NASA Contractor Report 194473

Influence of Geometry and Flow Variation on Jet Mixing and NO Formation in a Model Staged Combustor Mixer With Eight Orifices

M.S. Hatch, W.A. Sowa, and G.S. Samuelsen
UCI Combustion Laboratory
University of California
Irvine, California

June 1996

Prepared for
Lewis Research Center
Under Grant NAG3–1110

National Aeronautics and
Space Administration

TABLE OF CONTENTS

LIST OF FIGURES

LIST OF TABLES

LIST OF SYMBOLS

DR	- jet to mainstream density ratio
AR	- aspect ratio (long/short dimension)
ϕ	- equivalence ratio
J	- jet to mainstream momentum-flux ratio
MR	- jet to mainstream mass ratio
θ	- orifice angle with respect to mainstream
VR	- jet to mainstream velocity ratio
f	- mixture fraction
MOD1	- eight-hole baseline geometry
MOD2	- 8:1 aspect ratio slanted slots, $\theta = 45^o$
MOD3	- 4:1 aspect ratio slanted slots, $\theta = 0^o$
MOD4	- 4:1 aspect ratio slanted slots, $\theta = 22.5^o$
MOD5	- 4:1 aspect ratio slanted slots, $\theta = 45^o$
MOD6	- 4:1 aspect ratio slanted slots, $\theta = 67.5^o$
MOD7	- 4:1 aspect ratio slanted slots, $\theta = 67.5^o$
R	-Radius of Mixing Section
RQL	- Rich-Burn/Quick-Mix/Lean-Burn combustor
RZ	- rich zone
QM	- quick mix
OA	- overall
Z	-axial distance from orifice leading edge

ABSTRACT

A series of non-reacting parametric experiments was conducted to investigate the effect of geometric and flow variations on mixing of cold jets in an axis-symmetric, heated cross flow. The confined, cylindrical geometries tested represent the quick mix region of a Rich-Burn/Quick-Mix/Lean-Burn (RQL) combustor. The experiments show that orifice geometry and jet to mainstream momentum-flux ratio significantly impact the mixing characteristic of jets in a cylindrical cross stream. A computational code was used to extrapolate the results of the non-reacting experiments to reacting conditions in order to examine the nitric oxide (NO) formation potential of the configurations examined. The results show that the rate of NO formation is highest immediately downstream of the injection plane. For a given momentum-flux ratio, the orifice geometry that mixes effectively in both the immediate vicinity of the injection plane, and in the wall regions at downstream locations, has the potential to produce the lowest NO emissions. The results suggest that further study may not necessarily lead to a universal guideline for designing a low NO mixer. Instead, an assessment of each application may be required to determine the optimum combination of momentum-flux ratio and orifice geometry to minimize NO formation. Experiments at reacting conditions are needed to verify the present results.

CHAPTER 1
INTRODUCTION

1.1 Overview

The development of a new generation U. S. built supersonic civil aircraft is currently the focus of a multi-phase study led by NASA. This long-range, Mach 2-3 aircraft is projected to be commercially available as early as the year 2000 (Ott, 1989). There are, however, a number of technical and environmental obstacles that need to be overcome before the viability of this supersonic aircraft is proven. To identify these challenges, the High Speed Research (HSR) program was launched in 1988. The program, which involves the NASA Lewis, Langley and Ames Research Centers, is initially focusing on environmental issues such as engine emissions, community noise and sonic booms.

One of the requirements of the HSR program is to develop the technology for an economically attractive flight alternative for the airline passengers of the year 2000 and beyond. To meet this requirement, the High Speed Civil Transport (HSCT) is designed to fly in the stratosphere at a cruise speed of Mach 2-3. The flight in the stratosphere, and the direct release of engine exhaust emissions in the earth's ozone layer, cause a major environmental concern with the operation of a fleet of such supersonic aircraft (Shaw, 1991).

The exhaust gases of today's conventional aircraft engines contain oxides of nitrogen, generally known as NO_X that includes nitric oxide (NO), nitrogen dioxide (NO_2), and nitrous oxide (N_2O). NO has been shown to play a significant role in the depletion of the earth's ozone layer through a series of known chemical reactions. Therefore, for the operation of a supersonic airplane to be environmentally acceptable, the HSR program is required to develop and demonstrate a combustion system with a ten-fold NO reduction as compared to todays conventional combustors.

Nitric oxide is formed in the combustion process when the nitrogen in the air oxidizes at high temperatures. The rate of NO production in the combustion chamber increases exponentially with reaction temperature. Therefore, the amount of NO produced is determined by the stoichiometry of the reaction and the residence time in the combustor.

Today's conventional combustors operate with a near stoichiometric primary zone where both the reaction temperature and NO production rate are high. The maximum temperature leaving the combustor, however, is limited by the turbine blade material. Therefore, more air is added downstream of the primary zone to dilute the high temperature gases to an overall lean equivalence ratio.

To reduce the emissions of nitrogen oxides, combustors can be designed to operate with a primary zone at an off-stoichiometric condition where the reaction temperature is reduced and, as a result, the NO production is decreased.

One of the promising low NO_x combustor concepts is the Rich-Burn/Quick-Mix/Lean-Burn (RQL) combustor (Novick and Troth, 1981). In this concept, the primary zone is designed to operate rich at an equivalence ratio of 1.2 to 2.0. The products of combustion, high in carbon monoxide concentrations, then enter the quick mix region and are rapidly mixed with the remaining air to complete the combustion process. In some cases, a portion of the air is added in the dilution zone to bring the gas temperature down to an acceptable level for the first stage turbine blade material. The RQL combustor is one of the approaches being considered by NASA and engine manufacturers for future HSCT aircraft (Shaw, 1991).

A key to the success of the RQL combustor concept is achieving rapid and uniform mixing in the quick mix region of the combustor. Poor mixing in this section can form near stoichiometric packets at high temperatures, and allow them sufficient time to form large amounts of NO. Non-uniform mixing can also result in hot spots which may severely degrade the combustor liner

material. To ensure the success of the RQL approach, it is essential to understand the mixing mechanisms in the quick mix region and the role of these processes on NO formation and material integrity. This knowledge can then be used to optimize the design of the quick mix section to achieve the lowest NO_x levels possible. To address this need, the present study focuses on (1) understanding, and (2) optimizing the mixing mechanisms in the quick mix region of a RQL combustor.

1.2 Research Goals and Objectives

The goals of the present study are to (1) understand the mechanisms responsible for NO formation in this region of the combustor, and (2) optimize the mixing process to reduce the formation of NO. To achieve these goals, the objectives of this effort are to:

1. Conduct a literature search identifying the previous studies on mixing of jets in a cross flow and the past RQL developmental efforts,
2. Based on previous research, identify the first and second order parameters influencing mixing of jets in a confined cross flow,
3. Design and build a test facility with preheat capability and high flow rates to perform atmospheric mixing studies,
4. Select and implement the appropriate diagnostics,
5. Establish an analysis procedure,
6. Conduct a series of parametric studies to determine the effect of first order parameters on mixing characteristics of jets in a heated cross flow,
7. Demonstrate the influence of the second order parameters on mixing of jets in a cross stream,
8. Identify the low NO quick mix configuration for subsequent evaluation under practical conditions in the UCI Combustion Lab high pressure, high preheat test cell, and
9. Provide a data base for numerical modeling and CFD code validation.

CHAPTER 2

BACKGROUND

2.1 Overview

With the approach of the 21st century, and the increase in the number of international flights, the need for a long range, supersonic commercial transport has increased. To respond to the projected need, the United States is exploring the development of the first U.S. built high speed civil aircraft. Concord's economic failure in the supersonic transport area, however, has proved that such aircraft must be fuel efficient, reliable, and economically competitive to present a successful flight alternative.

In an effort to identify the key technology requirements for a supersonic transport, NASA has sponsored a number of independent studies known as the high speed research program (HSRP) studies. These investigations address the technical, economical, and environmental issues related to the development of a high speed commercial transport. Preliminary designs project a 250- 300 passenger aircraft with a 5500-6500 nautical mile range, flying at the cruise speed of Mach 2.8. To meet the noise and fuel consumption requirements, the aircraft is projected to fly in the stratosphere at altitudes of approximately 60,000 ft where the air density is low and the drag on the aircraft body is minimized.

The flight in the stratosphere, where the Earth's ozone layer is located, has introduced a major environmental challenge with the operation of a fleet of such supersonic aircraft. The depletion of the Earth's ozone layer has already been linked to the emissions of oxides of nitrogen released in the troposphere by conventional aircraft engines and other sources. The flight of a fleet of supersonic aircraft in the stratosphere presents an even greater danger to the ozone layer because: 1) NO emissions will be directly released in the ozone layer, and 2) NO emissions levels predicted for a conventional gas turbine combustor operating at the HSCT high inlet pressure and

temperature are substantially higher than those of the subsonic fleet currently in service. Therefore, one of the primary objectives of the HSRP is to demonstrate an advanced gas turbine combustor with NO emissions at one tenth of a conventional combustor operating at the HSCT cruise condition.

2.2 Gas Turbine Combustor

2.2.1 Overview

Gas turbine engines have been described as the main power plant of the twentieth century. They are widely used in aircraft and stationary applications as well as power sources for ships, trains, trucks and buses. Gas turbine engines operate on a three-step, open cycle known as the Brayton cycle. First, the air is compressed adiabatically in a compressor. The compressed air then enters the combustion chamber where fuel is introduced and burned at constant pressure. Finally, the products of combustion are expanded through a turbine and released in the atmosphere. The pollutants are formed in the combustion chamber where the chemical energy of fuel is converted to heat.

Figure 2.1 presents the schematic of a typical gas turbine combustor. As shown, fuel and a portion of combustor air enter the primary zone through separate delivery circuits. Typically a swirler is fitted around the fuel injector to induce recirculation in the primary zone in order to mix the hot combustion products and the incoming fuel/air mixture and stabilize the reaction. The function of the primary zone is to provide high temperatures and enough time for the combustion process to complete. The intermediate zone of the combustor is designed to provide the time and available oxygen to complete the CO oxidation process. Approximately 20-40 percent of the air is added in the dilution zone of the combustor to provide an exit temperature distribution acceptable to the turbine blade material. The remaining air is injected through the cooling slots to protect the combustor liner from high temperatures inside the chamber.

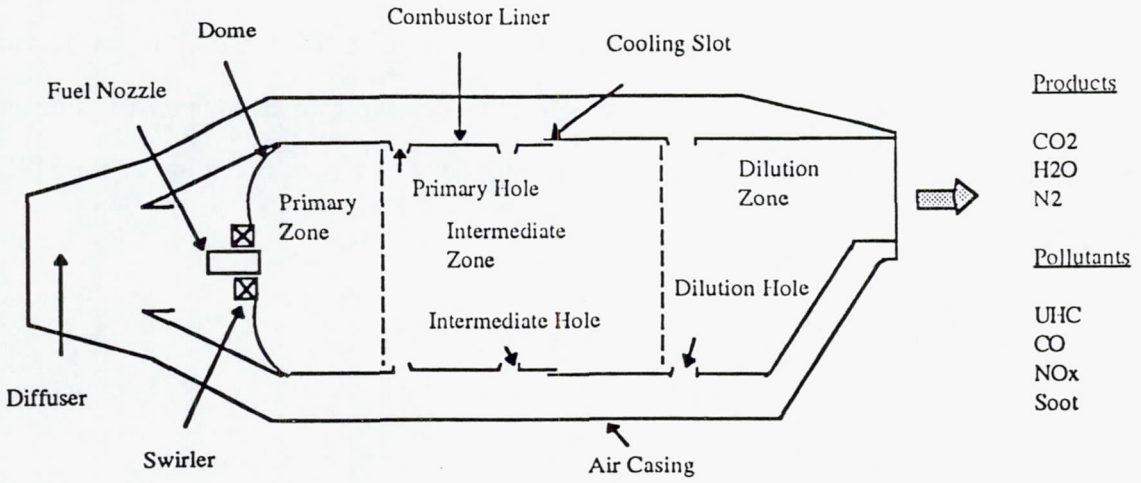

Figure 2.1: Schematic of a Gas Turbine Combustor

The ratio of air to fuel determines the stoichiometry of reaction in a combustion chamber. In a stoichiometric or theoretical reaction, all combustible elements in the fuel are completely converted to carbon dioxide and water, and no excess fuel or oxygen is present in the products.

$$\text{Fuel + air} \quad \text{----------->} \quad CO_2 + H_2O + N_2 + \text{Heat}$$

The mass based ratio of fuel to air required to achieve complete combustion is the stoichiometric fuel/air ratio. In an actual combustion process, the equivalence ratio ϕ, is used to describe the stoichiometry of reaction. ϕ is defined as follows:

$$\phi = \frac{(\text{Fuel/air})_{\text{actual}}}{(\text{Fuel /air})_{\text{stoichiometric}}}$$

$\phi > 1$ fuel rich
$\phi = 1$ stoichiometric
$\phi < 1$ fuel lean

The exhaust of a typical gas turbine combustor, contains CO_2, H_2O, N_2, and pollutants such as CO, unburned hydrocarbons, soot, and oxides of nitrogen or NO_x. These pollutants form less than one percent of the total exhaust gases. Despite their relatively small amounts, their impact

on air quality is significant. Photochemical smog, for example, is formed by the action of sunlight on oxides of nitrogen and reactive hydrocarbons. The role of nitric oxide on the depletion of the ozone layer however, is the reason for reducing the oxides of nitrogen in the HSRP.

2.2.2 Nitric Oxides Emissions

At full engine power, over 90% of NO_x consists of nitric oxide or NO. Therefore, NO and NO_x are often used (inappropriately) interchangeably. In a gas turbine combustor, NO can be formed by three mechanisms (Lefebvre, 1989) : Prompt NO is formed very early in the combustion process in especially fuel rich regions. Prompt NO typically forms a small fraction of the total NOx emissions. Currently, there are no known mechanisms available to control prompt NO. Fuel-bound NO is formed by oxidation of nitrogen in the fuel and may be controlled by reducing the nitrogen content of the fuel. Thermal NO constitutes the majority of NO formed in gas turbine engines and is formed by oxidation of nitrogen at high temperatures. Controlling thermal NO is of specific interest to the HSRP.

The kinetics of thermal NO formation were first identified in 1946 (Zeldovich, 1946), and are referred to as the Zeldovich chain mechanism:

$$N_2 + O \quad \text{------->} \quad NO + N \qquad (1)$$

$$N + O_2 \quad \text{------->} \quad NO + O \qquad (2)$$

Reaction (1) takes places more slowly than reaction (2) and requires elevated temperatures to initiate. Therefore, reaction (1) is the rate limiting step in the NO formation mechanism. The reaction rate for NO formation can be derived based on the Zeldovich mechanism.

$$\frac{d[NO]}{dt} = K_1 [N_2] [O]$$

where (Glassman, 1987, p. 329)

$$K_1 = 2 \times 10^{14} \exp (-76{,}500 / R_u T)$$

Figure 2.2, shows the exponential dependence of the NO production rate on temperature. K_1 is especially significant in temperatures in excess of 1900 K or 2800° F.

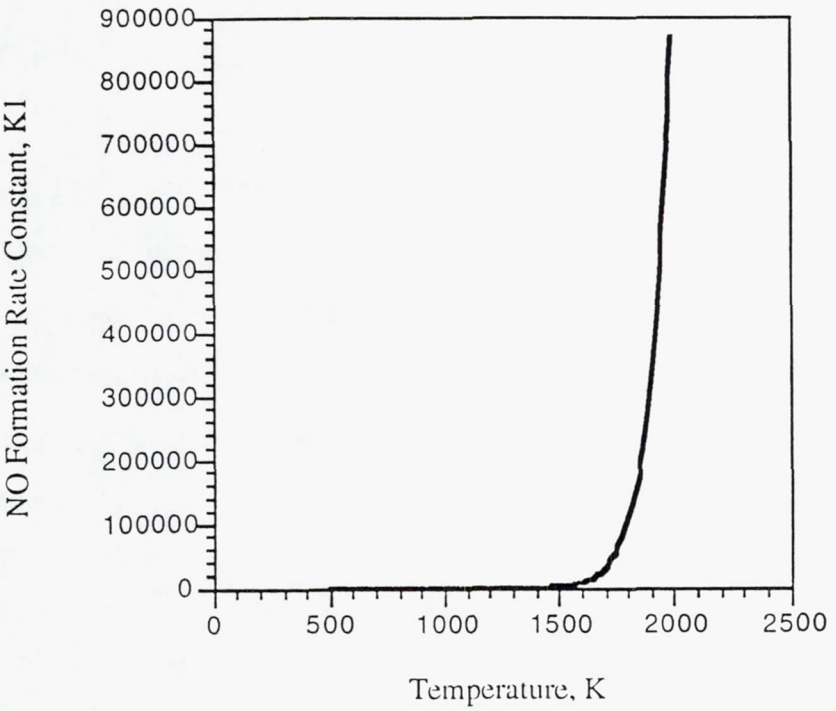

Figure 2.2: Dependence of NO Formation Rate on Temperature

(Samuelsen, 1975, p. 276)

2.3 Impact of NO on the Ozone Layer

The mechanisms involved in maintaining the balance of ozone in the stratosphere have been the subject of investigation for many decades. The source of ozone in the stratosphere is the photodissociation of molecular oxygen by radiations of wavelength shorter than 242 nm. In 1930, Chapman developed the basic theory of stratospheric ozone removal based on the air motions and

the photochemistry of pure air (Brasseur, 1973). According to Chapman's hypothesis, there are two photochemical and two chemical reactions involved in formation and removal of ozone:

formation	$O_2 + h\upsilon$	------->	$O + O$	(1)
	$O + O_2$	---M-->	$O_3 + M$	(2)

Where M represents the radical species, and

removal	$O_3 + h\upsilon$	------->	$O_2 + O$	(3)
	$O + O_3$	------->	$O_2 + O_2$	(4)

The rate constants for the above reactions were measured in the laboratory and the solar intensity above the atmosphere was calculated based on Plank's radiation equation and a temperature for the sun surface. Chapman's mechanism appeared to provide a satisfactory balance of ozone production and destruction in the stratosphere.

During the period 1930-1961, as a result of more advanced laboratory measurement techniques, new values for the rate constants for reactions 1- 4 were obtained. In addition, the actual distribution of the solar radiation was measured by rocket flights. The new data revealed a large unbalanced ozone production based on Chapman's model, indicating the need for a modified theory.

In 1965, Hunt postulated the reactions of free radicals based on water, H, HO, HOO (Johnston and Whitten, 1973).

$HO + O_3$	------->	$HOO + O_2$	(5)
$HOO + O_3$	------->	$HO + O_2 + O_2$	(6)

Further study of the above reactions and their rate constants revealed the inadequacy of the mechanism to entirely account for the unbalanced production of stratospheric ozone in altitudes

below 40 Km (~130,000 ft), further emphasizing the need for a mechanism other than pure air or water reactions to explain the global balance of ozone in the lower stratosphere.

The interaction of oxides of nitrogen with the Earth's ozone layer was first postulated by Crutzen (1970).

$$NO + O_3 \text{ -------> } NO_2 + O_2 \quad (7)$$

$$NO_2 + O \text{ -------> } NO + O_2 \quad (8)$$

$$NO_2 + h\upsilon \text{ -------> } NO + O \quad (9)$$

The rate constant for reactions 7 and 8 have been measured repeatedly by various investigators and good agreement among the measurements has been demonstrated (Johnston and Whitten, 1973).

Studies have shown that at elevations below 20 Km (~65,000 ft), another catalytic cycle of the oxides of nitrogen may be important (Johnston and Whitten, 1973):

$$NO_2 + O_3 \text{ -------> } NO_3 + O_2 \quad (10)$$

$$NO_3 + h\upsilon \text{ -------> } NO + O_2 \quad (11)$$

$$NO + O_3 \text{ -------> } NO_2 + O_2 \quad (12)$$

The above reactions, along with the ozone removal mechanisms based on pure air and water radical, and the transport to the troposphere, appear to provide a satisfactory picture of the photochemical balance of stratospheric ozone. It has been noted, however, that the oxides of nitrogen are the most important factor in maintaining the ozone balance in altitudes between 15 and 35 Km (49,000 ft - 115,000 ft) (Johnston and Whitten, 1973).

The presence of NO in the stratosphere was at first attributed to the photolysis of diatomic nitrogen in altitudes above 90 Km and its downward transportation by eddy diffusion. In 1970, Nicolet identified a main natural source of NO in the stratosphere due to the dissociation of

nitrous oxide by the excited oxygen atoms (Brasseur, 1973). The average range of natural NO flux in the stratosphere has been estimated to be 0.35 - 1.2 x 108 molecules cm-2 sec-1 (Johnston and Whitten, 1973).

The emissions of oxides of nitrogen from supersonic aircraft have been identified as the main sources of artificial NO in the stratosphere. Johnston and Whitten (1973), concluded that the operation of a full fleet of supersonic transport would approximately double the natural flux of NO in the stratosphere. This conclusion was based on the average NOx emissions of 15 g/Kg fuel per aircraft which is over three times less than the level predicted for a conventional combustor operating at the HSCT cruise condition. At predicted NO emissions level of 50 g/Kg fuel for the HSCT combustor, the potential impact on the ozone layer is far too great, and requires the demonstration of an "ultra low" NO_x combustion system, a prerequisite to the HSRP development.

2.4 Low NO Combustor Concepts

In recent years, environmental issues have become a growing concern due to the increased public awareness of phenomena such as the green house effect, global warming, and ozone layer depletion. Studies have shown that the combustion systems of mobile and stationary sources generate over 90% of the pollutant emissions released in the atmosphere. Stringent air quality regulations have been proposed and implemented to control the emissions of combustion systems including gas turbine combustors. To meet the air quality standards, engine manufacturers have concentrated their efforts on developing low emissions combustors.

There are two fundamental approaches to the design of a low NO combustor: 1) control the NO formed during the combustion process, and 2) eliminate the NO produced through a series of chemical reactions in a post-combustion process. Examples of the first approach include "dry" low NO combustor concepts such as lean premixed and RQL. Selective Catalytic Reduction (SCR), typically used in stationary applications, is an example of the second approach. The dry

low NO capability is preferred in an aircraft application where the engine size and weight are important design parameters. The development of a dry, ultra low NO combustor is the focus of the HSRP combustor design effort.

As discussed earlier, the NO formation rate increases exponentially with the reaction temperature. Therefore, there are two factors that influence NO production in the combustion process: 1) temperatures inside the chamber and, 2) time available for N_2 oxidation. Controlling these parameters, forms the basis for most dry low NO concepts.

In the combustor environment, the reaction temperature varies with the fuel/air stoichiometry. Figure 2.3 shows the variation of the combustor reaction temperature with equivalence ratio for Jet A fuel at representative HSCT cruise conditions. It is shown that the combustion reaction temperature is highest for a fuel/air mixture near equivalence ratio of unity, and decreases as the fuel/air mixture approaches a lean or a rich composition. The mole fraction of NO on the other hand, peaks on the lean side due to the abundance of oxygen, and reaches ultra low values for very rich or very lean mixtures (Figure 2.4).

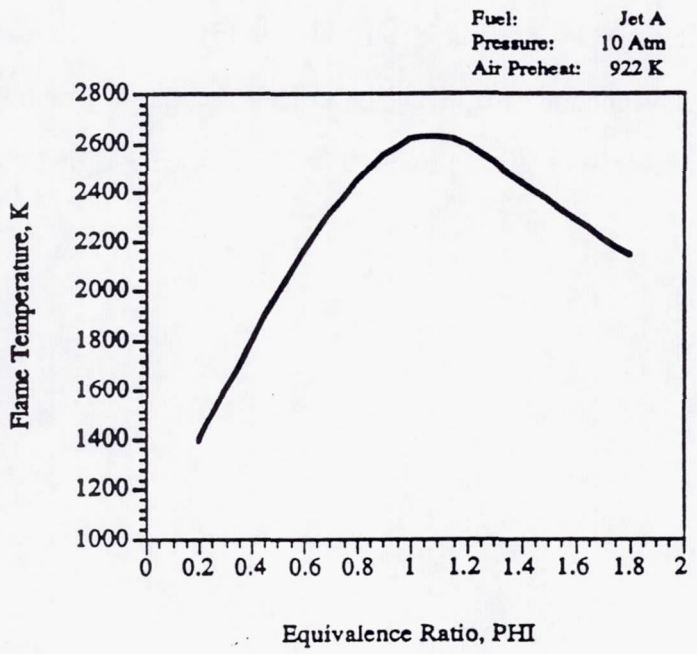

Figure 2.3: Variation of Reaction Temperature with Equivalence Ratic
Source: NASA Equilibrium Program

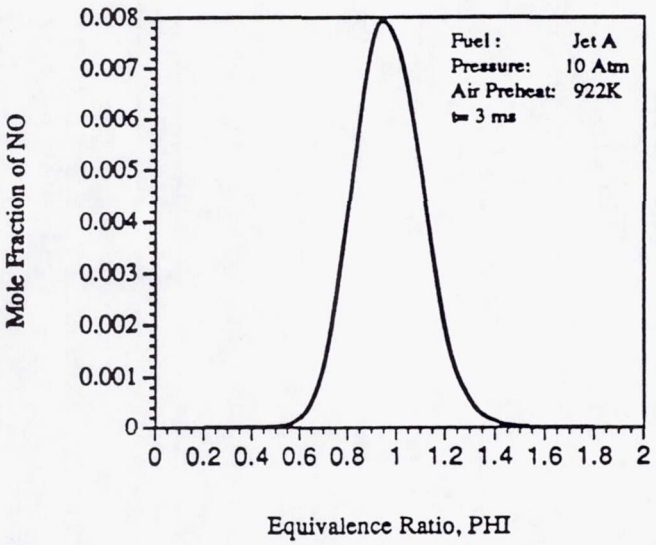

Figure 2.4 : Variation of NO Mole Fraction with Equivalence Ratio

Source: CHEMKIN Kinetics Code

The effect of residence time on NO formation is illustrated in Figure 2.5. In this figure, the mole fraction of NO is plotted as a function of equivalence ratio and time. It is shown that increasing residence time significantly increases the mole fraction of NO formed at a given equivalence ratio.

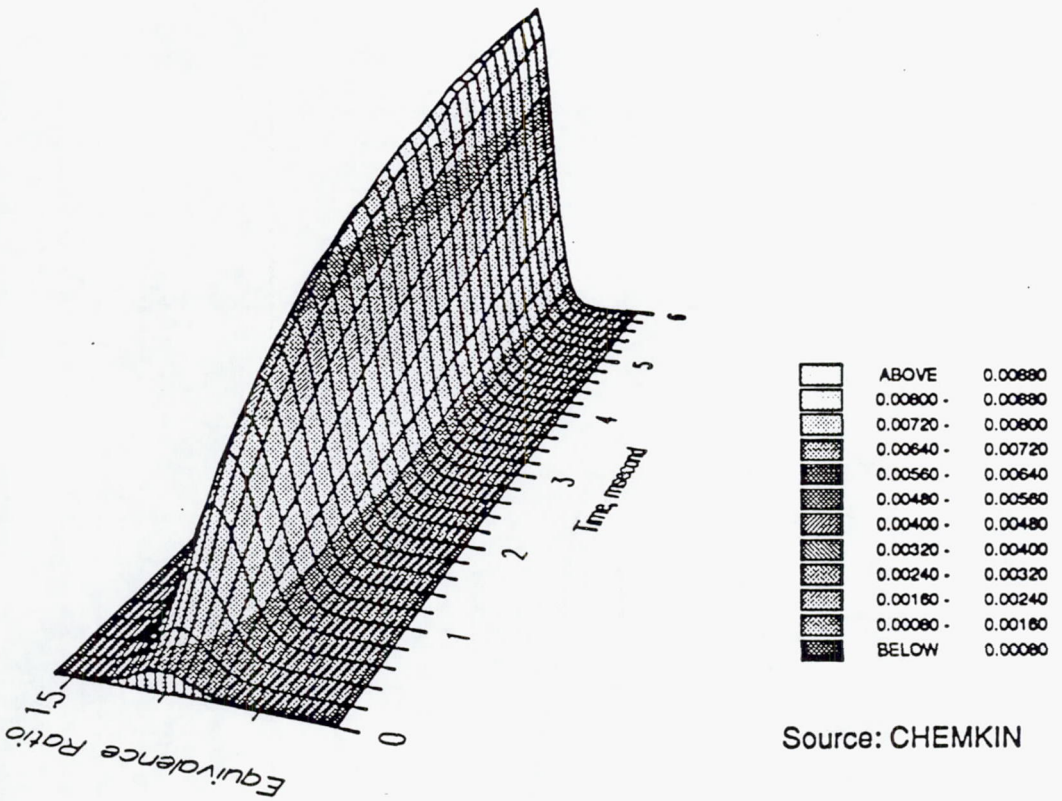

Figure 2.5: Effect of Residence Time on Mole Fraction of NO Formed

Today's conventional combustors are designed with a stoichiometric primary zone. At the severe HSCT operating conditions, especially the high inlet temperature, a stoichiometric primary zone produces large amounts of NO as illustrated in Figure 2.4. Therefore, a conventional combustion system is not suitable for achieving the NO emissions goal of the HSRP and an alternative low NO approach is necessary.

Among the promising low NO_x combustor concepts are the Lean-Premixed/Prevaporized (LPP) and the Rich-Burn/Quick-Mix/Lean-Burn (RQL) combustors. In a LPP combustor, the fuel and air are premixed and burned in a lean primary zone at an equivalence ratio in the range of 0.5-0.7. Very little NO_x is produced due to the low temperatures inside the combustor chamber. The ultra low NO capability of the LPP combustor has been demonstrated in practice (Tacina, 1990). The Lean-Premixed combustor however, has a narrow stability range, and is susceptible to flashback and auto-ignition. Figure 2.6 presents a schematic of a LPP combustor.

The RQL concept was first developed in the 1970's to reduce the NO emissions of alternate fuels containing large amounts of fuel-bound nitrogen (Tacina, 1990). In this approach, combustion takes place in two stages. First, fuel and air react in a fuel rich environment at equivalence ratios in the range of 1.2 to 2.0. NO formation is suppressed due to the lack of oxygen and low temperatures associated with the fuel rich mixture. The products of combustion, rich in carbon monoxide, then enter the quick mix region where 2 to 3 times the primary air is added to the mixture to complete the combustion process. Typically, a contraction occurs at the inlet to the quick mix section to avoid backflow and reduce the residence time required for mixing (Smith et al., 1991). CO oxidation continues into the lean zone and, if necessary, more air is introduced to provide an acceptable temperature profile at the exit of the combustor. The RQL combustor requires more complex hardware than the Lean-Premixed combustor, but has a wide stability range and can be operated with lower grade fuels. Available emissions data however, have shown higher NO emissions for the RQL combustor than predicted (Tacina,1990). Figure 2.7 presents a schematic of a RQL combustor.

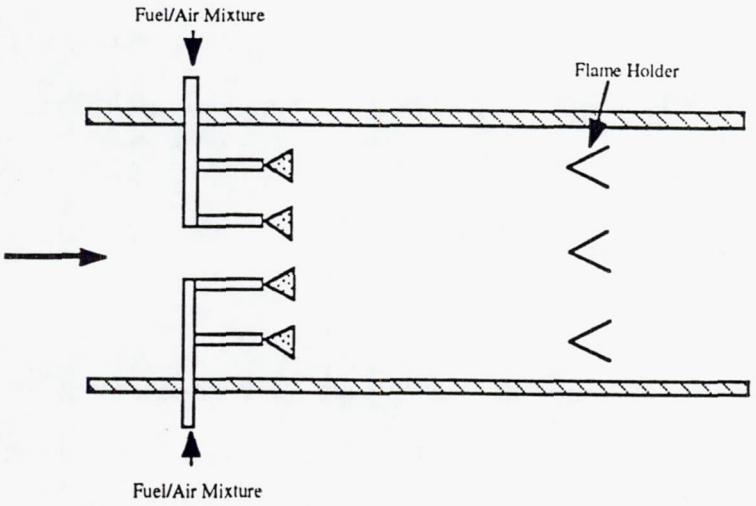

Figure 2.6: Lean Premixed/ Prevaporized (LPP) Combustor

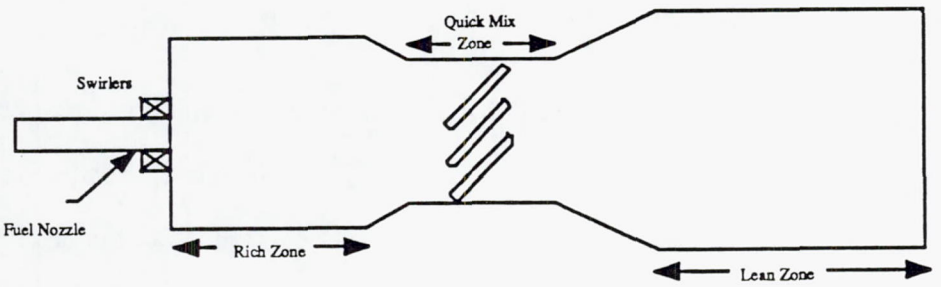

Figure 2.7: Rich-Burn/Quick-Mix/Lean-Burn (RQL) Combustor

Mixing processes in the quick mix zone are of significant importance for the optimum performance of a low NO_x RQL. First, the transition from the rich to lean fuel/air mixture must take place rapidly to minimize the residence time of near stoichiometric compositions (Figure 2.8). Secondly, mixing must be uniform to control the mean temperature and fluctuating instantaneous high temperature peaks where large amounts of NO are formed (Figure 2.9).

Experience shows that low NO emissions for the RQL concept depends on the mixing effectiveness in the quick mix region. The higher than expected NO emissions levels from RQL combustors are probably due to stoichiometric burning in the quick mix zone (Tacina,1990). To optimize the quick mix step, it is essential to 1) understand the parameters that influence mixing processes and the role of these mechanisms on NO formation, and 2) select the parameters that optimize mixing relative to NO production.

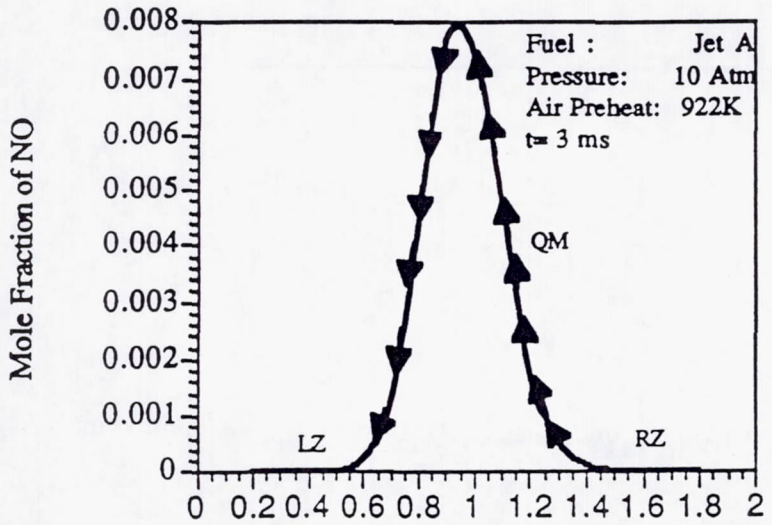

Figure 2.8 Rich-Burn/Quick-Mix/Lean-Burn Concept

Source: CHEMKIN Kinetics Code

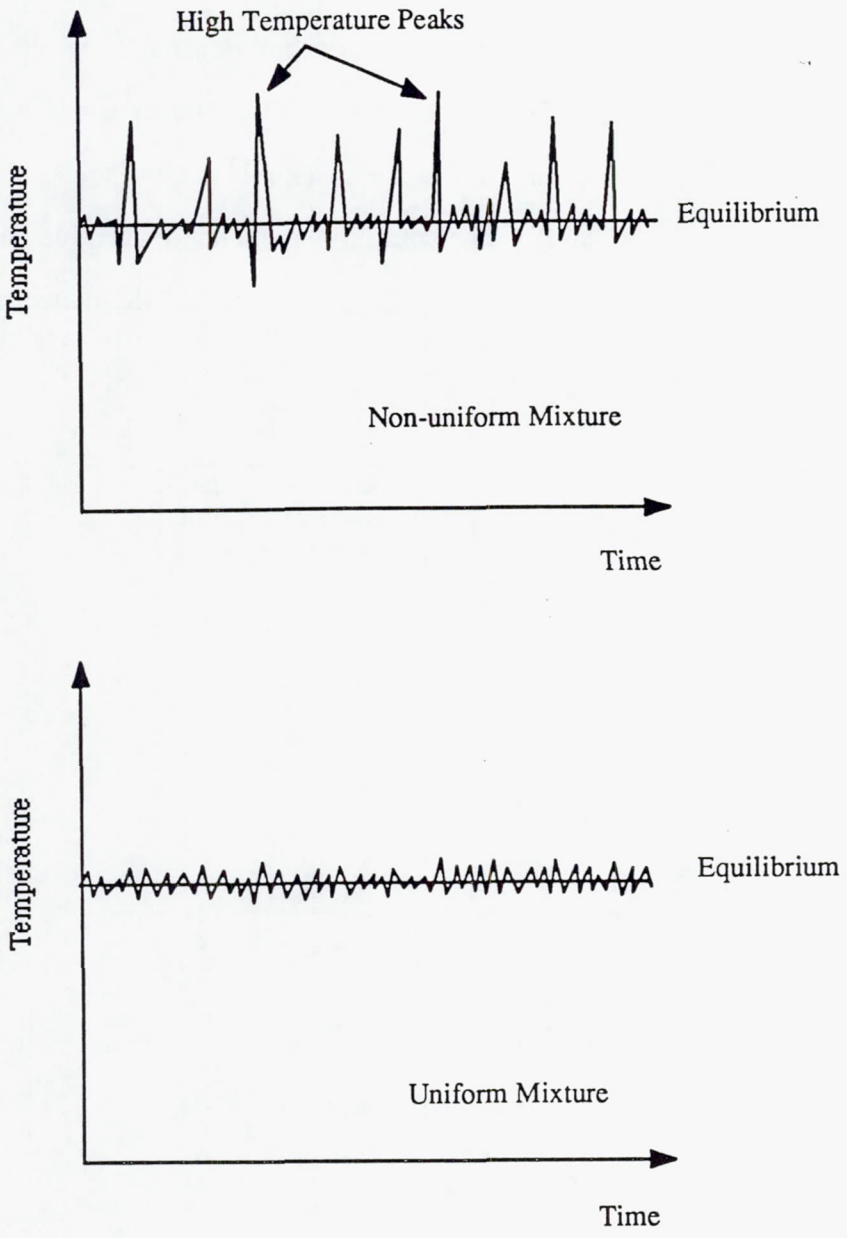

Figure 2.9 Comparison of Uniform and Non-uniform Mixtures

2.5 Mixing of Jets in a Cross Flow

Mixing of relatively cold jets in a confined cross flow has a variety of practical applications and has motivated a number of studies over the past decades. In a gas turbine combustor for example, jet mixing is important in the dilution zone where the products of combustion are mixed with air to reduce the temperatures to the acceptable levels for the turbine section material. Poor mixing in this region can result in hot spots and high pattern factor which degrade the engine life. Jet mixing in a cross flow is also important in applications such as discharge of effluents in water, and in transition from hover to cruise of V/STOL aircraft.

This section will describe the previous research conducted on mixing of jets in a cross stream by focusing on: 1) the experimental and numerical studies of mixing of jets in a cross flow performed primarily to understand the mixing processes in a dilution zone of a combustor, and 3) the recent mixing studies motivated by the HSRP. Table 2.1, presented at the end of Chapter 2, summarizes the relevant experimental mixing studies.

2.5.1 Previous Mixing Research

As a jet is injected into a cross flow, it causes a blockage in the main stream which decelerate the flow and increases the pressure upstream of the jet. The pressure immediately downstream of the jet, however, decreases and this non-uniform pressure distribution, deflects the jet, creating the kidney shape structure characteristic of a jet in a cross flow. Downstream of the injection point, the cross flow forms a pair of vortices behind the jet which persist long after the original jet disappears. The rate of entrainment and large scale mixing between the two streams are determined by the action and strength of these vortices. Figure 2.9, illustrates the main features of a jet injected into a cross stream.

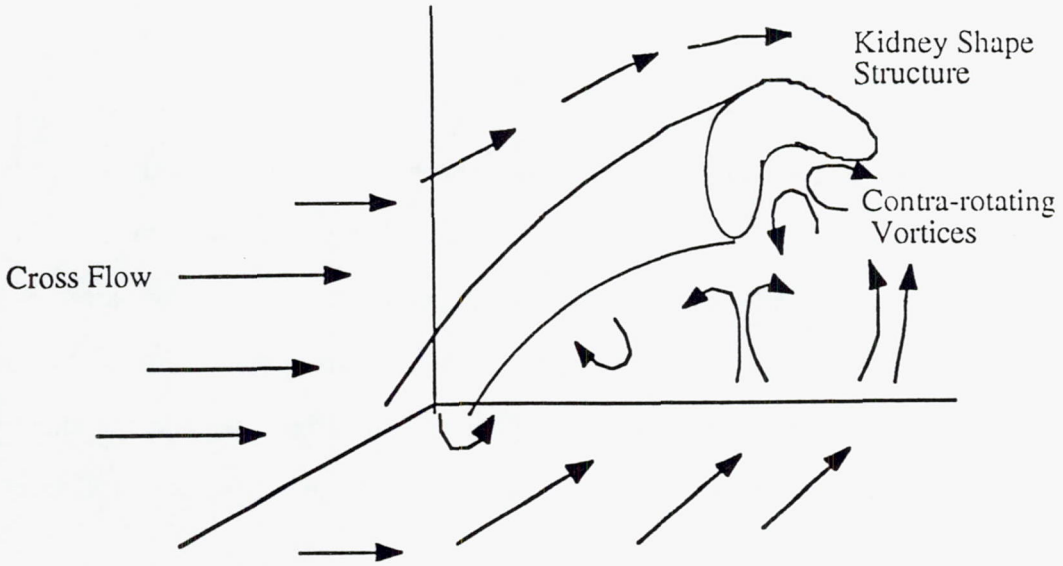

Figure 2.10 : Jet in a Cross Flow

Kamotani and Greber (1972), measured the velocity and temperature distribution downstream of a heated turbulent round jet injected into a subsonic cross flow for several momentum-flux ratios . The results showed that the jet structure is primarily dominated by a vortex pair formed behind the jet. At lower momentum-flux ratios, the jet is deflected sharply and the vortices do not have time to develop. Therefore, the kidney shape structure remains present into the far downstream. At higher momentum-flux ratios, however, the vortices become stronger and dominate the flow field. The results also indicated that the jet velocity and temperature trajectories, defined as the locus of the maximum value in the plane of symmetry, strongly depend upon the jet to cross stream momentum-flux ratio.

To present a quantitative measure of the vortex structure observed downstream of a jet injected into a cross stream, Fearn and Weston (1974) proposed two, two-dimensional models to predict the location, and strength of the vortices. In the vortex filament model, the strength and location of vortices are determined by the measured upwash velocities. In the other model, it is assumed

that each vortex is composed of a Gaussian distribution of vorticity. The parameters used in each model are based on the measured velocity field in a vortex cross section. The models showed that the vortex pair is formed very close to the injection point, and the strength of the vortex structure is directly proportional to the orifice diameter and jet speed.

Based on the two-dimensional vortex filament assumption proposed by Fearn and Weston, Le Grives developed a simple expression for the mass entrained by the contra-rotating vortex pair (Le Grives, 1978). In addition, Le Grives obtained closed form equations for the vortex strength and spacing in terms of jet angle, vortex trajectory with respect to the cross stream velocity, and the ratio of jet to mainstream velocities. The theoretical model proposed by Le Grives to approximate the jet penetration process, identified the following forces acting on a jet control volume: 1) the centrifugal force oriented along the normal direction to the jet centerline, 2) the overall drag force, opposite to the relative jet velocity, and 3) the rate of variation of momentum along the jet trajectory (Le Grives, 1978). Theoretical predictions based on Le Grives model were found to be in fair agreement with experimental results and flow visualizations.

Karagozian, Nguyen, and Kim, (1980) used an analytical model to examine the nature of the contra-rotating vortices associated with a jet in a cross flow. The model showed that a component of vorticity, parallel to the jet axis, is generated by the interaction of the jet with the cross flow and dominates the near field. Another component of vorticity, formed by the jet impulse, lies parallel to the cross flow and dominates the far field. Numerical solutions for the vortex trajectory compared well with the experiment and showed that vortex separation is a two-dimensional, viscous phenomena and can be theoretically predicted.

The behavior of the contra-rotating vortices for a spanwise jet injection was numerically examined by Karagozian et al. (1986) and compared to available experimental results. The solutions showed that the multiple vortices interact with each other and cause less penetration of the cross

flow. The model also showed that closely spaced orifices quickly approach a two-dimensional slot (Karagozian, et al. 1986).

In order to predict the behavior of jets in a cross stream, various correlations have been proposed. In 1976, Cox used the experimental data obtained from a single row of cold jets injected into a heated cross stream to develop a correlation to predict the temperature pattern inside the dilution zone of a gas turbine combustor. The experiments were performed in a rectangular geometry (Walker and Kors, 1973). The flow variables included jet to mainstream density ratio and velocity ratios. Geometric variables were jet diameter and spacing. The correlation accurately predicted the mixing characteristics of a single row of jets at conditions representative of gas turbine annular combustors.

Holdeman and Walker (1977), used the same set of experimental data to develop an empirical model to: 1) predict the temperature downstream of the row of jets, and 2) study the effect of the independent variables on mixing. The independent flow and geometric variables included the momentum-flux ratio, the ratio of jet spacing to orifice diameter, the ratio of duct height to orifice diameter, and the ratio of the downstream distance to duct height. The model was based on the assumption that properly normalized temperature profiles are self-similar. The scaling factors were expressed in terms of the independent flow and geometric variables. The model showed excellent agreement with experimental data accept for the cases that resulted in strong impingement on the opposite wall. The study also concluded that the momentum-flux ratio was the most significant parameter that influences the penetration and mixing. Density ratio on the other hand, appeared to have only a second order effect on mixing for the range examined.

To examine the mixing characteristics of jets in a rectangular duct at conditions representative of gas turbine combustors, Holdeman et al. (1984), extended the experimental variations to include variable density ratio, flow area convergence, variable mainstream temperature, and opposed in-

line and staggered injection. The results showed a coupling between momentum-flux ratio, J, and normalized orifice spacing, S/H_o, described by the following expression:

$$C = \frac{S}{H_o}\sqrt{J}$$

where C is a constant. For a single row of jets, isothermal temperature distribution was obtained in a minimum distance downstream of the injection plane for C=2.5. Values of C, a factor of _ 2 larger or smaller, resulted in over or under-penetration, respectively. Flow area convergence, especially injection wall convergence, significantly improved downstream mixing (Holdeman, et al., 1984). The study also concluded that the optimum orifice spacing for double sided in-line injection is one-half of the optimum spacing for single sided injection. For opposed rows of staggered jets, the optimum spacing is double the optimum value for single sided injection.

Wittig et al. (1984), measured the temperature distribution downstream of a single and opposite-wall jet injection into a hot cross flow. The results showed that the correlations derived from single wall jet injection developed by Cox (1977), and Holdeman and Walker (1977), can be applied to opposite-wall injection at identical and low momentum-flux ratios. The correlations however, do not hold well at high momentum-flux ratios when the jets penetrate beyond the mid-plane. Modified correlations resulted in better agreement between the predicted and measured temperature distribution downstream of opposite-wall jet injection (Wittig et al., 1984).

The effects of geometry on jet trajectory and penetration has been investigated in several studies. Weston and Thames (1979) experimented with 4:1 aspect ratio rectangular nozzles and showed that these jets decay faster than round jets of equivalent diameter, due to increased viscous effects caused by their larger perimeter. It was also shown that streamwise nozzles have characteristics similar to those of round holes, while jets oriented normal to the freestream exhibit significantly different properties.

Detailed velocity and Reynolds stress measurements of twin jets injected normally to a cross stream was performed by Isaac and Jakubowski in 1985. Their results showed a striking similarity in terms of mean velocities and turbulent parameters between the tandem jets and a single jet in a cross flow.

Mixing characteristics of small aspect ratio elliptic jets were the subject of experimental investigation by Ho and Gutmark (1987). The results showed a significant increase in cross flow entrainment for small aspect ratio elliptic jets (2:1- 3:1) as compared to circular holes. Most of the mass entrainment for this geometry occurred around the jet minor axis.

The influence of swirl and high turbulence was investigated in an experimental study conducted by Kavsaoglu and Schetz (1989). Pressure and velocity distributions were obtained for a 90^{o} circular hole at low and high-exit turbulence and different swirl levels. The results showed that both swirl and high turbulence decrease jet penetration to center of the main flow and reduces the negative pressure regions on the surface. Inlet swirl also introduces asymmetries into the flow field, the effects of which are more pronounced at low velocity ratios.

Numerical studies by Smith (1990) examined the mixing patterns of opposed, staggered holes in a rectangular geometry, to determined the effects of jet inlet turbulence and hole spacing. Both symmetric and asymmetric flow patterns were seen for the conditions numerically tested. Jet mixing was strongly influenced by the type of flow pattern where improved mixing occurred for symmetric flow patterns. The result suggested that there is an optimum hole spacing for a given flow condition and geometry, and that mixing improves as the jet inlet turbulence is increased.

2.5.2 Recent Studies

In the past few years, a number of jet mixing studies have been conducted with the specific goal to understand the mixing processes in the quick mix region of a RQL combustor. The majority of these studies have focused on the numerical analysis of the flow field.

Howe, et al. (1991), developed a computer program to investigate the mixing characteristics for both reacting and non-reacting conditions in a configuration simulating the quick mix region of a RQL combustor. Jet to mainstream momentum-flux ratio was shown to have a significant impact on jet penetration depth while reaction appeared to reduce the penetration depth. No NOx measurements were reported for this study.

The impact of momentum-flux ratio on mixing and NO formation in a can geometry was numerically investigated by Talpallikar, et al. (1990). Momentum-flux ratios of 32 and 40 produced the "best" mixing for a 12-slot geometry under non-reacting and reacting conditions, respectively. The study also investigated the mixing characteristics of two asymmetric geometries designed to produce large scale vortices. The overall mixing was improved for the asymmetric configurations, but higher NO was calculated due to the presence of hot spots.

Smith, et al. (1991), conducted a CFD study to examine the effect of reduced flow area on mixing and NO_x emissions. Their calculations showed that mixing is unaffected by the reduction in the flow area , while NO_x formation is reduced due to shorter residence time.

One of the few experimental studies of jet mixing in a cylindrical duct was conducted by Vranos, et al. (1991). The primary variables in this experiment were the momentum-flux ratio, injector geometry, and density ratio. Planar digital imaging was used to measure the concentration of an aerosol seed uniformly mixed with the jet stream, in several planes downstream of the mixing orifices. The first axial location examined in this experiment was 1.2-radius downstream of the injection point. The results showed that for an axis-symmetric geometry, mixedness is more sensitive to circumferential uniformity rather than jet penetration. Therefore, above a certain momentum-flux ratio, mixing with slanted slots is better than with round holes.

Reference	Configuration	Test Parameters	Measurements	Diagnostics	Major Conclusion
Kamotani and Greber, (1972)	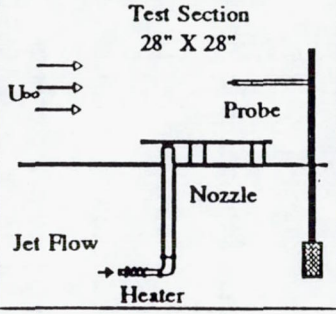	J : 15- 60 U∞ : 20- 30 fps Re: 2800- 4200 T jet: 75 F- 400 F	Flow Visualization Velocity Turbulent Intensity Temperature	Smoke Photograph Hot Wire Thermocouple	• Momentum flux ratio determines the jet trajectory. Turbulent intensity increases with momentum flux ratio. • Temperature trajectory is a weak function of density ratio. • Downstream temperature and velocity distribution is dominated by vortex motion.
Fearn and Weston (1974)	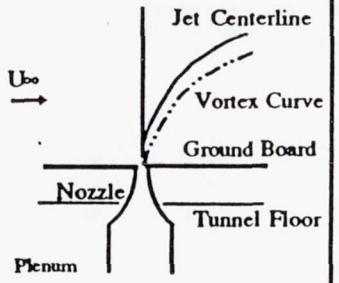	VR: 3 to 10 U∞ : 100- 175 fps T jet: 75 F- 400 F	Jet Velocity Field	Yaw Pitch Probe	• Developed two models to define contrarotating vortices. • The pair of vortices is the dominant feature of flowfield. • The vortex pair is formed close to the injection point • Vortices initial strength is proportional to nozzle diameter and jet speed.
Cox (1976)	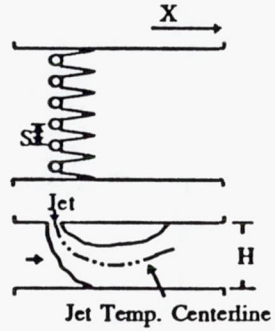	13 ≤ J ≥ 63 0.1≤MR ≥ 0.6 2.5 ≤ VR ≥ 5.3	Temperature Pressure	Thermocouple Not reported	• Developed a correlation method to predict temperature field downstream of one row of closely spaced holes injected into a hot confined cross flow. • The model provided good comparison beteem predicted and measured flow field within the range of parameters representative current GTE combustors.

Table 2.1: Summary of Selected Jet Mixing Experiments

Holdemen and Walker, (1977)	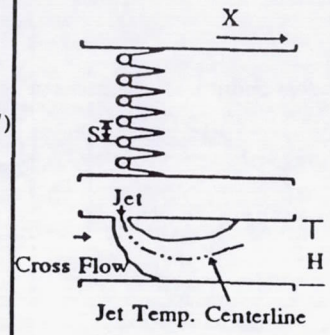	13 ≤ J ≥ 63 0.1≤ MR ≥ 0.6 2.5 ≤ VR ≥ 5.3	Temperature Pressure	Thermocouple Not reported	• Developed an empirical model to predict mixing of of one row of jets injected into a hot cross flow. • The model provided good comparison beteem predicted and measured flow field. • Momentum flux ratio was found to be the most important factor influencing mixing.
Weston and Thames (1979)	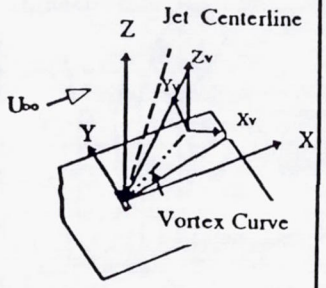	4:1 Aspect Ratio Jets Blunt & Streamwise Vel. Ratio: 4, 8, 10 Jet Angle: 15-90 Deg	Pressure Velocity Flow Angularity	Yaw Pitch Probes	• Penetration and vortex strength of blunt jets are less than those of streamwise jets. • Nominal properties of stream-wise jets are similar to those of circular jets. • Rectangular jets decay much faster than round jets due to the increased viscous effects on larger perimeter.
Wittig et. al. (1984)	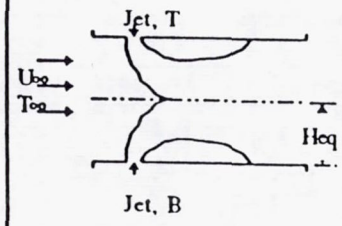	JT: 8.9- 57.8 JB: 24.0- 60.24 Uoo : 14.4- 18.4 m/s T jet: 309 K- 318.7 K Too: 430.8 K- 558.4 K	Total Temperature Total Pressure Velocity	NiCr-Ni TC Total Pressure Probe Not Reported	• One-sided wall injection correlations can be used for opposite-wall jet injection at low momentum flux ratios. • Modified correlations to give better agreement at higher momentum flux ratios.

Table 2.1: Contd.

Holdeman, et al. (1985)	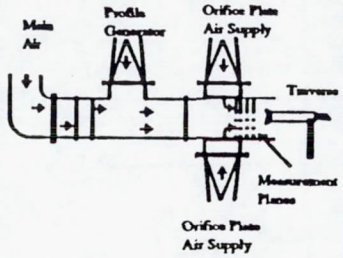	Ho/D: 4, 8 S/D: 2, 4 DR: 0.75, 2.2	Temperature Pressure	TC Total & Static Pressure Probes	• Density ratio has a second order effect on mixing. • Injection wall convergence significantly improves mixing. • Optimum orifice spacing for opposed in-line jets is half of the optimum value for single sided case. • For staggered jets the optimum value is twice the one of single side injection.
Isaac and Jakubowski (1985)	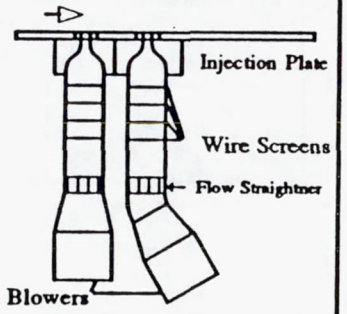	VR = 2 Single Jet Tandem Jets	Mean Velocities Reynolds Stresses	Hot-Wire	• Similarity was observed in details of flow within the cross sections of single and tandem jets. • The transvers velocity profiles were found to be significantly different than axial and vertical profiles. • Initial conditions are important in determining the jet trajectory.
Ho, and Gumark (1987)	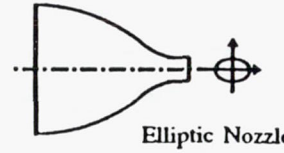	Vj= 21.9 m/s Aspect ratio: 2:1	Velocities	Hot Wire	• Mass entrainment by a 2:1 aspect ratio ellipttic jet is significantly higher than that of a round hole.

Table 2.1: Contd.

Kavsaoglu, and Schetz (1989)	Top of Test section 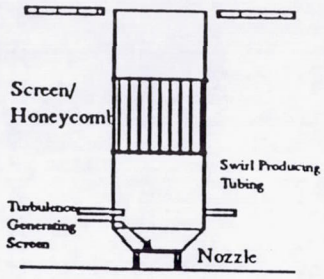	VR: 2.2, 4, 8 Turbulence: 3%, >10% Swirl: 40%, 58%	Pressure Velocity Turbulence Data	Yawhead Probe Hot wire X-wire Probe	•Swirl and high turbulence reduce penetration and decrease negative pressure surface area. • Swirl produces asymmetry in pressure distribution, especially for low velocity ratios, and high swirl ratios.
Stevens and Carrotte (1990)	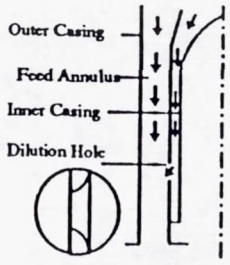	$13 \leq J \geq 63$ $0.1 \leq Mj/M\infty \geq 0.6$ $2.5 \leq Vj/V\infty \geq 5.3$	Temperature Pressure	Thermocouple Not reported	• Developed an empirical model to predict mixing of of one row of jets injected into a hot cross flow. • The model provided good comparison beteem predicted and measured flow field. • Momentum flux ratio was found to be the most important factor influencing mixing.
Vranos et al. (1991)	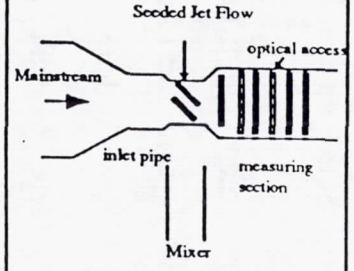	4:1 & 8:1 AR Slots and Round Holes Slot Angle: 45 deg J: 5, 18, 78	Seed Concentration	Mie Scattering Planar Digital Imaging	• Slanted slots are better mixers above a certain J. •Mixing decreases at increased density ratios. • Mixedness is independent of mass flow rate.

Table 2.1: Contd.

CHAPTER 3

TASKS

The present effort consisted of four tasks designed to accomplish the objectives outlined in Chapter 1:

I. Literature Survey

II. Experimental Protocol

III. Parametric Studies

IV. Demonstration Experiments

Task I. Literature Survey. To gain understanding of the mechanisms involved in mixing of jets in a cross flow, it was required to first determine the parameters that most likely affect the mixing process. To do so, the following approach was employed: First, a literature survey was conducted with specific reference to mixing of jets in a cross flow. The survey also included the industrial RQL research conducted in the early 80's. Secondly, discussions were held with experts in the field of jet mixing with the objective to apply the knowledge gained from previous research to specific requirements of the HSR program. Discussions and literature survey, identified a list of important mixing parameters summarized in Table 3.1.

Task II. Experimental Protocol. Task II included the 1) design and construction of a test facility with preheat capability and high flow rates, 2) design of test matrices for the experimental parametric studies and demonstration tests, and 3) selection of the appropriate diagnostics and analysis procedure. A detailed discussion of above subtasks is presented in Chapter 4.

Task III. Parametric Studies. A series of parametric studies, designed as part of Task II, were conducted in Task III of the present effort. The experiments were designed to investigate the influence of the first order mixing parameters, identified in Task I, on mixing characteristics of jets in an axis-symmetric configuration.

First Order Mixing Parameters
• Jet to mainstream momentum-flux ratio, J
• Orifice Geometry and Spacing
Second Order Mixing Parameters
• Jet to mainstream mass ratio
• Jet to mainstream density ratio
• Reference velocity
• Reaction

Table 3.1: Important Mixing Parameters

Task IV. Demonstration Experiments. Following the parametric phase, a number of demonstration studies were performed to determine the influence of the second order parameters on mixing, for selected geometry and flow conditions. Flow visualization and time series measurements were also conducted for a number of configurations. Details of the parametric and demonstration experiments are presented in Chapter 4.

CHAPTER 4

EXPERIMENT

4.1 Experimental Facility

As part of the present effort, an atmospheric test facility (TS-5), was designed and constructed at the UCI Combustion Laboratory to conduct the quick mix experiments. The facility was designed to provide high air flow rates as well as preheat capabilities.

A schematic of the flow control is provided in Figure 4.1. House air, filtered and regulated, branches into two isolated main and jet circuits. The jet circuit incorporates four independently metered flow legs. Each leg is designed to provide flow rates as high as 150 SCFM. The main circuit consists of a coarse and a fine leg which provide a total of 150 SCFM for the mainstream flow. Each leg is regulated independently to eliminate the effects of pressure fluctuations caused by other experiments in the laboratory. All circuits are metered by sonic venturies designed and fabricated in house, and calibrated using a Laminar Flow Element. The pressure upstream of the venturi determines the flow rate. The mainstream air may be heated to 600° F by passing through a 20 Kw air preheater (Watlow, P/N 86036-2). The outlet temperature is monitored by a type J thermocouple and controlled by a heater controller (Watlow, series 800). At present, the test facility does not have the capability to preheat the jet flow.

The flow panel incorporates a separate seeding circuit designed to seed either the jet flow or the mainstream flow, or both, for laser anemometry and flow visualization purposes. Two aluminum fluidized bed seeders, designed and fabricated in house, disperse the 5-micron, alumina particles used to illuminate the flow field.

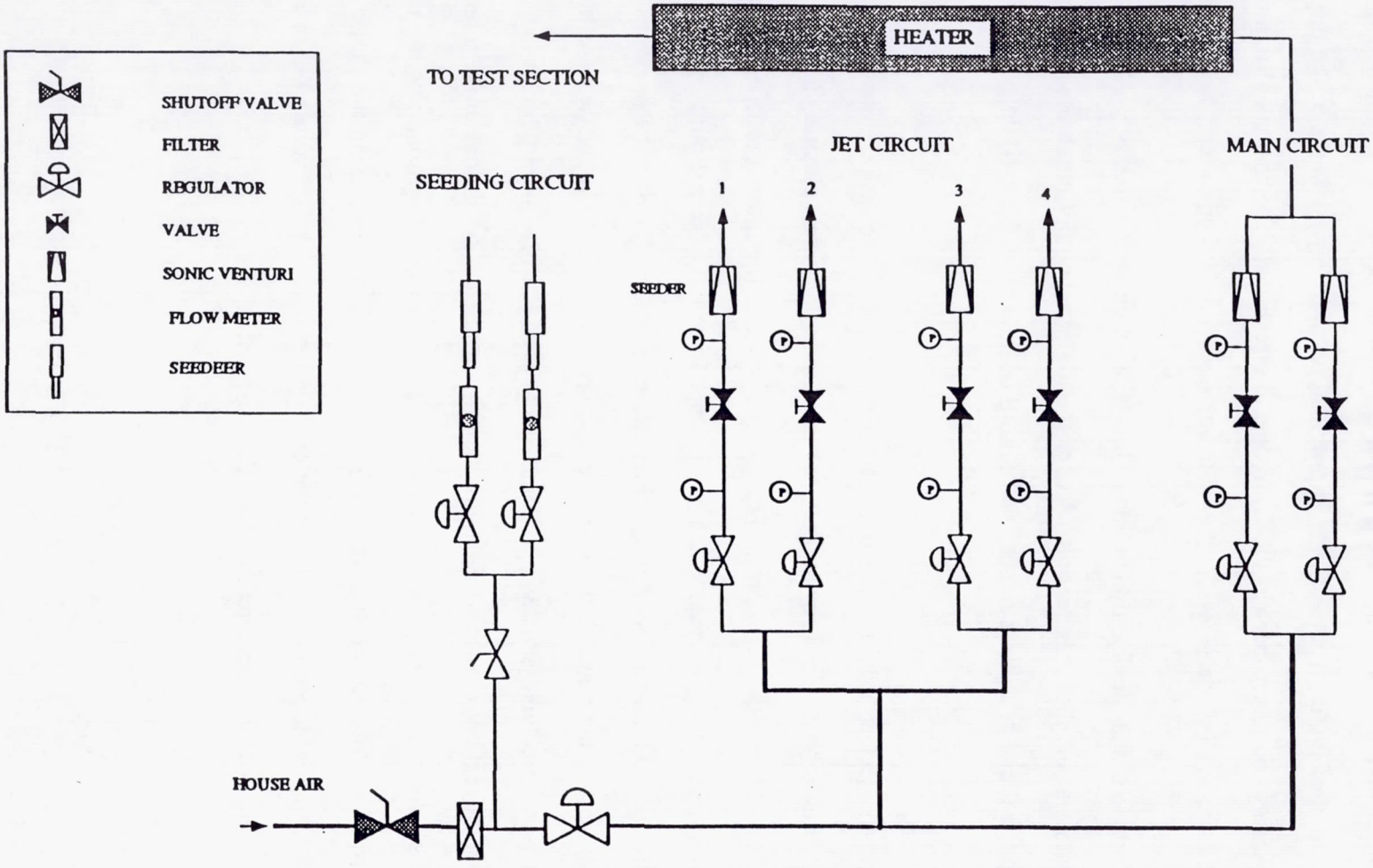

Figure 4.1: Schematic of Test Stand 5 Flow Panel

Figure 4.2 shows a schematic of the QMM test facility. The mainstream air, metered and heated, is passed through a 2-inch insulated carbon steel pipe to the vertically mounted test bed. A five-ft long section of 2-inch flexible tubing is provided immediately upstream of the test setup to facilitate traversing the experiment in the X, Y, and Z directions. The test stand is traversed manually, and a Mitutoya (Model PM-33l) digital traverse readout is used to read the coordinates.

The transition from a 2-inch flexible tubing line to a 4-inch, thick wall stainless steel pipe occurs 23 inches upstream of the quick mix section. A combination honeycomb/screen provides uniform flow at the inlet to the quick mix module. All piping upstream of the module is insulated to minimize the heat loss.

The 3-inch quick mix section used in the parametric phase is positioned inside a concentric Pyrex manifold as shown in Figure 4.3. The manifold has a 5.5-inch (140 mm) outside diameter with a wall thickness of 0.125 inches (3.18 mm). The jet manifold incorporates four openings on top and four on the bottom, each 90^{o} apart, and placed 1 inch from the edges. Four discrete jets are supplied at right angle to the manifold through the bottom openings. Two of the openings on the top are used to measure the manifold temperature and pressure, and the other two are blocked. Each jet circuit is metered individually, and equal lengths of silicone tubing between the flow control panel and the test section are used to provide symmetric flow conditions at the inlet to the manifold. A 1-inch thick, doughnut shaped honeycomb section installed upstream of the orifices, provides uniform flow at the injection point. A fixed probe holder installed on the optical table, incorporates either the thermocouple probe or the cold wire sensor. An aluminum exhaust stack, with variable suction, is positioned directly above the experiment.

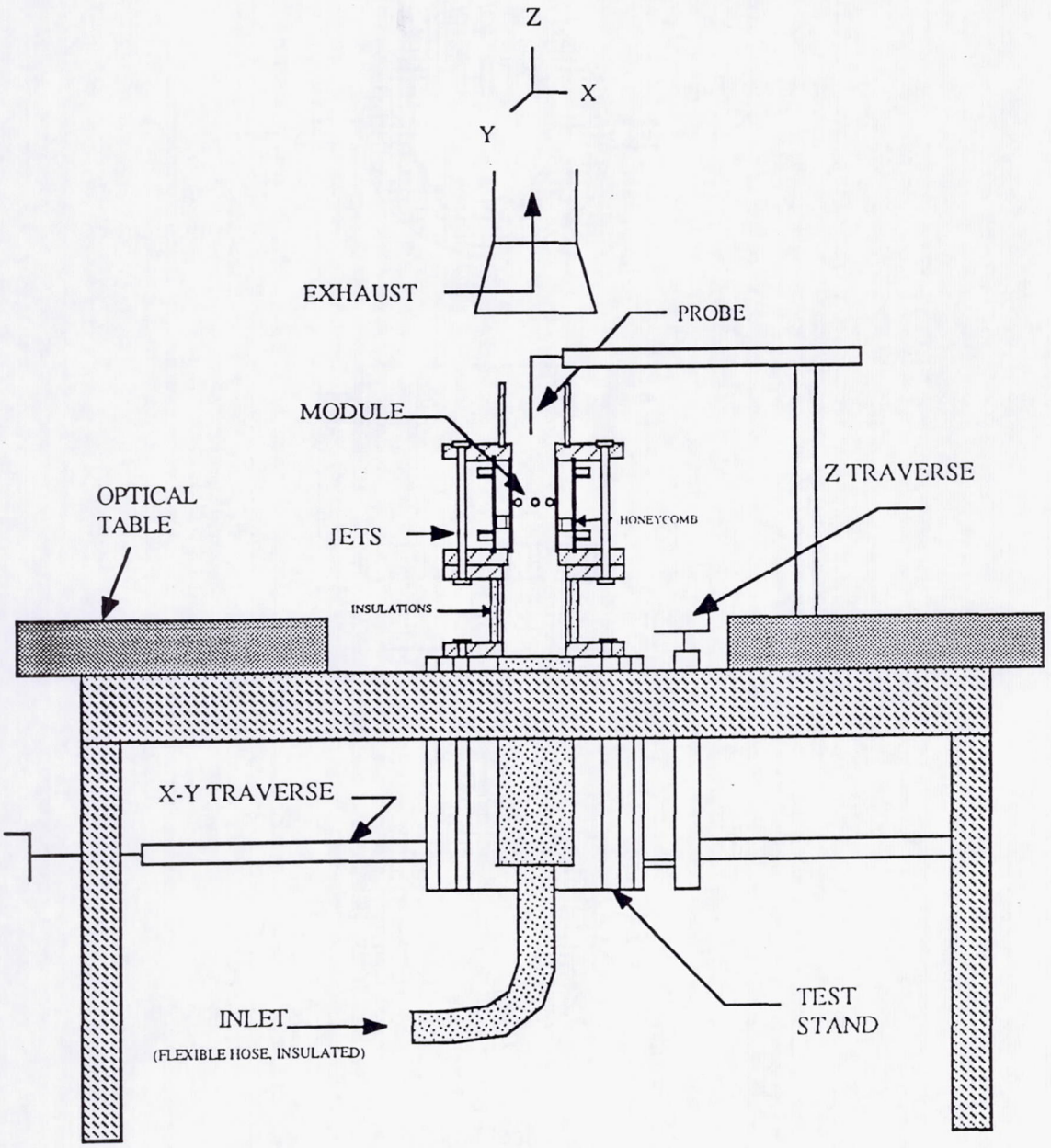

Figure 4.2 Schematic of the Test Facility

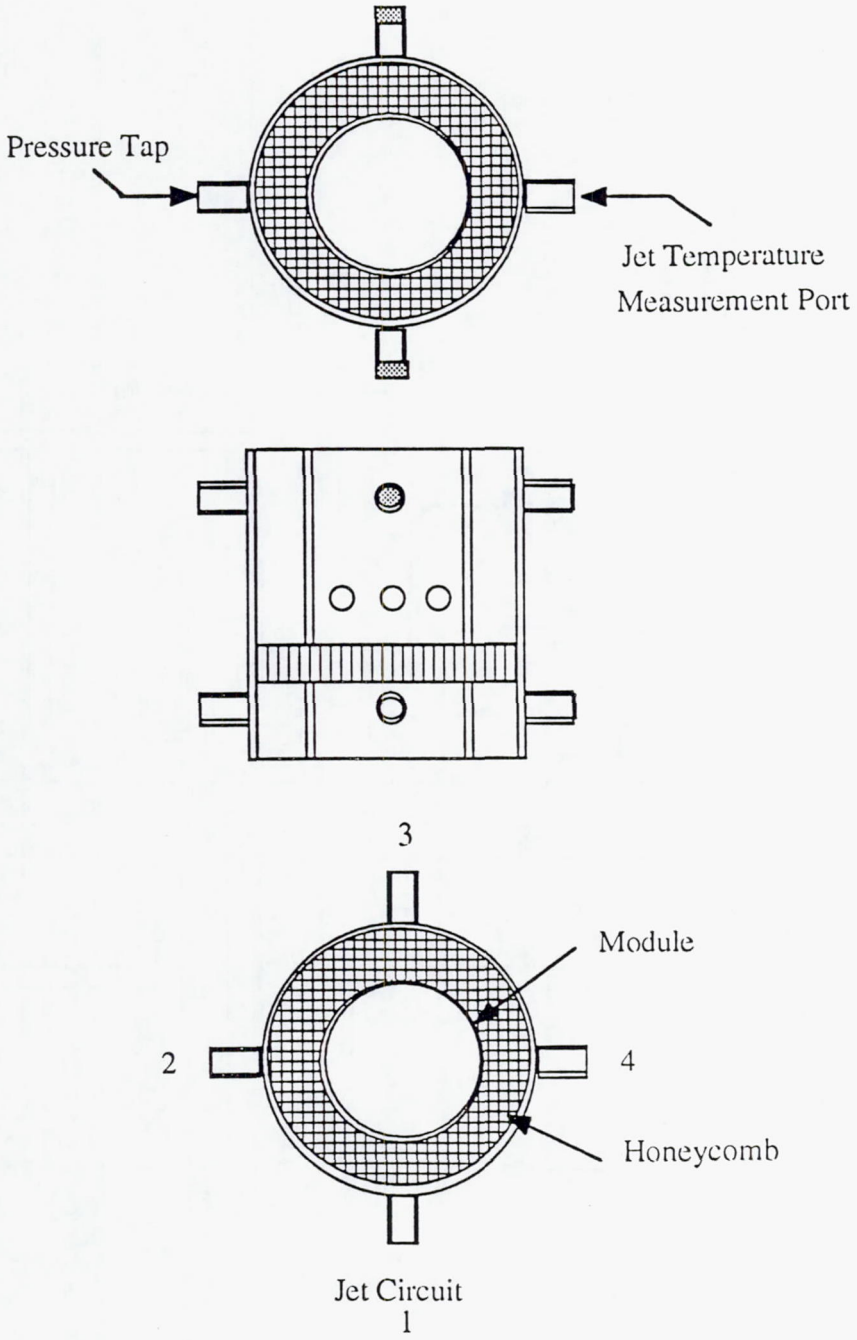

Figure 4.3: Schematic of the Test Section

4.2 Parametric Studies

The jet to mainstream momentum-flux ratio, J, and orifice geometry as the primary variables for the parametric studies. These parameters were selected based on their significant impact on mixing characteristics established by previous research.

The range of J values for these experiments was determined based on the projected HSCT cruise conditions given in Table 4.1.

ϕ, RZ	ϕ, OA	V_{ref} (ft/sec)	Inlet T (°F)	Inlet P (psia)	RZ Dia. (in)	QM Dia. (in)
1.6	0.5	40	1250	150	6	5

Table 4.1: HSCT Baseline Conditions (Tacina, 1991)

In practice, the dilution holes in a gas turbine engine are designed based on the dilution air flow and a given pressure drop. The pressure drop parameter, usually quoted as a percentage, is the ratio of the total pressure loss across the combustor to the inlet total pressure. For a conventional gas turbine combustor, pressure drop ranges between 2-4%.

For a RQL combustor operating at the HSCT cruise condition, the pressure loss parameter determines the jet to mainstream momentum-flux ratio, J. A typical pressure loss of 3% at the HSCT cruise condition corresponds to a momentum-flux ratio of 25. At this stage of the HSCT developmental effort, however, the design pressure loss value for the aircraft combustor has not yet been specified and it may or may not correspond to the conventional range of 2%-4%. In fact, to meet the HSRP goal of a ten fold reduction in NO emissions, it may be necessary to design the quick mix orifices for optimum mixing at a higher pressure drop percentage. Therefore, the parametric experiment was designed to investigate a relatively broad range of J values including 25, 52, and 80.

To vary the momentum-flux ratio at fixed jet and mainstream densities, either the orifice area or the jet to mainstream mass ratio can change. Table 4.1 shows that for the HSCT baseline condition, a jet to mainstream mass ratio of 2.2 is required to dilute the primary zone equivalence ratio of 1.6 to an overall equivalence ratio of 0.5. Therefore, for the parametric studies phase, a mass ratio of 2.2 was maintained at each tested J value. An area discharge coefficient of 0.80 was assumed in designing the orifices.

The modules tested in the parametric studies were fabricated from a 3-inch (76 mm) inside diameter, 0.125-inch (3.18 mm) thick Plexiglas tubing. Plexiglas was selected for its good optical quality, and easy and inexpensive fabrication. The disadvantage of Plexiglas material was its temperature limit of 212° F, which restricted the full use of the facility preheat capability of 600° F.

For each J value, a baseline configuration with eight, equally spaced round holes was selected. The modules designed for J of 25, included ones with eight , 4:1 aspect ratio slots oriented at 0, 22.5, and 45 degrees with respect to the mainstream flow direction. The set of modules for J of 52 also included a 4:1 aspect ratio geometry oriented at 67.5°, while the J of 80 set incorporated an additional 4:1 aspect ratio configuration oriented at 90°. Each set also included a module with eight, 8:1 aspect ratio orifice oriented at 45°. All modules are 6.5-inch (165 mm) long, with the center of the orifice row placed at one radius from the edge. The orifice area for each module at the design J value was kept constant. Schematics of the modules are provided in Figures 4.4 through 4.6.

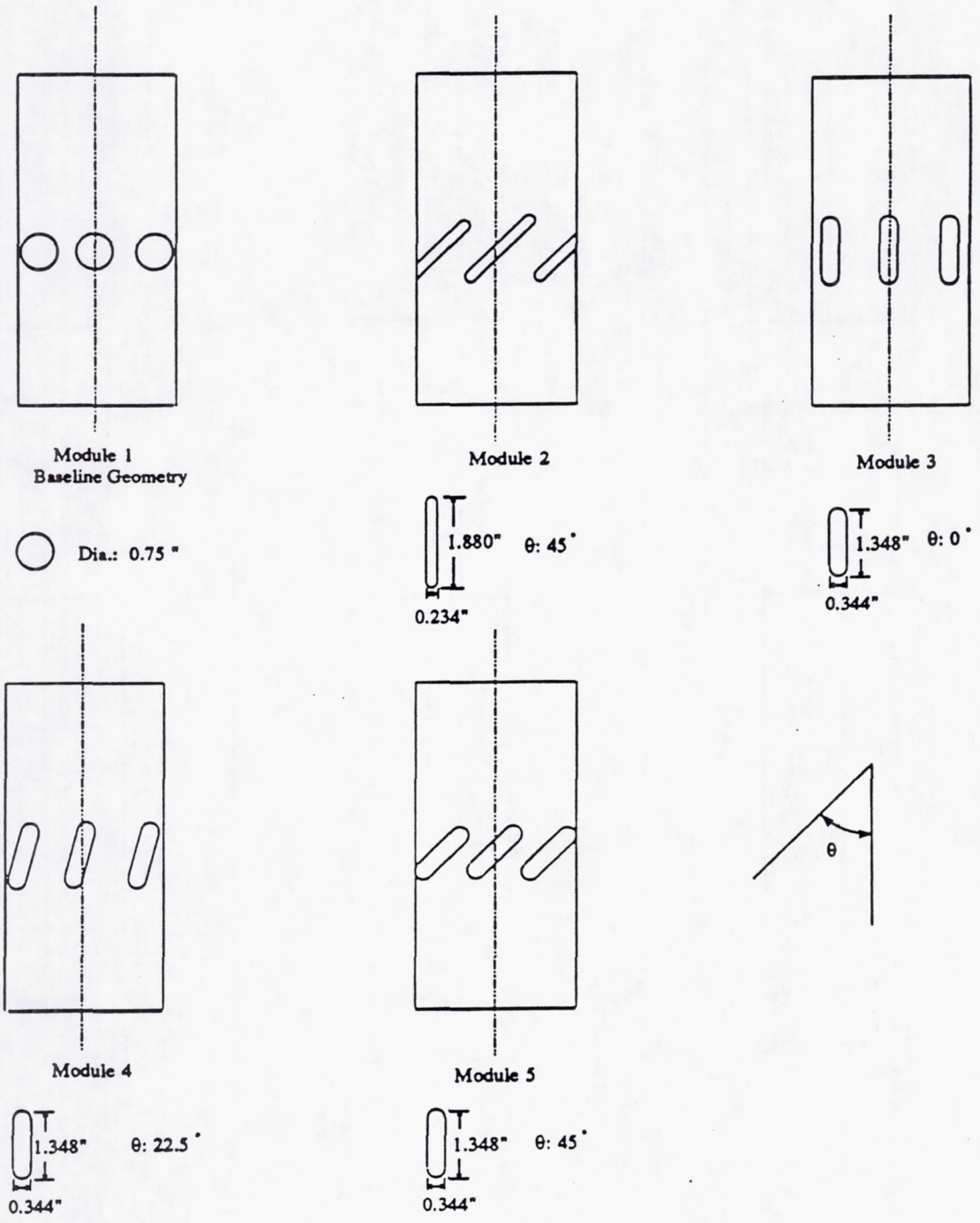

Figure 4.4: Schematic of Modules for J = 25

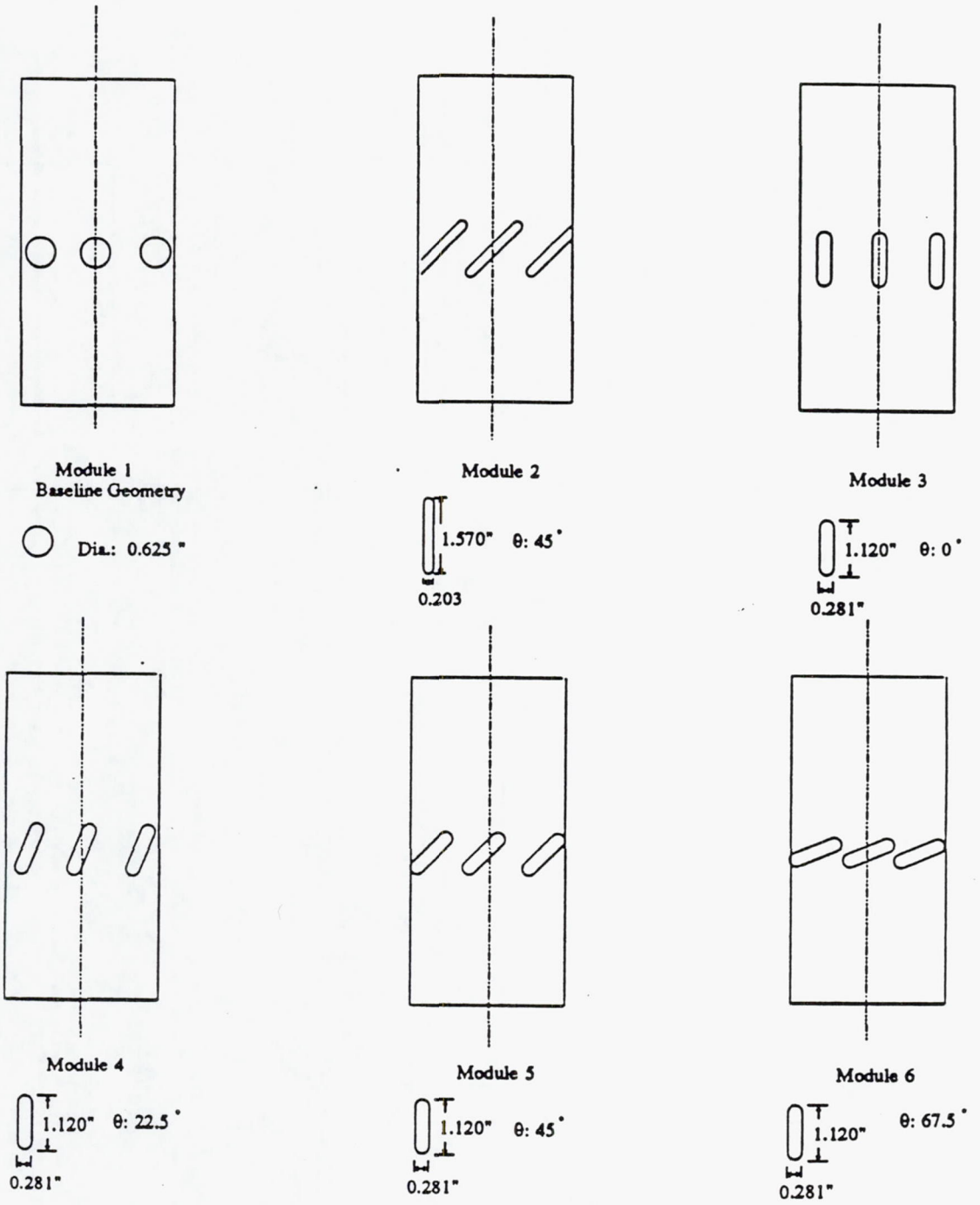

Figure 4.5: Schematic of Modules for J = 52

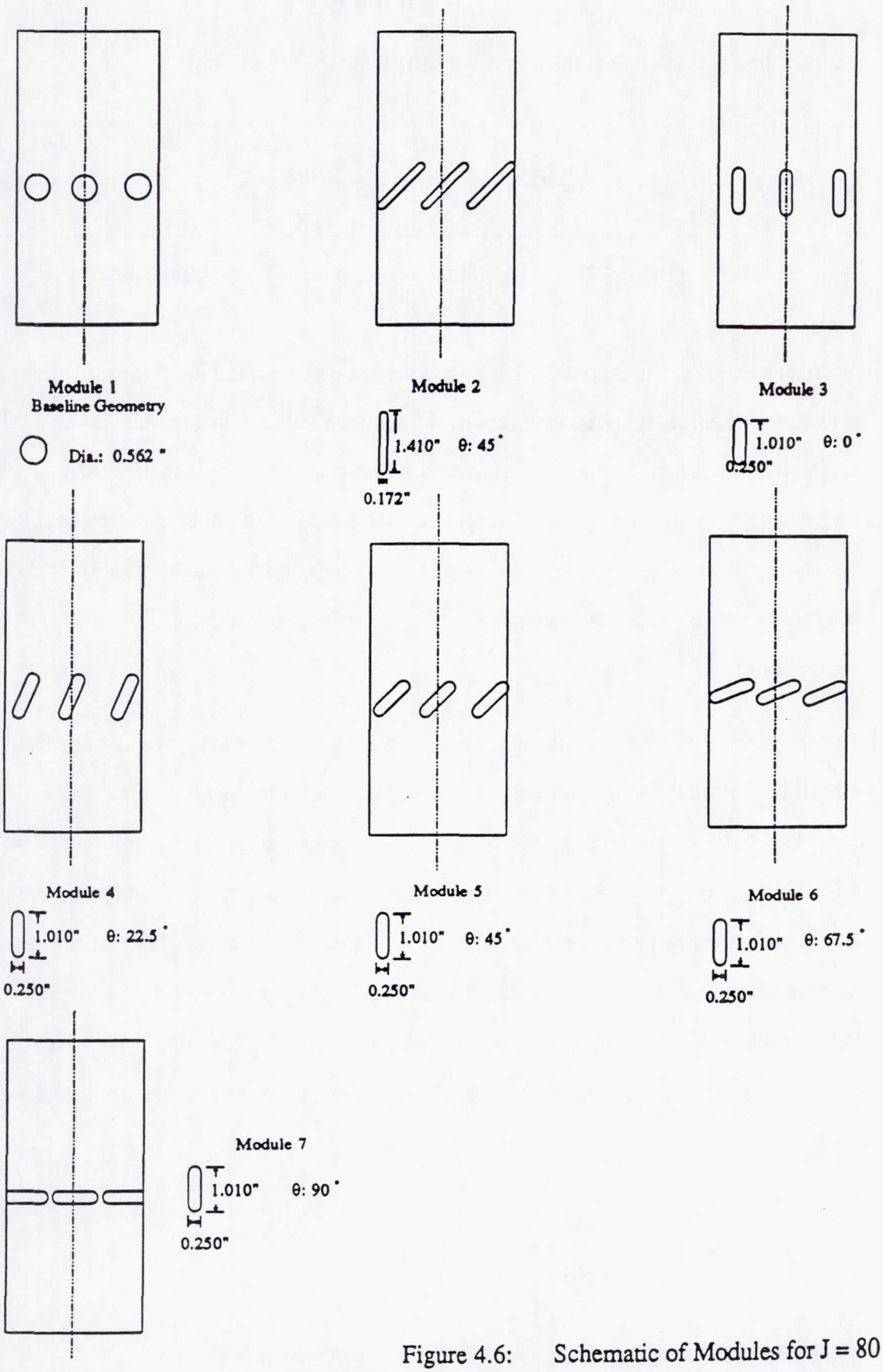

Figure 4.6: Schematic of Modules for J = 80

The operating conditions for the parametric studies are given in Table 4.2.

T_{main} (°F)	T_{jet} (°F)	P (psia)	V_{main} (fps)	M_{main} (pps)	MR	DR
212	74	14.7	34.5	.10	2.2	1.26

Table 4.2: Operating Conditions for Parametric Studies

The mainstream temperature of 212°F was determined by the Plexiglas temperature limitation. Jets were introduced at room temperature. Reference velocity was defined as the velocity at the inlet to the quick mix section, calculated based on the mainstream temperature and pressure. A reference velocity of 34.5 fps (10.5 m/s) was maintained throughout the parametric experiments. The actual value of momentum-flux ratio was determined for each case by measuring the jet manifold pressure drop. A magnehelic ΔP gage (Dwyer, Model 2050) was used to read the pressure drop.

Mixing between the heated mainstream and cold jets was examined by recording the spatial distribution of the mean temperature downstream of the leading edge of each jet orifice. Temperature was measured at 50 points in a quarter sector of the modules, in five planes throughout the mixer. A 90° sector was selected to examine the interaction of the adjacent jets and the asymmetries of the flow field. Figures 4.7a, and 4.7b show the measurement points and the axial planes. The five planes examined in this study were located between Z/R=0.08, and Z/R=1.0 where Z was measured from the leading edge of the orifices. The mainstream and jet temperatures were monitored throughout the experiment. The variations recorded were less than 2° F.

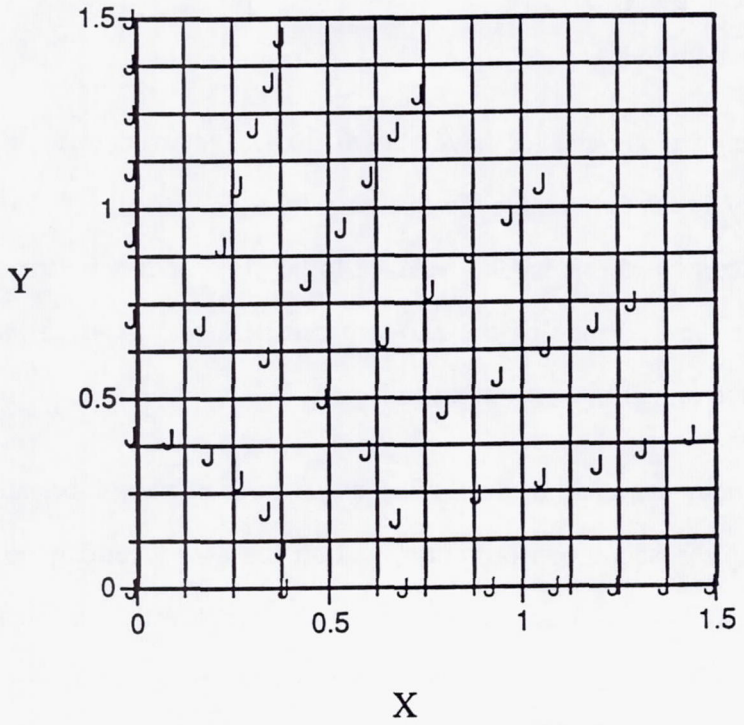

Figure 4.7a: Measurement Points

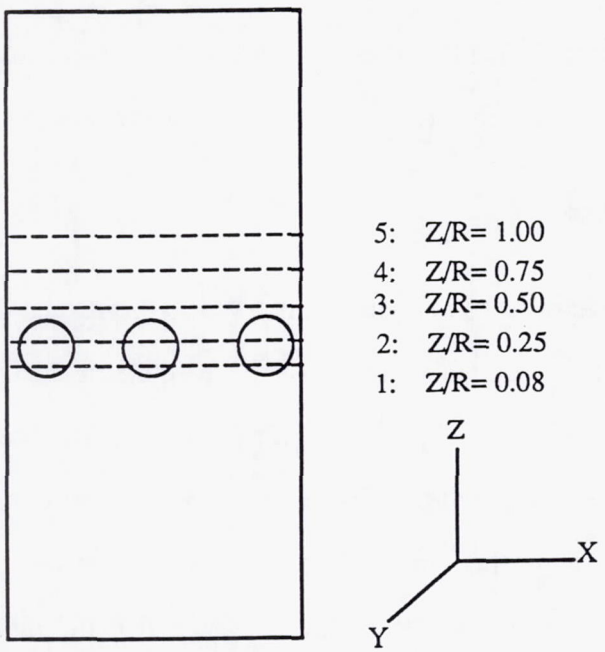

Figure 4.7b: Measurements Planes

4.3 Demonstration Experiments

Mixing studies in rectangular geometries have shown that jet to mainstream mass and density ratios have a secondary effect on mixing processes (Holdeman et al., 1987) . The effect of reference velocity on mixing patterns, is also believed to be of secondary importance (Holdeman, 1991). To demonstrate the influence of the above parameters on mixing in an axis-symmetric geometry, a number of experiments were conducted.

For the purpose of the demonstration studies, two quartz modules were fabricated. The modules incorporated an eight-hole baseline configuration, and an 8:1 aspect ratio geometry oriented at 45° as shown in Figure 4.8. A laser drilling technique was employed to fabricate the holes and slots with a tolerance of $\pm$ 0.01 inch (0.25 mm). Quartz was selected for its good optical quality and broad temperature limit required for the high temperature case. The quartz tubing used to fabricate the modules was a 3.35-inch x 3.15-inch (85 mm x 80 mm) tubing, slightly larger than the Plexiglas tubing used in the parametric phase. Therefore, the mainstream flow rate was increased to maintain the same reference velocity as used in the parametric studies. The following sections summarize the conditions for the demonstration experiments.

4.3.1 Case1: Effect of Mass Ratio

To demonstrate the influence of jet to mainstream mass ratio on mixing, the mixing characteristics of the quartz modules were compared to those of the baseline geometry (MOD1), and the 8:1 aspect ratio configuration (MOD2) designed for J of 52 (Figure 4.5). The operating conditions of the parametric studies were maintained for this experiment. Because of the smaller orifice size of the quartz modules, maintaining the same reference velocity, density ratio, and J, provided a smaller mass ratio (MR=1.5) as compared to J52MOD1, and J52MOD2 cases (MR=2.2). Table 4.3 shows the operating conditions for this experiment. The results of the mass ratio demonstration experiments (Case1) were used as the baseline for comparison to Case2 and Case3.

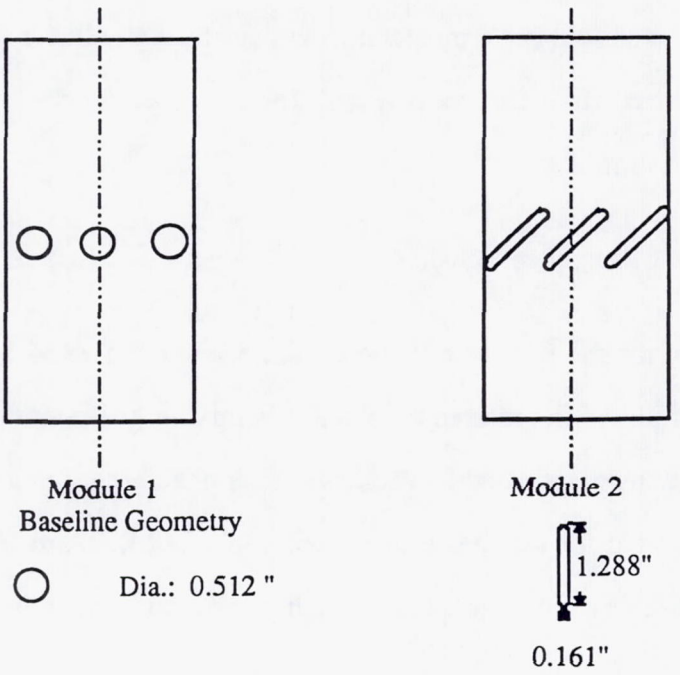

Figure 4.8: Schematic of Quartz Modules

Module	T_{main} (^oF)	T_{jet} (^oF)	P (psia)	V_{main} (fps)	M_{main} (pps)	MR	J	DR
Baseline	213	82	14.7	34.5	.11	1.4	56.5	1.2
8:1 Slot	212	74	14.7	34.4	.11	1.5	51.1	1.3

Table 4.3: Mass Ratio Demonstration Experiment

4.3.2 Case2: Effect of Density Ratio

For the parametric studies, the mainstream air was heated to 212° F due to the temperature limitation of Plexiglas material. To examine the effect of density ratio on mixing, the mainstream air was heated to 482° F (250° C). To maintain the reference velocity of 34.4 ft/s, the main mass flow rate was decreased to compensate for lower mainstream density. Because of the decrease in the main flow rate, the mass ratio was increased by 20 percent to maintain the J value. The

temperature inside the manifold (jet temperature) was substantially higher than room temperature due to the heat transferred from the mainstream. Table 4.4. shows the operating conditions for the density ratio demonstration case.

4.3.3 Case3: Effect of Reference Velocity

The reference velocity for the parametric studies was maintained at 34.5 ft/sec (10.5 m/s). To demonstrate the effect of varying reference velocity on mixing, the mainstream flow was reduced while maintaining the density ratio and J. The lower limit of reference velocity was determined by the minimum flow required for safe heater operation (48 SCFM). A mainstream flow rate of 60 SCFM was selected for this experiment. The operating conditions are presented in Table 4.5.

Module	T_{main} (°F)	T_{jet} (°F)	P (psia)	V_{main} (fps)	M_{main} (pps)	MR	J	DR
Baseline	482	93	14.7	33.7	0.08	1.7	56.7	1.7
8:1 Slot	482	92	14.7	34.4	0.08	1.7	51.3	1.7

Table 4.4: Density Ratio Demonstration Experiment

Module	T_{main} (°F)	T_{jet} (°F)	P (psia)	V_{main} (fps)	M_{main} (pps)	MR	J	DR
Baseline	212	82	14.7	23.8	0.08	1.4	56.2	1.2
8:1 Slot	212	80	14.7	23.8	0.08	1.5	54.2	1.2

Table 4.5: Reference Velocity Demonstration Experiment

4.4 Diagnostics

4.4.1 Flow Visualization

Flow visualization was used in the first stage of the parametric studies to provide a qualitative assessment of the flow field for a number of modules geometries. Laser sheet lighting was used to illuminate the test section. The laser beam from a 5-watt cw Argon-ion laser (Spectra Physics 2020-05) was passed through a cylindrical lens to form a horizontal sheet. The sheet was then collimated to illuminate the test module as shown in Figure 4.10. Alumina particles (9-micron) were used to seed the mainstream flow. A mirror, oriented at 45° was installed at the exhaust of the vertical test section to reflect the image of the flow field at the illuminated plane. The flow field was documented by obtaining photographs at each condition.

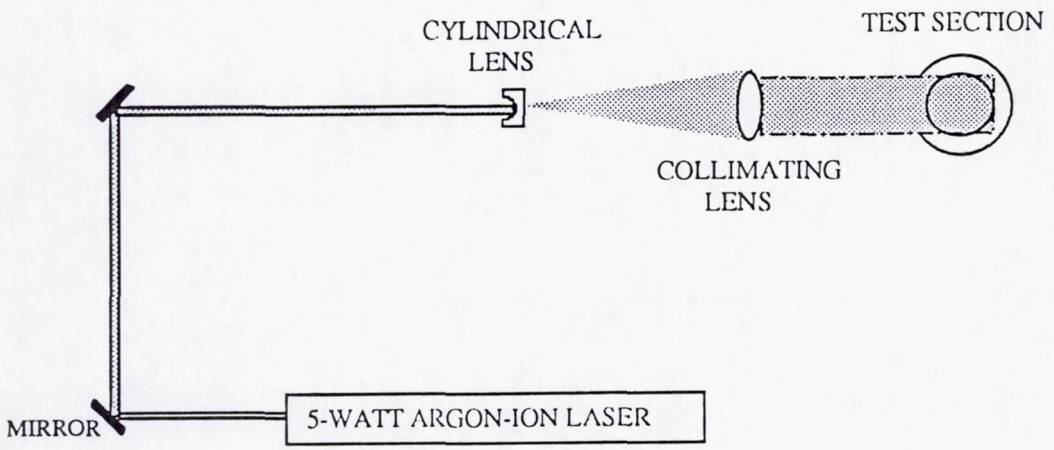

Figure 4.9 : Flow Visualization Optics

4.4.2 Time-Averaged Temperature Measurements

The main diagnostics used in the parametric and demonstration studies was the time averaged temperature measurements conducted in five planes for each module configuration. A 12-inch long, 0.125-inch type K thermocouple was used to measure the temperatures. The thermocouple was held in a fixed position while the test stand traversed in X, Y, and Z directions. The probe was positioned in the center of the modules with respect to four, 90° apart, reference points marked on each module as shown in Figure 4.10.

Temperature Distributions were recorded using a Fluke temperature readout (Model 2160A). A Beckman temperature indicator (Model 500T) was used to monitor the mainstream and jet temperatures throughout the experiment.

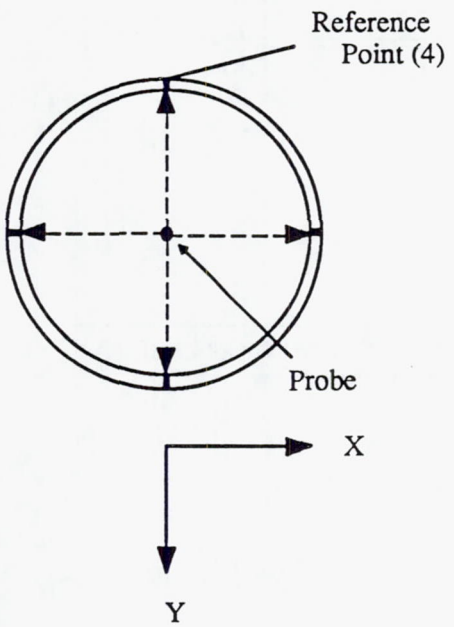

Figure 4.10: Probe Positioning

4.5 Analysis

One of the objectives of the present study was to identify a quick mix configuration that provides the most effective mixing and the lowest NO emissions level. Therefore, it was necessary to establish an analysis procedure that quantified both the mixing uniformity, and NO formation potentials of a given module based on the non-reacting temperature measurements.

4.5.1 Mixture Uniformity

To compare the mixing characteristics of different modules, the temperature measurements were normalized by defining the mixture fraction, f, at each point in the plane:

$$f = \frac{T_{measured} - T_{jet}}{T_{main} - T_{jet}}$$

A value of f=1.0 corresponds to the mainstream temperature, while f=0 indicates the presence of the pure jet flow. Perfect mixing is achieved when f is at the equilibrium value determined by the mass ratio of the jet and main streams. Note that $f = 1 - \theta$, where θ appears in previous studies (Holdeman, 1991).

To quantify the mixing effectiveness of each module configuration, an area-weighted standard deviation parameter was used. This parameter was defined as Mixture Uniformity at each Z/R plane:

$$\text{Mixture Uniformity} = \sqrt{\frac{1}{A}\sum_{i=1}^{n} a_i (f_i - f_{equil})^2}$$

Where: $A = \sum(a_i)$, f_i is the mixture fraction calculated for each node, and f_{equil} is the equilibrium mixture fraction, defined as:

$$f_{equil} = \frac{T_{equil} - T_{jet}}{T_{main} - T_{jet}} = \frac{1}{MR+1}$$

Perfect mixing is achieved when the mixture uniformity parameter is zero.

4.5.2 Emissions Formation Potential

To examine the low emissions potential of the quick mix modules based on the results of the non-reacting studies, a computational code was developed at the UCI Combustion Lab. The code analyzes the mixture uniformity and emissions characteristics of each module using the following procedure:

- Mean temperature measurements in each plane, jet and mainstream mass ratio and temperatures, and the bulk flow residence time between planes Z/R=0.0, and Z/R=1.0 are provided as inputs to the program.

- The code superimposes the experimentally measured mixture fraction, f, onto a rectangular grid by interpolating the measured temperatures in each plane. Like the experiment, the computation is performed in a quarter sector plane only.

- The program then, interpolates the mixture fraction results to create 100 equally spaced planes between Z/R= 0.0 and Z/R=1.0. Since the first measured values are at Z/R = 0.08, values reported at Z/R = 0.0 are extropolated.

- To apply the results of the non-reacting experiments to estimate the mixer performance at the projected conditions of a RQL combustor, the assumption is made that the mainstream is composed of the products of combustion at ϕ=1.6, and air jets are introduced at 1250° F.

- The mixture fraction information, and the above assumption are used to assign an equivalence ratio to every point in the computational domain.

- Based on the calculated equivalence ratio and the residence time for each plane, the code determines the gas-phase temperature, NO, and CO concentrations based on a database generated using the SENKIN kinetic code (obtained from Sandia National Laboratory).

- The code predicts the mixture fraction, mole fractions of NO and CO concentrations, NO production and CO depletion rates, gas temperature, equivalence ratio, mixture uniformity, and standard deviations of each property. The code also keeps track of the total NO produced in each planar volume.

- NO production and CO depletion rates are described in terms of mole fractions of NO produced and CO depleted between adjacent planes in the computational domain .

CHAPTER 5

RESULTS AND DISCUSSION

5.1 Flow Visualization

Flow visualization experiments were conducted to 1) qualitatively examine the effects of varying momentum-flux ratio and geometry on mixing between the jets and the mainstream, and 2) detect the possible asymmetries of the flow field. This section presents examples of the flow visualization results for an eight-hole baseline module, and a 4:1 aspect ratio, 45° slanted slot configuration. Throughout the experiments, the mainstream flow rate was maintained at 100 SCFM corresponding to a reference velocity of 31 fps (9.4 m/s) at the inlet to the quick mix section. Both the mainstream and jets were introduced at room temperature, maintaining the density ratio of one. The momentum-flux ratio, J, was varied by increasing the jet flow. Therefore, the mass ratio also varied for each case.

Figures 5.1 and 5.2 present the mixing characteristics of the baseline geometry and the 4:1 aspect ratio slanted slot module at Z/R= 0.4 measured from the leading edge of the orifices. This distance was selected to minimize the interference of the light scattered from the edges of the orifices. The mainstream flow was seeded in this case, and the jets were unseeded. Therefore, the white areas indicate the presence of the mainstream flow, while the black areas represent the jet trajectories. The momentum-flux ratio, J, for this case was 36.

A comparison of Figures 5.1, and 5.2 shows that given the same momentum-flux ratio, the jet penetration to the center is less for the 4:1 aspect ratio geometry than for the round holes. This is evident by the high concentration of seed (bright white area) at the center of the module. For the baseline module, the jets penetrate farther into the mainstream, and the flow field appears symmetric. The flow field for the 4:1 aspect ratio geometry is also reasonably symmetric with some jets penetrating slightly further than others. The lesser degree of penetration for the 4:1

aspect ratio geometry is caused by a swirling component induced by the geometry of the slots. The counter clockwise swirling motion is seen in Figure 5.2.

Figure 5.3 presents the mixing pattern for the 4:1 aspect ratio geometry at momentum-flux ratio of 64. At this J value, the high concentration seed area at the center of the module is reduced, indicating higher jet penetration to the center. The presence of apparently undiluted seeded flow at the center of this module, however, indicates that the increase in momentum-flux ratio is insufficient to provide jet penetration to the center.

The swirling component on the other hand, appears stronger and is more noticeable as compared to J of 36 case. Figure 5.4 shows a downstream location of Z/R=1.0 for the 4:1 aspect ratio geometry at J=64. At this location, the individual jets are no longer distinguishable, and the jet fluid is mixed with the mainstream flow. The lack of optimum penetration to the center is evident from this picture where a high concentration of seed is observed at the core of the module. The high seed concentration indicates the presence of mainstream flow.

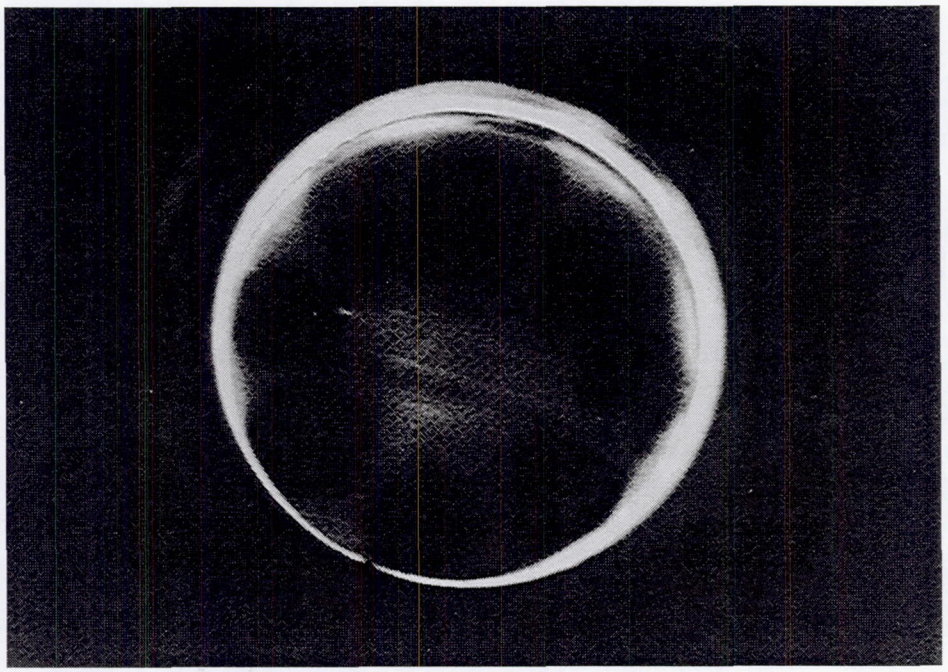

Figure 5.1 Mixing Pattern for a Baseline, 8-hole Geometry, Z/R = 0.4, J = 36

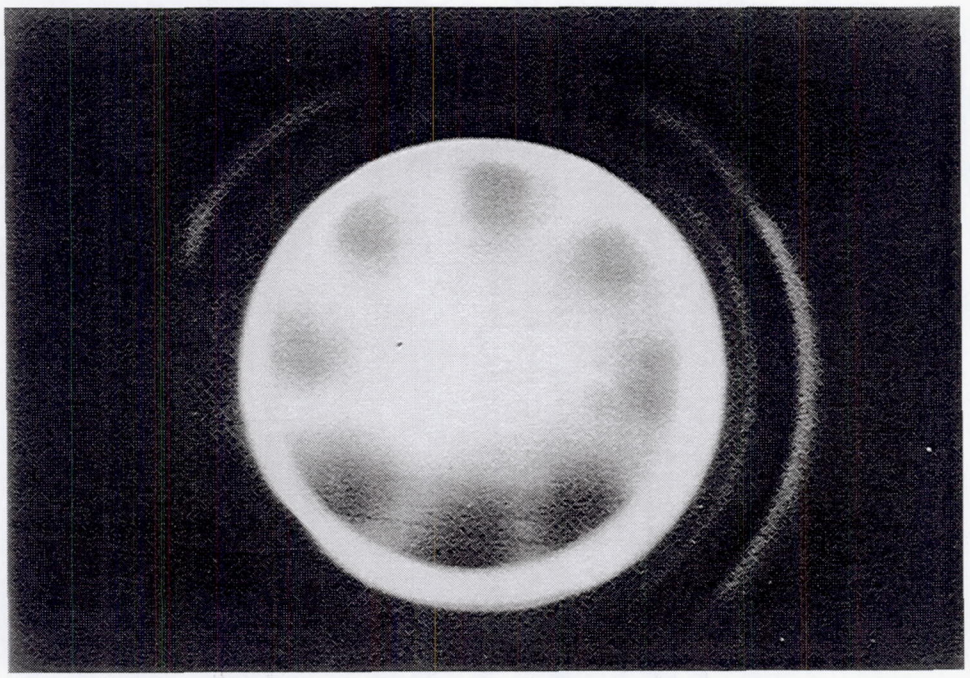

Figure 5.2 Mixing Pattern for an 4:1 Aspect Ratio Geometry, Z/R = 0.4, J = 36

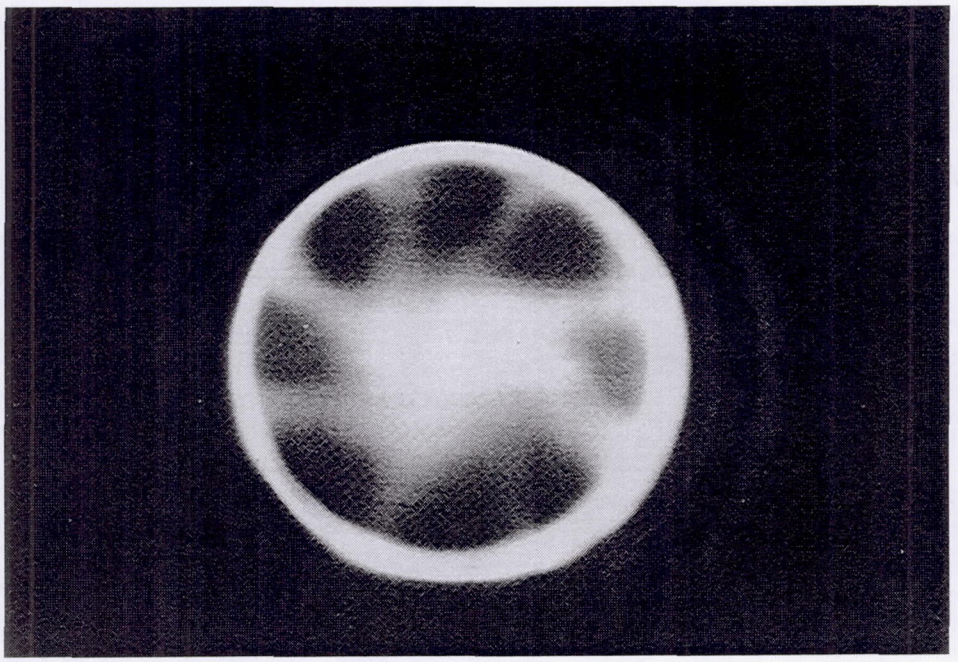

Figure 5.3 Mixing Pattern for an 4:1 Aspect ratio Geometry, Z/R = 0.4, J = 64

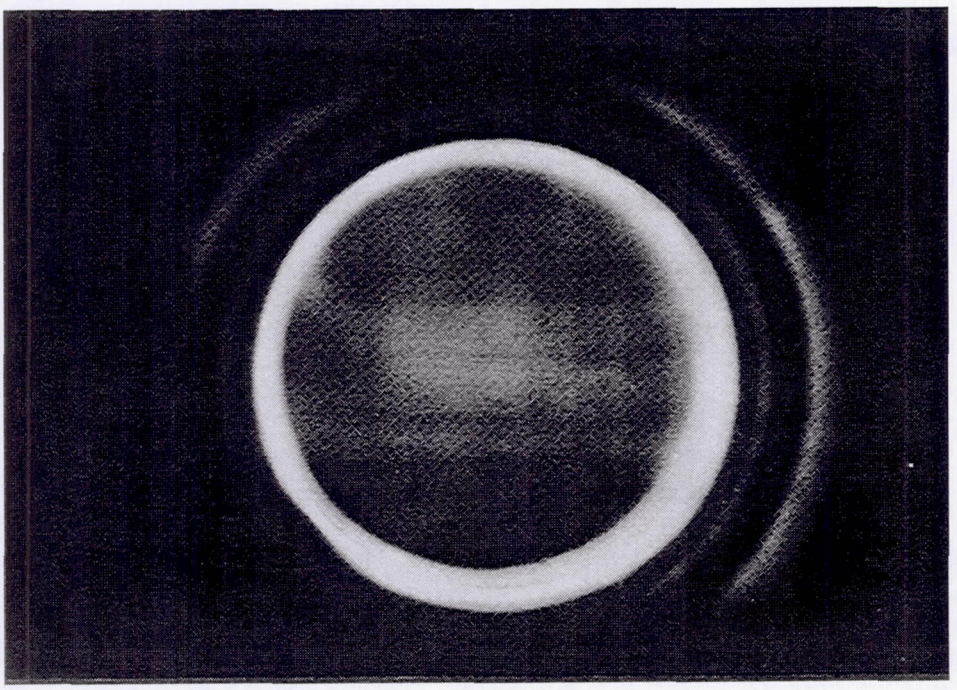

Figure 5.4 Mixing Pattern for an 4:1 Aspect Ratio Geometry, Z/R= 1.0, J = 64

5.2 Parametric Experiments

A series of parametric experiments was conducted to examine the influence of geometry and flow conditions on mixing in a cylindrical duct. 15 module geometries were tested as part of these experiments. All orifice geometries were designed to provide a jet to mainstream mass ratio of 2.2 at the design J values of 25, 52, and 80. A discharge coefficient, (C_d), of 0.8 was assumed in designing the orifices. The actual C_d, and J values for each geometry, were determined based on the measured orifice pressure drop:

$$J_{actual} = J_{design} * \left[\frac{C_d \text{ design}}{C_d \text{ actual}}\right]^2$$

Table 5.1, provides the test conditions, discharge coefficients, and the measured J value for the modules tested.

This section presents the results of the parametric studies by focusing on the "overall-mixing", and "NO-reduction" characteristics of each module tested. From an overall-mixing standpoint, an optimum mixer is defined as one that produces a uniformly mixed flow field, without a persistent unmixed core or unmixed near-wall regions, by the Z/R= 1.0 plane. From the NO-reduction standpoint, however, the best mixer is the one with the lowest NO formation potential.

Throughout this section, the following definitions are used for the terms "under-penetration", "slight penetration", and "over-penetration":

In an under-penetrated configuration, at Z/R = 0.0, the mixture fraction value (f) at the module center is near unity. According to the definition of mixture fraction, a value of f = 1 indicates the presence of pure main flow. An under-penetrated configuration is often accompanied by a persistent relatively unmixed core at the downstream axial locations.

Module	Mmain pps	Tmain F	Tjet F	Pressure psia	Amain ft^2	Vmain fps	DP " H20	DP (%)	Vjet fps	Orif. A in^2	C_d	J	DR	MR	VR
J25MOD1	0.1	212	74	14.7	0.049	34.5	5.7	1.38	158.9	0.441	0.75	26.7	1.26	2.2	4.6
J25MOD2	0.1	212	74	14.7	0.049	34.5	6	1.45	163	0.429	0.75	28.1	1.26	2.2	4.7
J25MOD4	0.1	210	76	14.7	0.049	34.5	6	1.45	163.3	0.428	0.75	28	1.25	2.2	4.7
J25MOD5	0.1	213	74	14.7	0.049	34.5	6.5	1.57	169.5	0.428	0.72	30.5	1.26	2.2	4.9
J52MOD1	0.1	212	73	14.7	0.049	34.5	12	2.86	228.6	0.307	0.74	55.4	1.26	2.2	6.6
J52MOD2	0.1	212	74	14.7	0.049	34.5	11	2.63	219.3	0.31	0.77	50.9	1.26	2.2	6.4
J52MOD3	0.1	214	74	14.7	0.049	34.5	11	2.63	219.3	0.313	0.76	51.1	1.26	2.2	6.4
J52MOD4	0.1	212	74	14.7	0.049	34.5	11.5	2.75	224.1	0.313	0.75	53.2	1.26	2.2	6.5
J52MOD5	0.1	212	74	14.7	0.049	34.5	12.5	2.98	233.4	0.313	0.71	57.7	1.26	2.2	6.8
J52MOD6	0.1	212	74	14.7	0.049	34.5	13	3.09	237.9	0.313	0.7	59.9	1.26	2.2	6.9
J80MOD1	0.1	212	76	14.7	0.049	34.5	18.5	4.34	282.5	0.248	0.74	84.2	1.25	2.2	8.2
J80MOD2	0.1	212	76	14.7	0.049	34.5	19.5	4.57	289.6	0.236	0.76	88.5	1.25	2.2	8.4
J80MOD3	0.1	214	76	14.7	0.049	34.5	20.5	4.79	296.6	0.236	0.74	93.1	1.26	2.2	8.6
J80MOD5	0.1	213	77	14.7	0.049	34.5	20.5	4.79	296.9	0.239	0.73	93	1.25	2.2	8.6
J80MOD6	0.1	212	76	14.7	0.049	34.5	22	5.12	306.8	0.239	0.71	99.3	1.25	2.2	8.9

Table 5.1: Parametric Test Conditions

For a slightly penetrated configuration, the f value at the center is in the range of 0.8 - 0.90 at Z/R = 0.0. This range of mixture fraction value indicates slight mixing between the jet flow and the mainstream. In a slightly penetrated configuration, there is no indication of a persistent unmixed core or unmixed near-wall regions at downstream locations.

The configurations labeled as over-penetrated in this section, show a central mixture fraction of less than 0.80. An over-penetrated case, however, is better identified by the presence of unmixed near-wall regions developed at downstream locations. An over-penetrated configuration is expected to be accompanied by back flow at the Z/R = 0.0 location upstream of the orifices.

The discussions are presented in the following order:

1. Mixing and emission potential of the baseline modules are examined.

2. Mixing and emissions potential of the 8:1 aspect ratio slanted slots are discussed.

3. Mixing and emissions potential of the 4:1 aspect ratio slanted slots are described.

4. The overall-mixing, and NO formation potential of the baseline geometries are compared to those of the 4:1 and 8:1 aspect ratio slanted slots.

5. The impact of jet to mainstream momentum-flux ratio on mixing is summarized.

6. The effects of slot angle and aspect ratio on mixing are examined.

5.2.1 Baseline Geometry (MOD1)

Three baseline geometries, one for each design J value, were tested as part of the parametric experiments. The baseline configurations incorporate one row of eight, equally spaced, round holes. Figures 5.5 through 5.7 present the mixture fraction variations between planes Z/R=0.0 to Z/R=1.0 for the baseline modules J25MOD1, J52MOD1, and J80MOD1, respectively.

A comparison of the mixture fraction distribution at the first axial location of these modules, shows a decrease in f at the center, with increasing momentum-flux ratio. For J25MOD1, f is in the range of 0.8 - 0.9 at the core of the module, indicating jet penetration to the center. For J52MOD1, and J80MOD1, the mixture fraction values at the center are 0.3- 0.4, and 0.2- 0.3, respectively. These f values are at or below f_{equil}, indicating over-penetration to the center.

At the jet injection locations for J25MOD1, f decreases monotonically in the radial direction, with the highest concentration at R= 0.0, and lowest at R= 1.5. The monotonic variation of f, indicates that no back flow exists for this configuration. The radial variation of f at Z/R=0.0 for J52MOD1, and J80MOD1, on the other hand, is non-monotonic. For these modules, at the injection location, f is relatively low at R=0.0, initially increases as R is increased, and approaches zero at the jet inlet. This non-monotonic variation of f indicates back flow and over-penetration of jets for these configurations.

Over-penetration of jets is evident at the downstream locations for J52MOD1, and J80MOD1, by the high f values near the wall. At Z/R= 1.0, Both J52MOD1 and J80MOD1 show low f values at the center, and unmixed regions along the walls, while J25MOD1 shows a more uniformly mixed flow field. The degradation in mixing for J52MOD1, and J80MOD1, occurs because the increased jet penetration to the module center directs a larger portion of the jet flow to the core, thus decreasing the circumferential mixing along the walls. In an axis-symmetric can geometry, where the majority of the mass is concentrated along the walls, good circumferential mixing is important in obtaining a well mixed flow field. Therefore, according to the definition presented

Page intentionally left blank

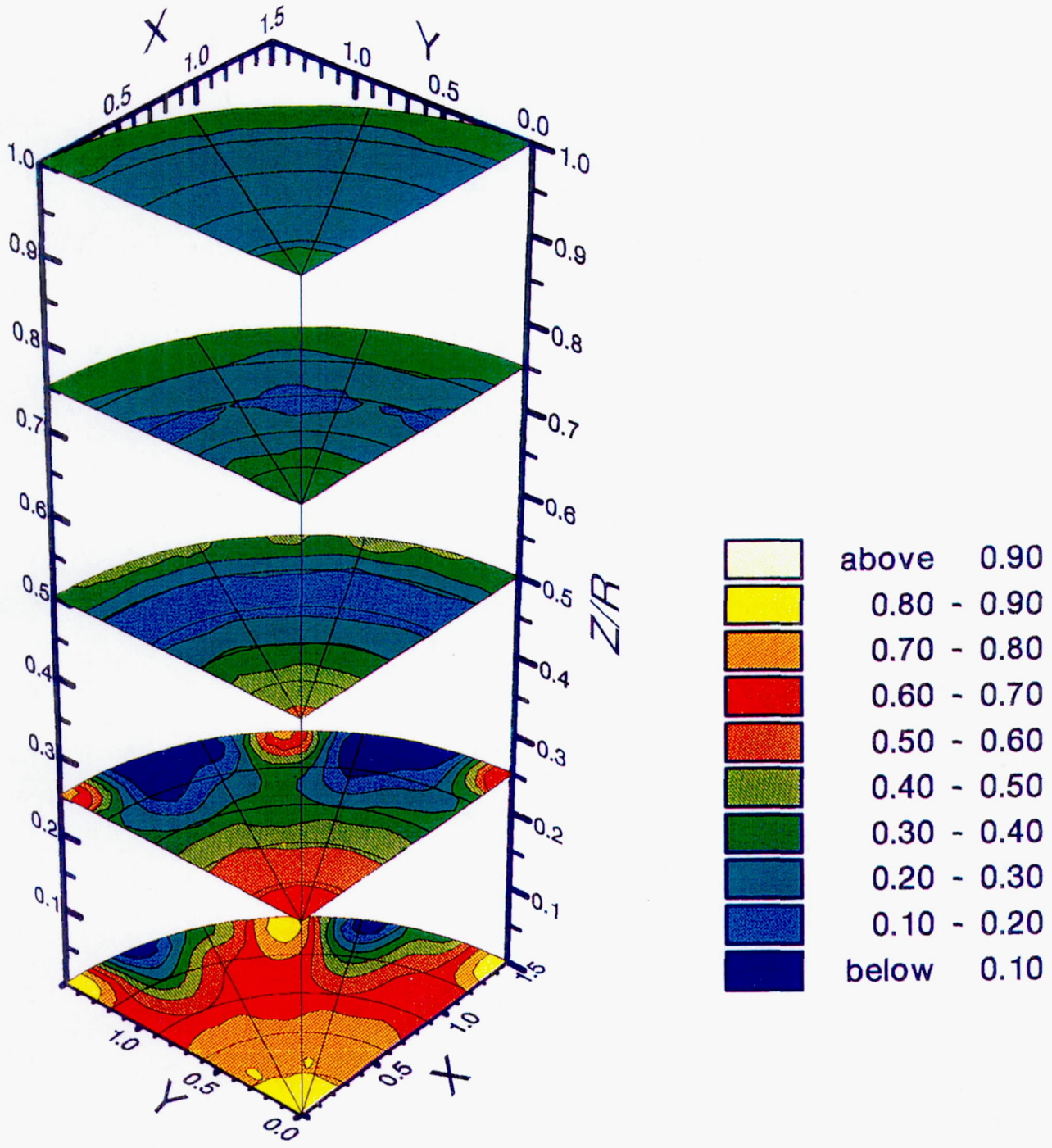

Figure 5.5: Mixture Fraction, J25MOD1, Baseline 8-hole, J = 26.7

Page intentionally left blank

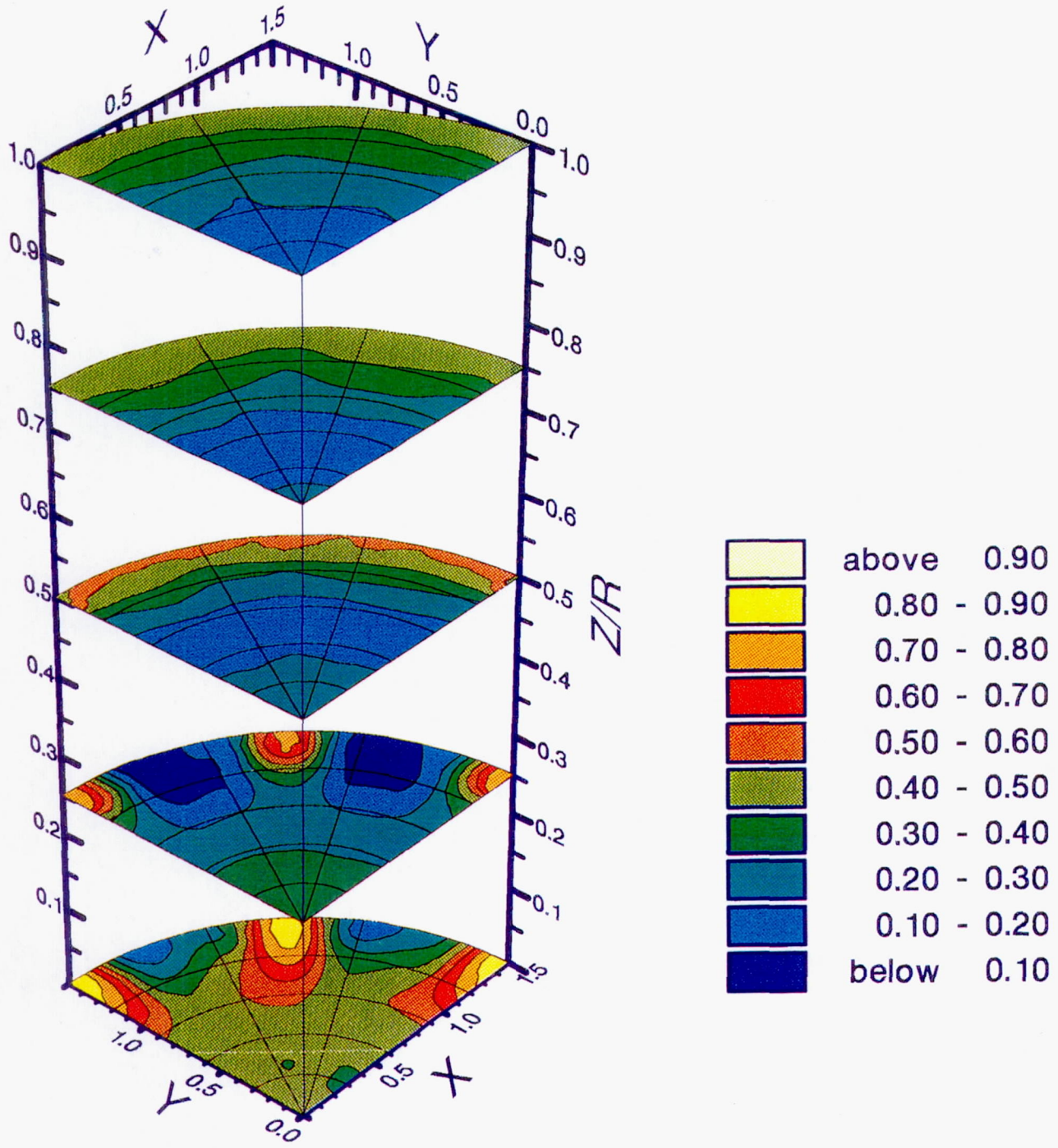

Figure 5.6: Mixture Fraction, J52MOD1, Baseline 8-hole, J = 55.4

Page intentionally left blank

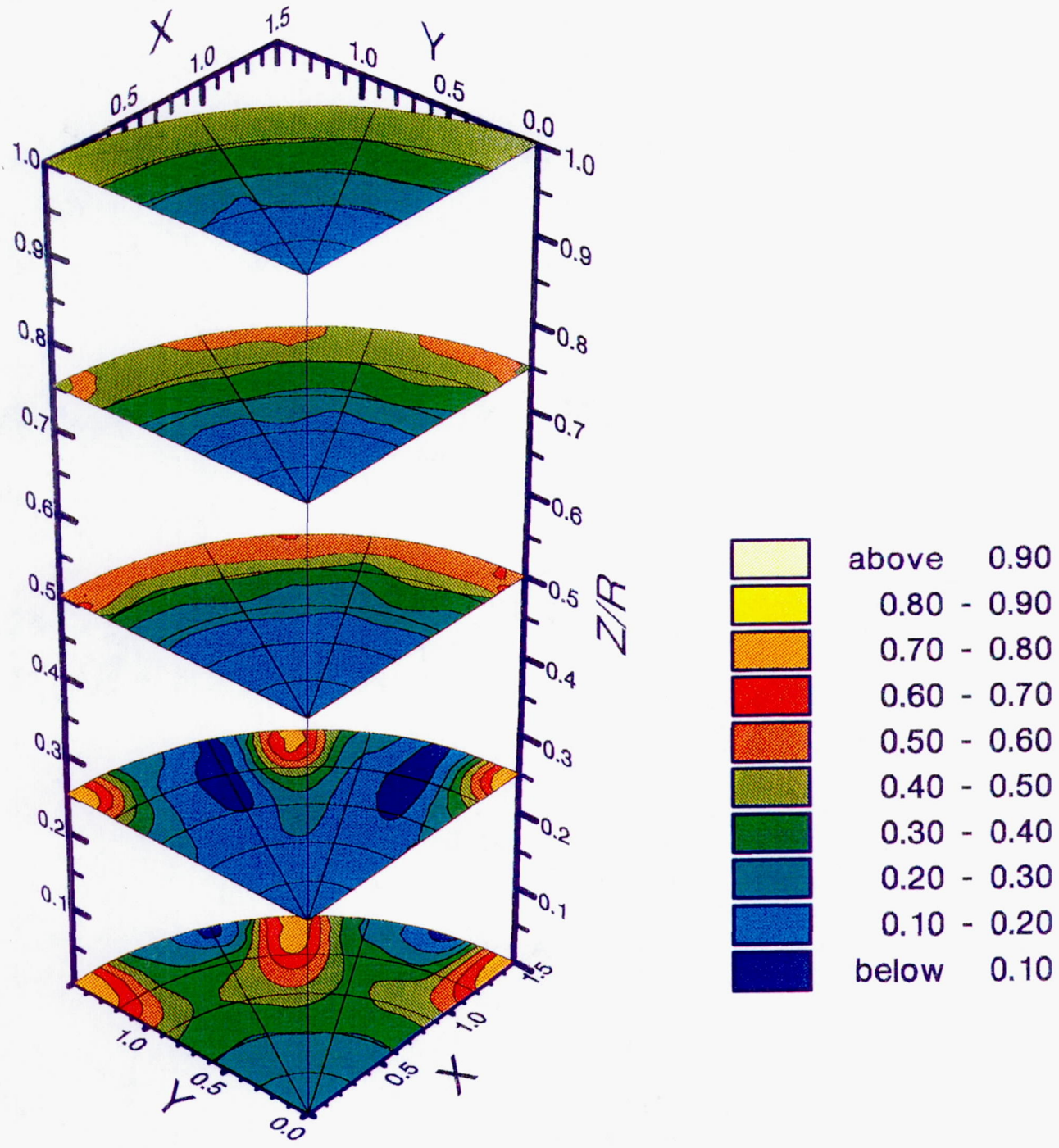

Figure 5.7: Mixture Fraction , J80MOD1, Baseline 8-hole, J = 84.2

Page intentionally left blank

earlier, J25MOD1 approaches the optimum overall mixer at Z/R =1.0, among the baseline geometries tested.

Figure 5.8 compares the mixture uniformity parameter for the baseline modules as a function of momentum-flux ratio. This plot confirms the qualitative observation that the increase in the momentum-flux ratio improves mixing at the initial planes, but degrades the overall mixing downstream of the injection plane.

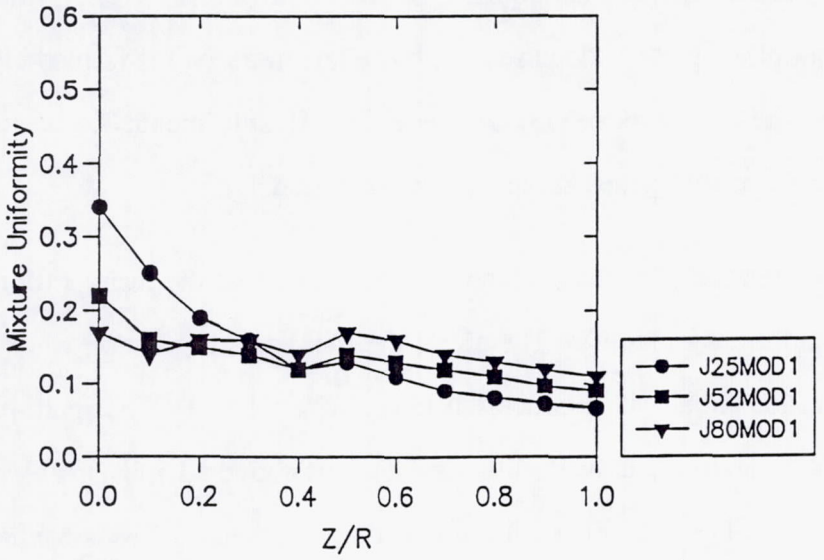

Figure 5.8: Mixture Uniformity for Baseline Modules

Figures 5.9 through 5.11 present the Equivalence Ratio and NO production potential for J25MOD1, J52MOD1, and J80MOD1, respectively. The NO Production plots show the mole fraction of NO produced between axial planes.

For J25MOD1, the majority of the NO is produced in planes below Z/R= 0.5. At the first axial location, Z/R=0.0, high concentrations of NO are produced at the shear layer formed between the jets and the mainstream, where a large near stoichiometric region is located. At Z/R= 0.25, the near stoichiometric region is concentrated at the center of the module where most of NO at this plane is formed. Further downstream relatively small amounts of NO are produced.

For J52MOD1, the near stoichiometric domain in the first axial location, is located in a relatively small region between the jets. The main portion of the flow field is at equivalence ratios below 1.0 due to the over-penetration of the jets. As expected, the highest NO produced at that axial location corresponds to the near stoichiometric region. Further downstream, NO production occurs mostly along the module walls. A similar pattern of NO production is observed for J80MOD1. In this module, the mixing in the first axial location is further enhanced due to higher jet penetration. Therefore, smaller amounts of NO are formed at the first axial location compared to previous modules. Further downstream, however, more NO is formed along the walls where mixing is poor and high temperature regions exist. This differential concentration of NO is low compared to the amount formed at the early axial stations.

The NO production plots for the baseline modules show that the main portion of NO is produced very early in the mixing process. Therefore, the mixing configuration which is most effective in the initial axial locations will produce the lowest overall NO. The multi-plane differential NO formation plots show qualitatively, that despite better overall mixing observed for J25MOD1, larger amounts of NO are produced for this module geometry. This is confirmed in Figures 5.12 and 5.13 in which the mean differential NO production, and the accumulated grams of NO produced at each plane, are compared for the baseline geometries. It can be seen that initially, the rate of NO production is highest for J25MOD1. As J is increased, the jets over-penetrate and mixing in the first axial location improves. Therefore, at the intermediate and highest J's (50.9, and 84.2) a significant reduction in the NO production rate at the initial planes is observed. It should be noted that the mixture uniformity and NO formation potentials for both J52MOD1, and J80MOD1 are similar, suggesting that once the jets over-penetrate, further over-penetration does not significantly improve the initial mixing nor reduces NO formation rate.

The accumulated NO production curves show that by Z/R= 1.0, the amount of NO produced for J25MOD1 exceeds the ones for J52MOD1, and J80MOD1 by a factor of two. The accumulated

NO graphs for the intermediate and higher J's, however, show a positive slope at Z/R = 1.0 suggesting further NO production potential beyond Z/R= 1.0. The positive slope is probably due to the on-going NO formation at the unmixed near-wall regions. It must be noted that the accumulated NO production plots do not take into account the potential NO produced upstream of the injection plane. Depending on the extent of the back flow, there may be substantial amounts of NO formed upstream of the mixing orifices for an over-penetrated configuration.

Figure 5.14 presents the mole fraction of CO as a function of axial distance for the baseline geometries. For J80 MOD1, the CO concentration at Z/R= 0.0 is lowest due to higher jet penetration and increased amount of oxygen available to oxidize CO. For all three geometries, the mechanism for CO depletion is most active at the injection plane. Beyond Z/R= 0.2, the projected CO concentration is the same for the three baseline geometries, and approaches zero by Z/R= 1.0.

Page intentionally left blank

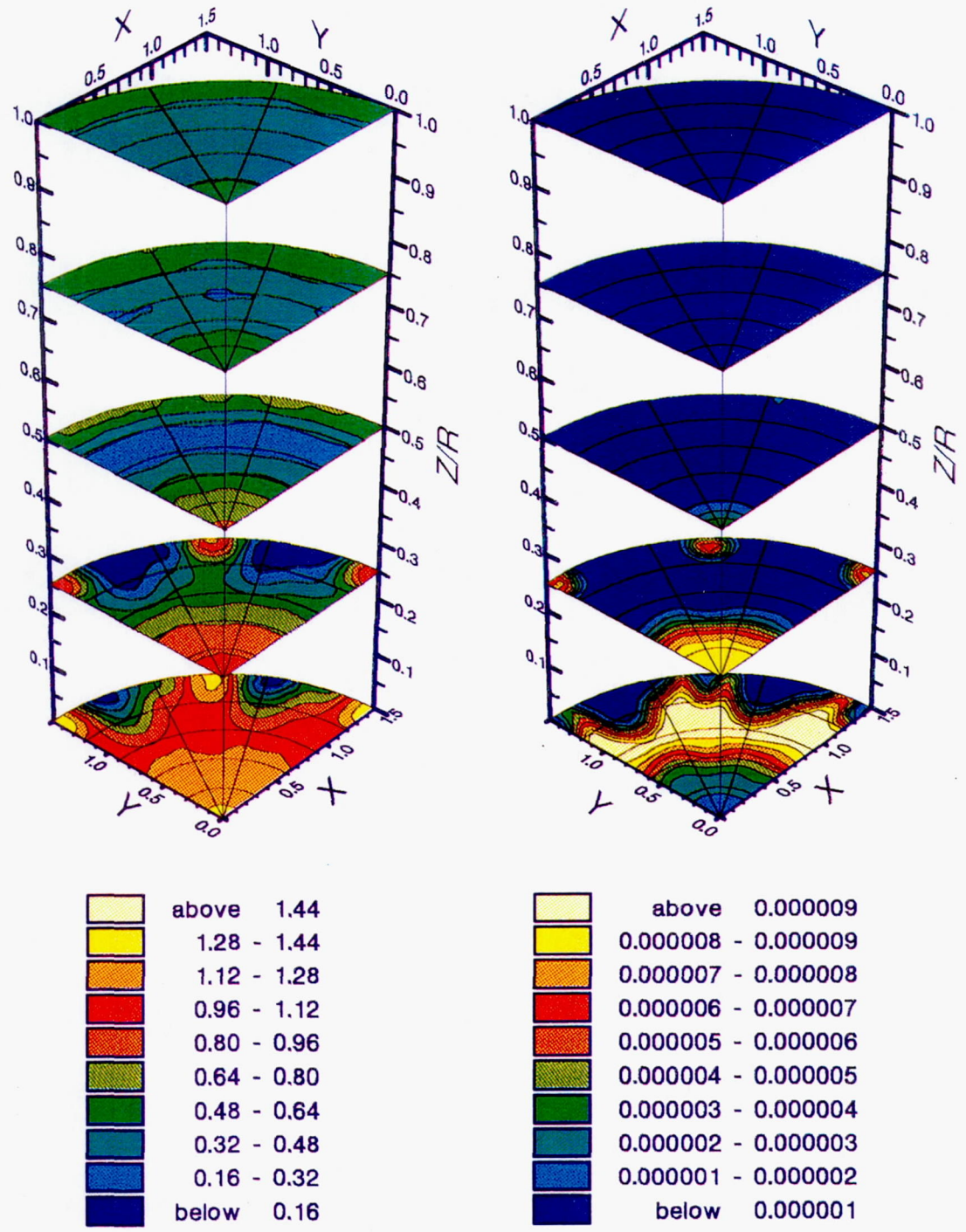

a) Equil. Ratio

b) NO Production (Mole Fraction)

Figure 5.9: Equivalence Ratio and NO Production, J25MOD1

Page intentionally left blank

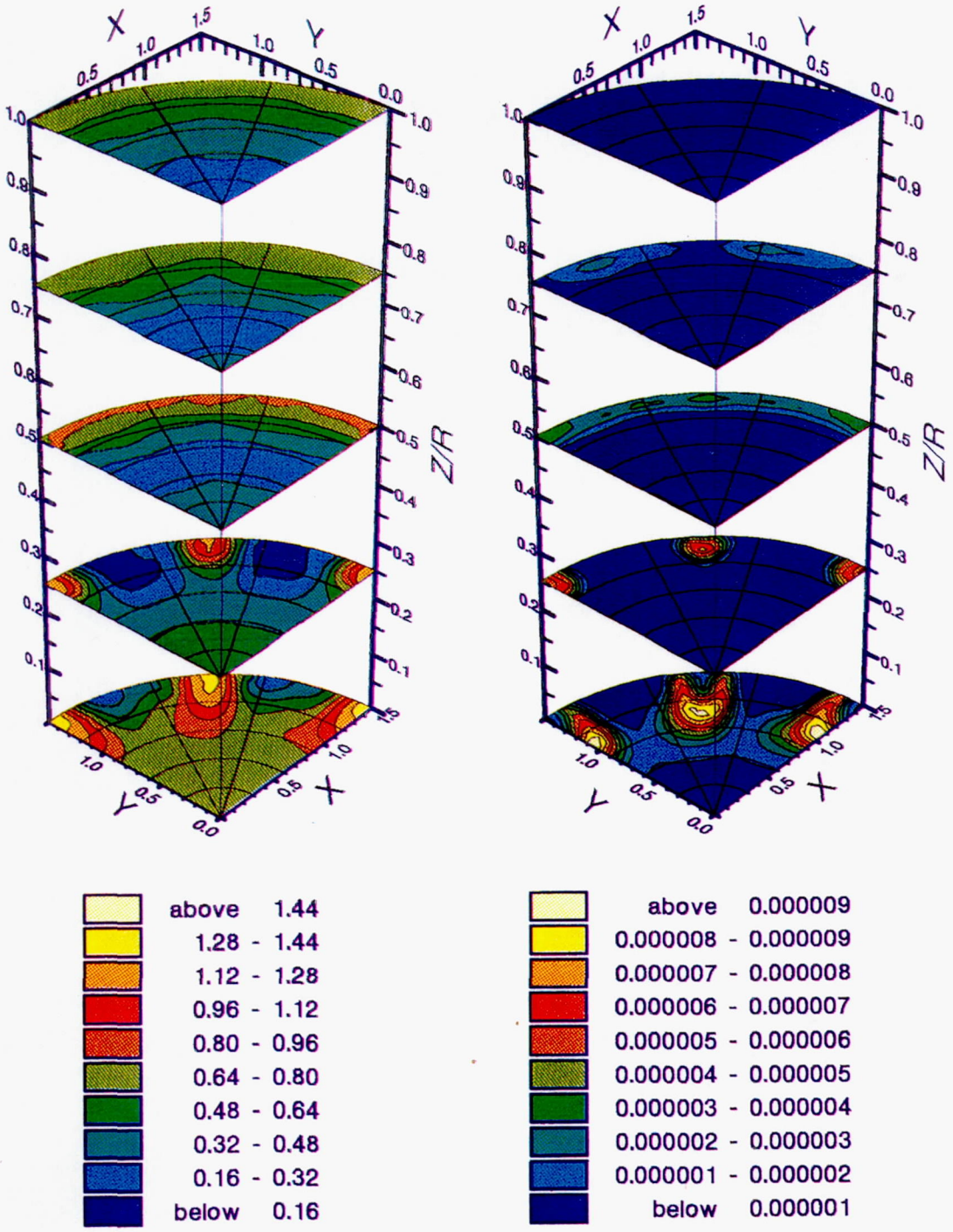

a) Equil. Ratio

b) NO Production (Mole Fraction)

Figure 5.10: Equivalence Ratio and NO Production, J52MOD1

Page intentionally left blank

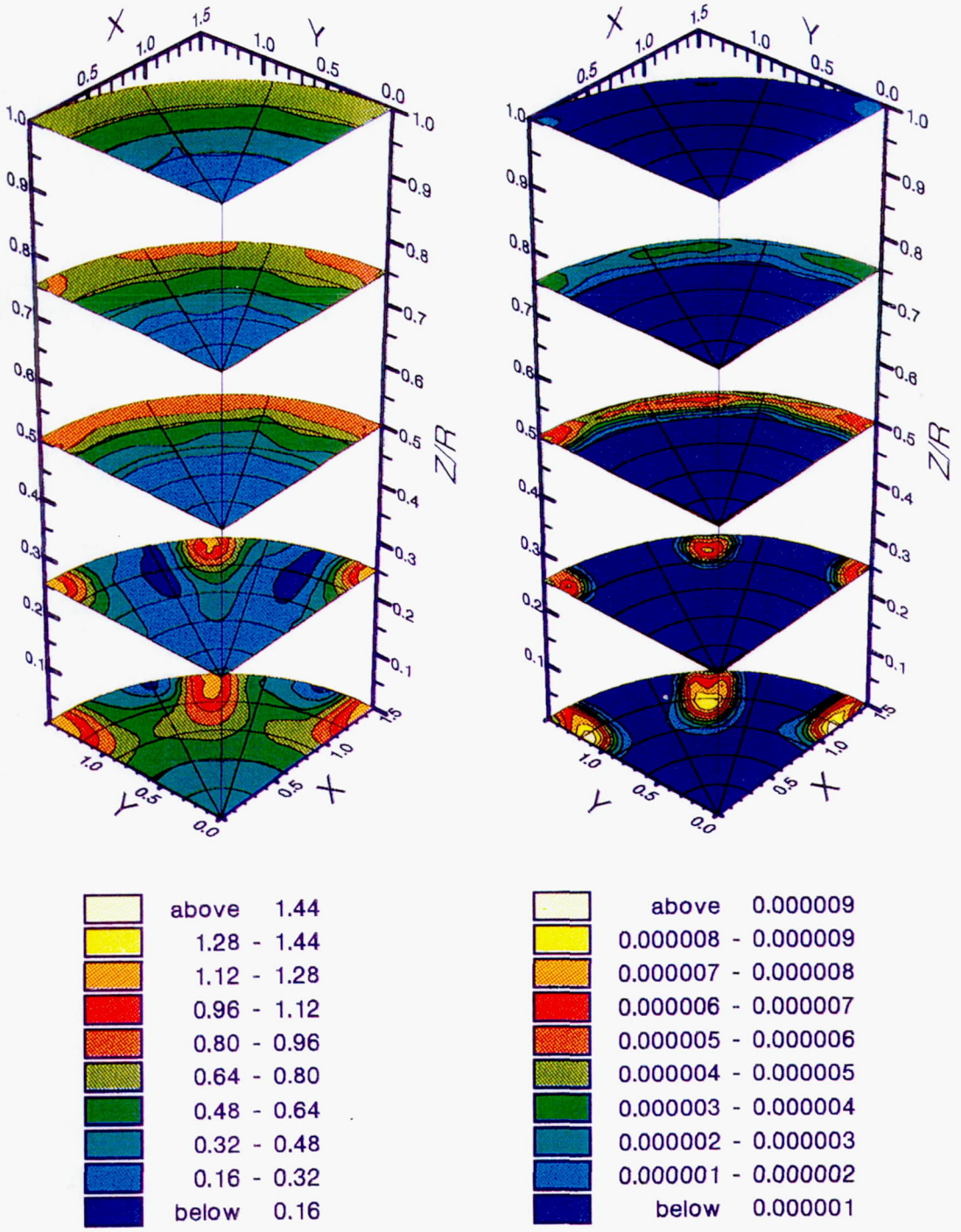

a) Equil. Ratio

b) NO Production (Mole Fraction)

Figure 5.11: Equivalence Ratio and NO Production, J80MOD1

Page intentionally left blank

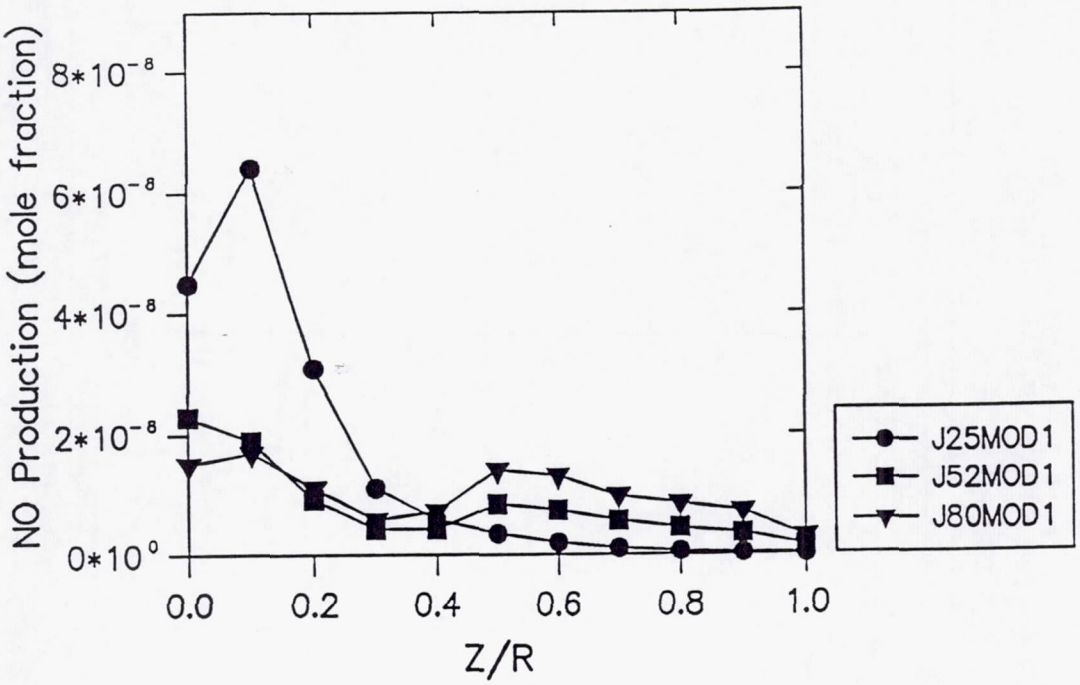

Figure 5.12 NO Production for Baseline Modules

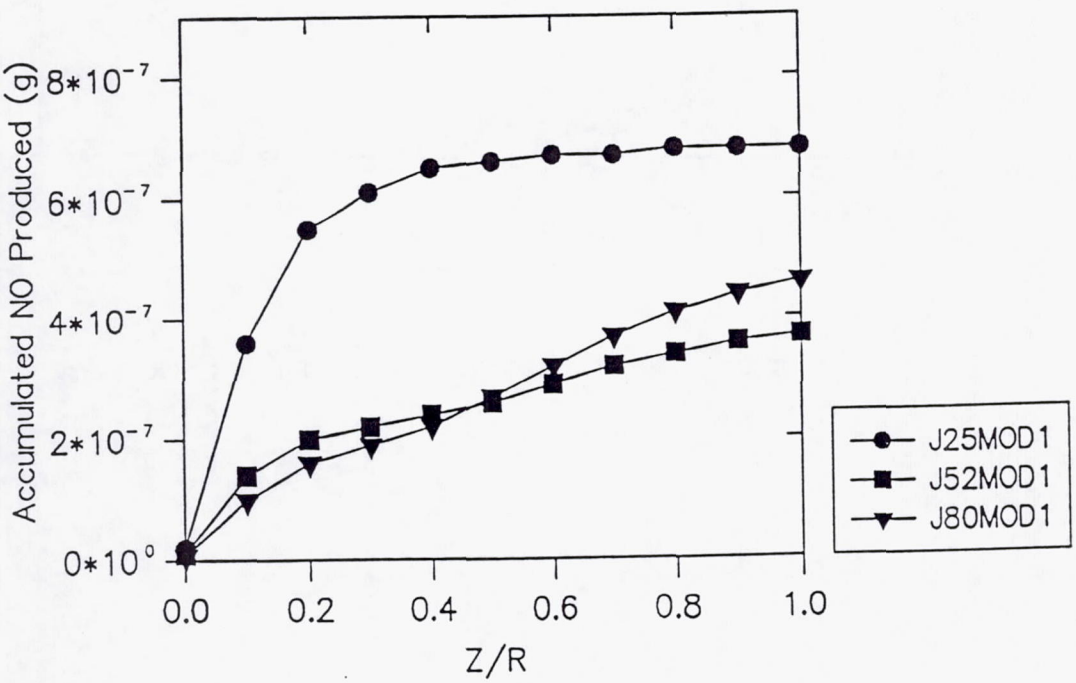

Figure 5.13 Accumulated NO Produced for Baseline Modules

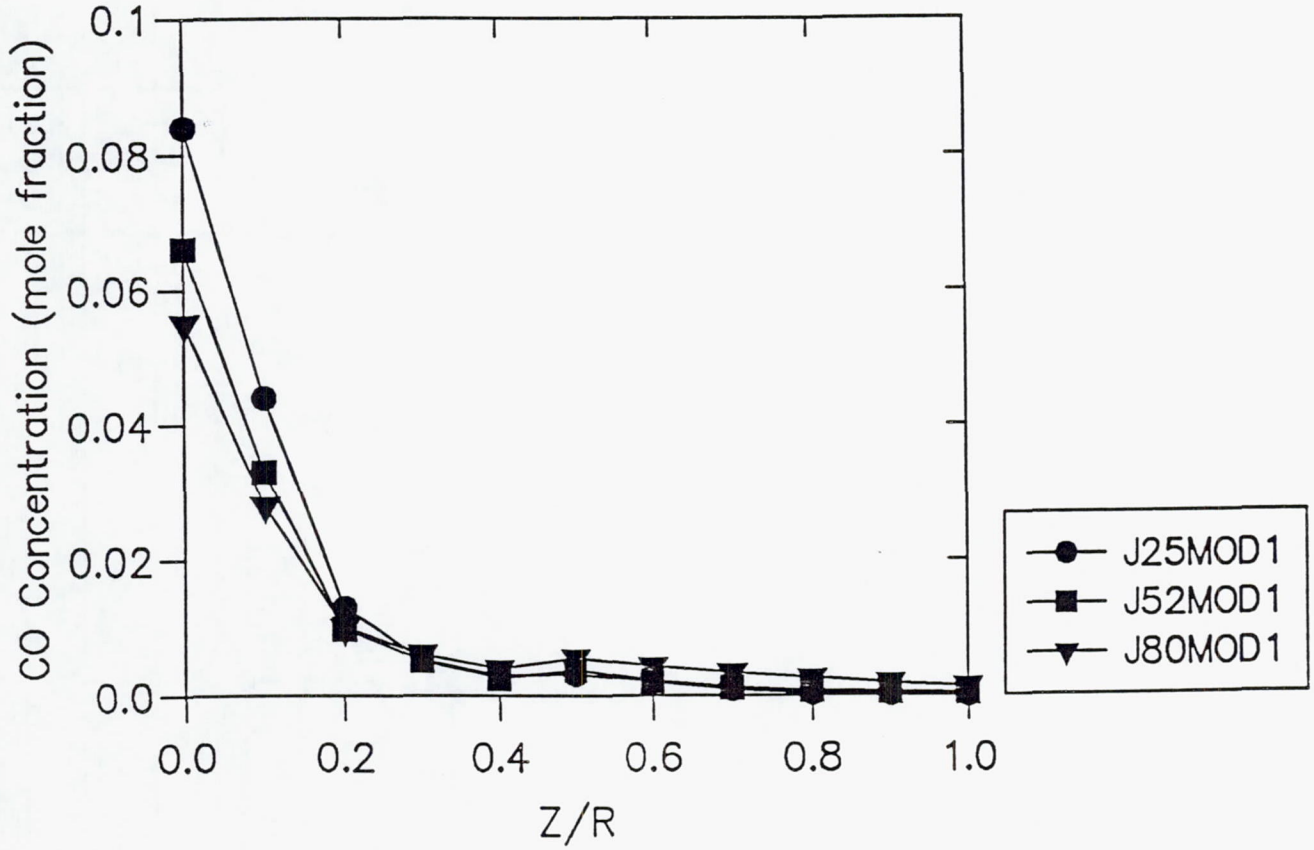

Figure 5.14: CO Concentration for the baseline Geometry

5.2.2 8:1 Aspect Ratio Geometry (MOD2)

Three 8:1 aspect ratio geometries were examined during the parametric studies. Figures 5.15 through 5.17 compare the mixture fraction distribution for these geometries.

The first axial location examined for J25MOD2, shows a large region at $f > 0.9$, indicating very small or no jet penetration to the center. For this configuration, the relatively unmixed core persists with increasing Z/R, and is present at the last axial location of Z/R=1.0. This configuration represents an under-penetrated case.

The presence of unpenetrated mainstream fluid is evident at the first axial location of J52MOD2 as well. Due to the increased jet momentum, however, the unpenetrated region is smaller compared to J25MOD2. The relatively unmixed core, similar in size and strength to that of J25MOD2, is observed in downstream locations, indicating that the increase in momentum-flux ratio has not significantly altered the overall mixing.

The first indication of jet penetration to the center, is observed at Z/R=0.0 plane of J80MOD2. The mixture fraction value at the core of this plane ranges between 0.8 - 0.9 suggesting that a portion of jet fluid is mixed with the mainstream. At the Z/R =1.0 plane, the main portion of the flow is at the equilibrium value, while a slightly larger f is seen at the center. The presence of the slightly warmer core shows that this configuration is still slightly under-penetrated. Mixing characteristics of this module are similar to those of J25MOD1.

A comparison of mixing characteristics of J25MOD2, J52MOD2, and J80MOD2 shows that 1) the impact of momentum-flux ratio on jet penetration for the 8:1 aspect ratio module geometry is less noticeable as compared to the baseline configuration, 2) Both J25MOD2 and J52MOD2, show under-penetration of jets which results in a persistent unmixed core.

Page intentionally left blank

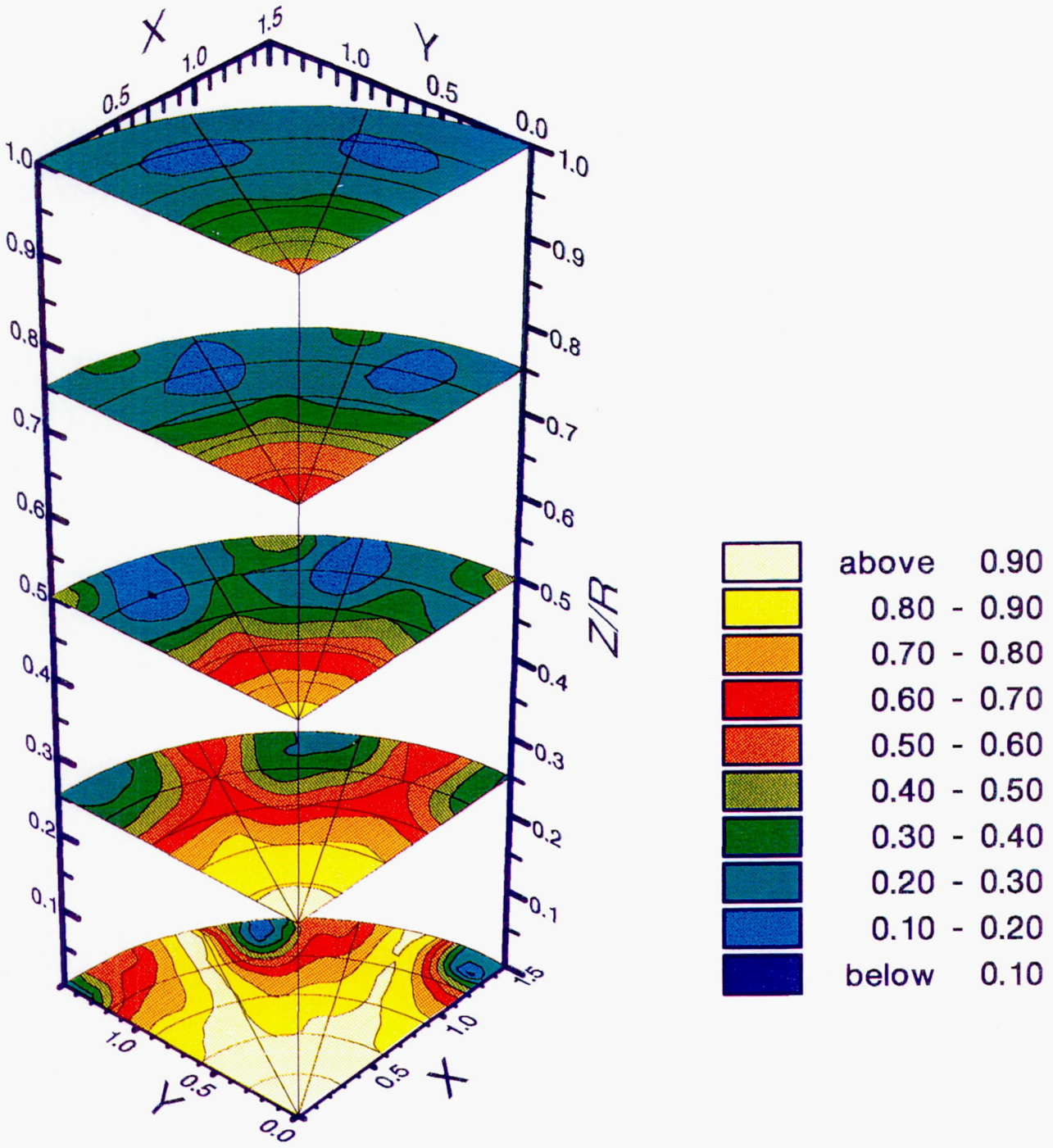

Figure 5.15: Mixture Fraction, J25MOD2, 8:1 Aspect Ratio Slanted Slots, J = 28.1

Page intentionally left blank

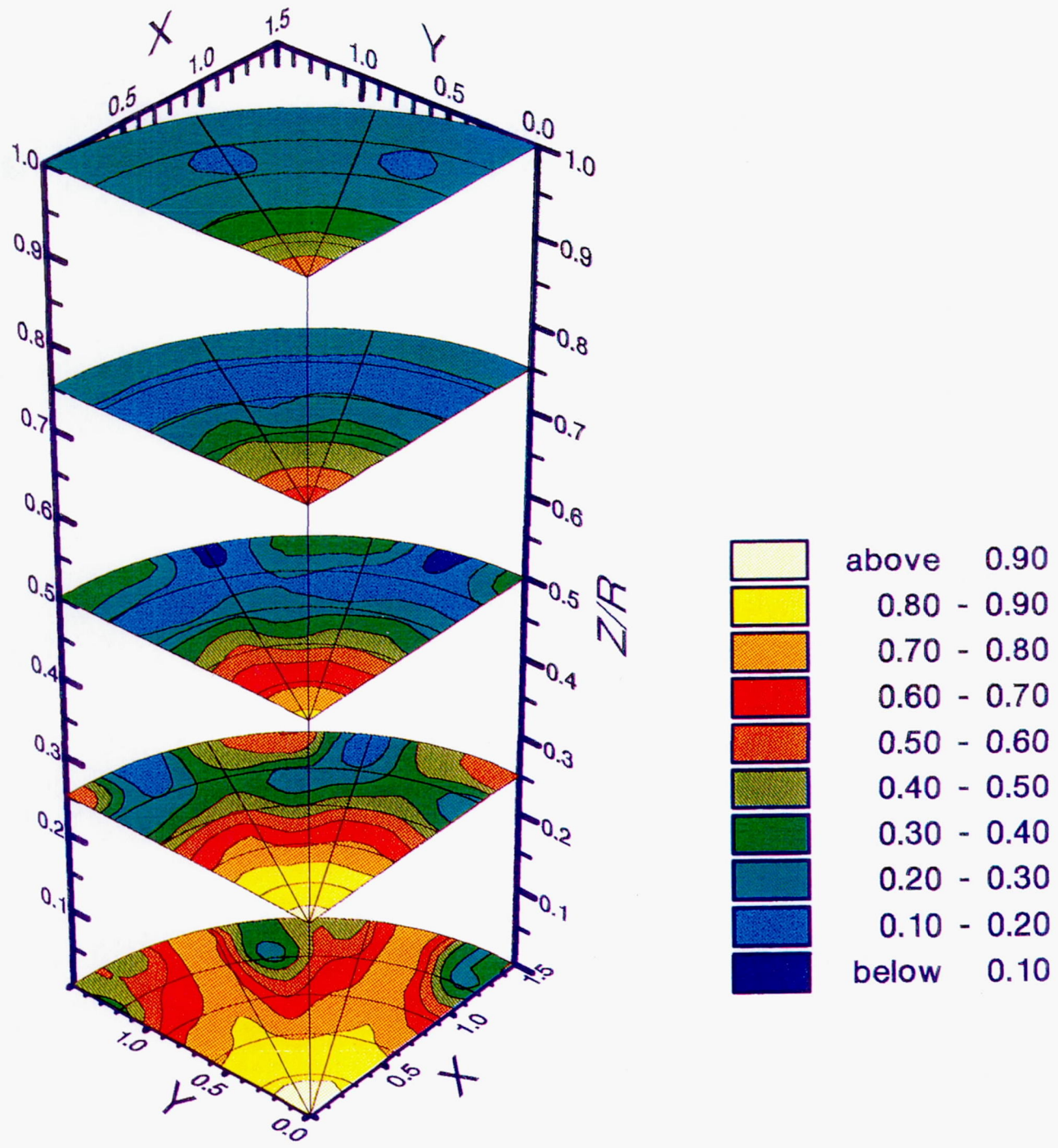

Figure 5.16: Mixture Fraction, J52MOD2, 8:1 Aspect Ratio Slanted Slots, J = 50.9

Page intentionally left blank

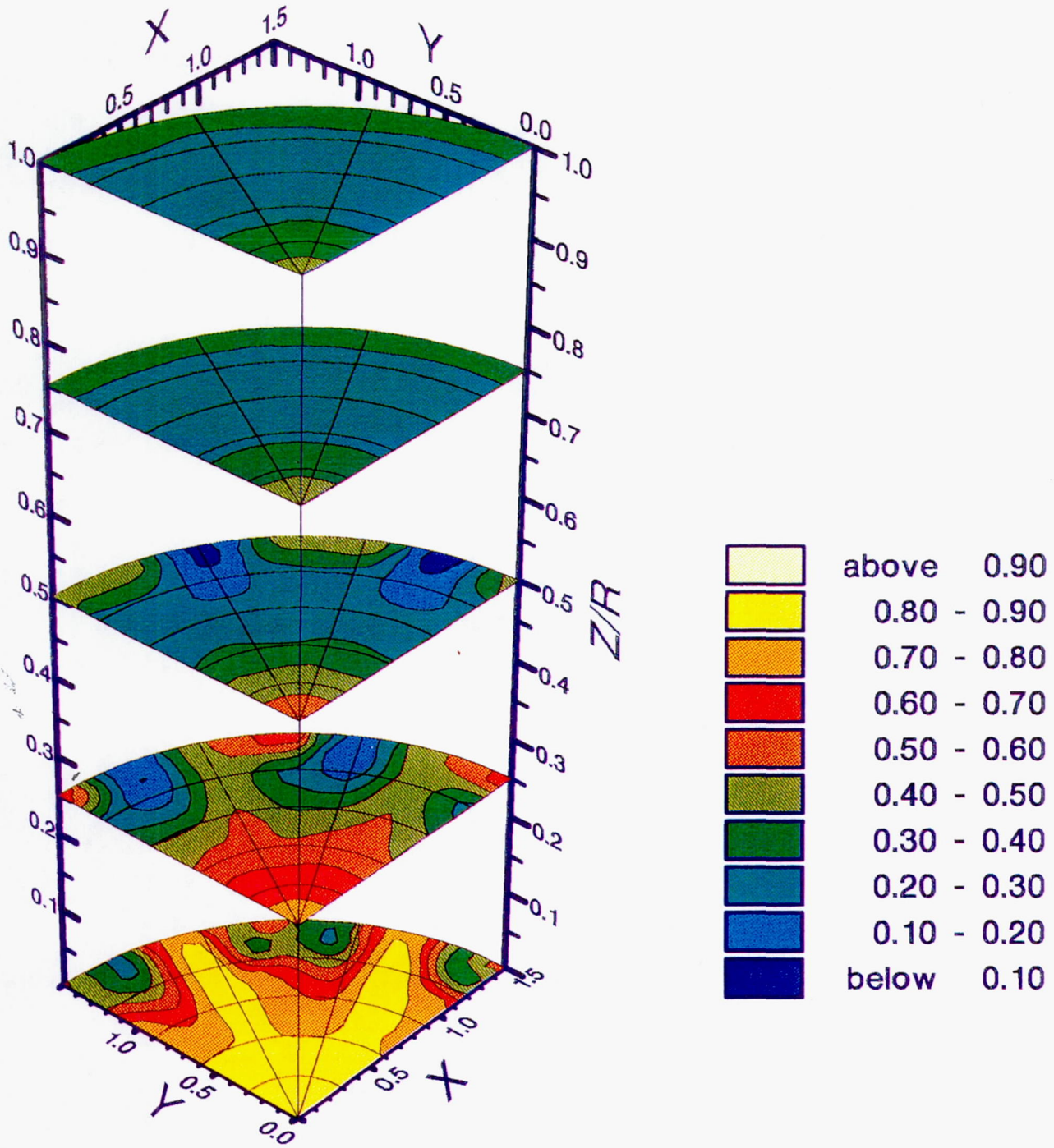

Figure 5.17: Mixture Fraction, J80MOD2, 8:1 Aspect Ratio Slanted Slots, J=88.5

Page intentionally left blank

Figures 5.18 compares the mixture uniformity parameter for the 8:1 aspect ratio geometries. At the first axial location, J25MOD2 is a poor mixer due to under-penetration. For increased J values, mixing at the first axial location is improved. The mixing performances of J52MOD2, and J80MOD2 are similar at the initial axial planes. Beyond Z/R=0.2, however, J80MOD2 is clearly a better mixer.

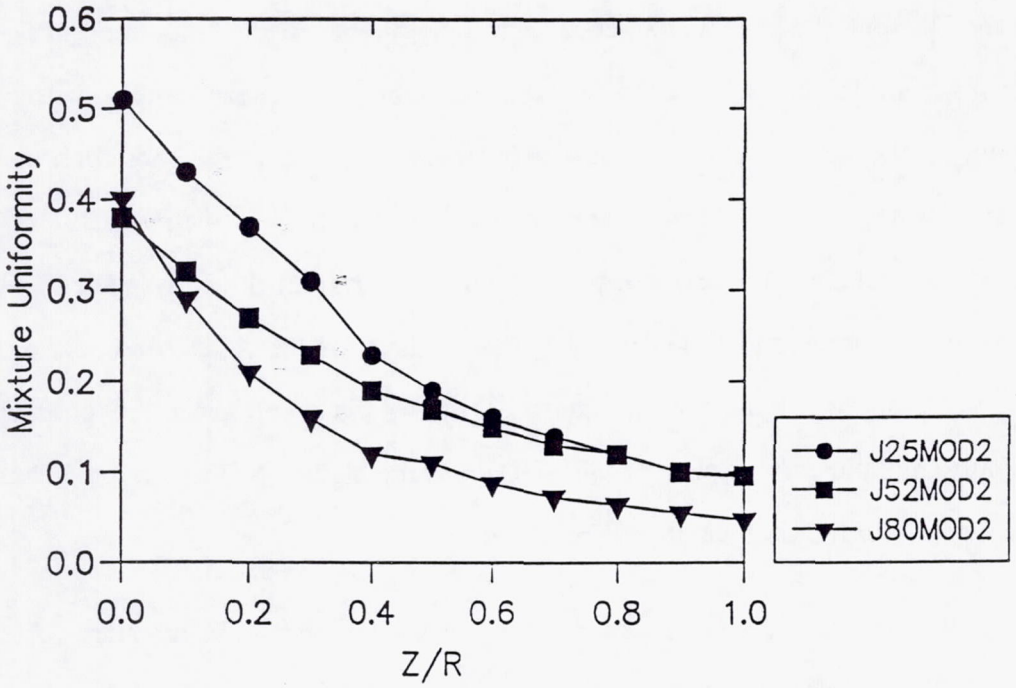

Figure 5.18: Mixture Uniformity for 8:1 Aspect Ratio Modules

Figures 5.19 through 5.21 present the equivalence ratio and NO production potential for the 8:1 aspect ratio geometries. At Z/R= 0.0, the near stoichiometric regions for all three geometries form at the shear layer between the jets and the mainstream. For J25MOD2, this region is smallest due to the under-penetration of the jets. At this axial location the main portion of the flow is at equivalence ratio of 1.28 - 1.44. Therefore, the rate of NO production for this module is lowest at the first axial location. Beyond Z/R= 0.25, however, most of NO formation for this modules occurs at the center where a high temperature region exists. As J is increased (J52MOD2, and J80MOD2), the jets penetrate farther and mixing in the first axial location improves. Despite the improved mixture uniformity, however, the amount of jet flow mixed with the mainstream is just enough to form larger regions of near stoichiometric composition. Additionally, the jets do not over-penetrate for these configurations. Therefore, the initial mixing between the jets and the mainstream is not quick enough to effectively reduce the near stoichiometric regions and decrease the NO formation rate at the early planes. As a result, the differential NO formation below Z/R= 0.2 is the highest for J80MOD2 despite the module's good mixing performance (Figure 5.22). Figure 5.23 shows the accumulated NO produced for the 8:1 aspect ratio modules. As expected, J80MOD2, has the highest NO formation potential due to the higher rate of NO formation at the initial planes.

Figure 5.24 presents the CO concentration for the 8:1 aspect ratio modules. At the first axial location, J25MOD2 has the highest CO concentration due to lack of jet penetration and mixing in the initial plane. With the increase in J, the initial CO concentration decreases. J80MOD2 appears to approach zero CO concentration more quickly than the other configurations due to enhanced mixing in the first axial locations. By Z/R=1.0, the CO concentration reaches very small amount for all three modules.

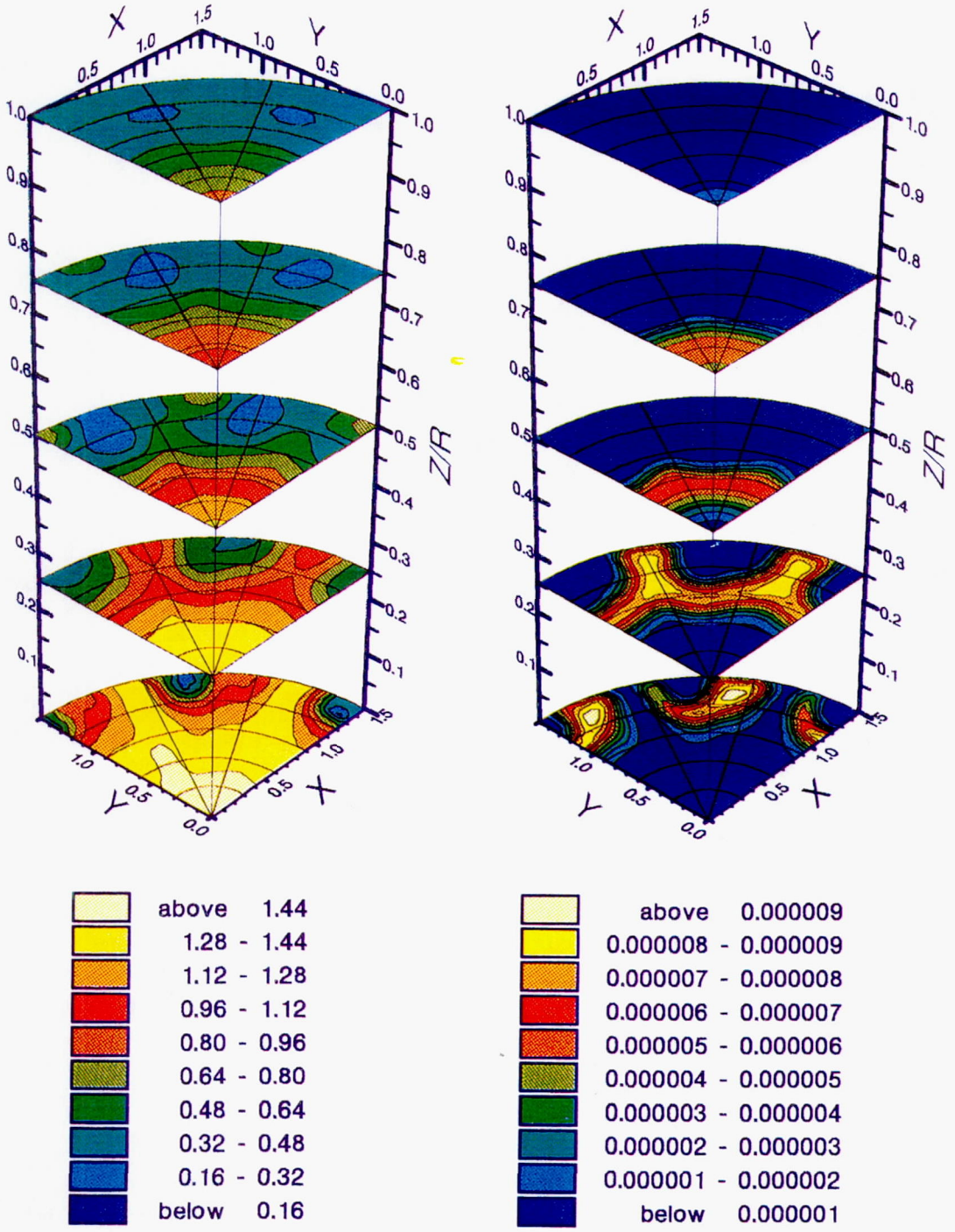

a) Equil. Ratio

b) NO Production (Mole Fraction)

Figure 5.19: Equivalence Ratio and NO Production, J25MOD2

Page intentionally left blank

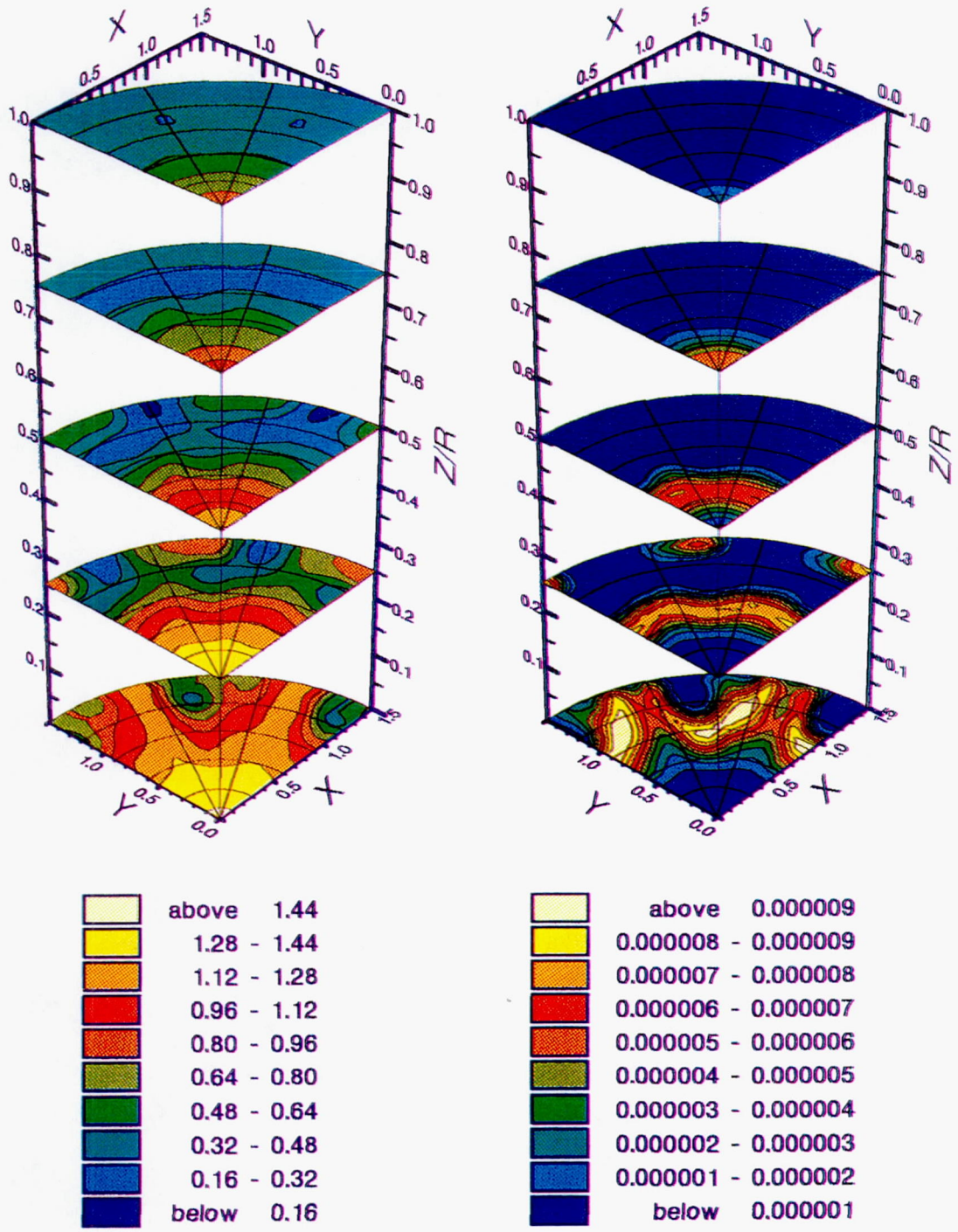

a) Equil. Ratio

b) NO Production (Mole Fraction)

Figure 5.20: Equivalence Ratio and NO Production, J52MOD2

Page intentionally left blank

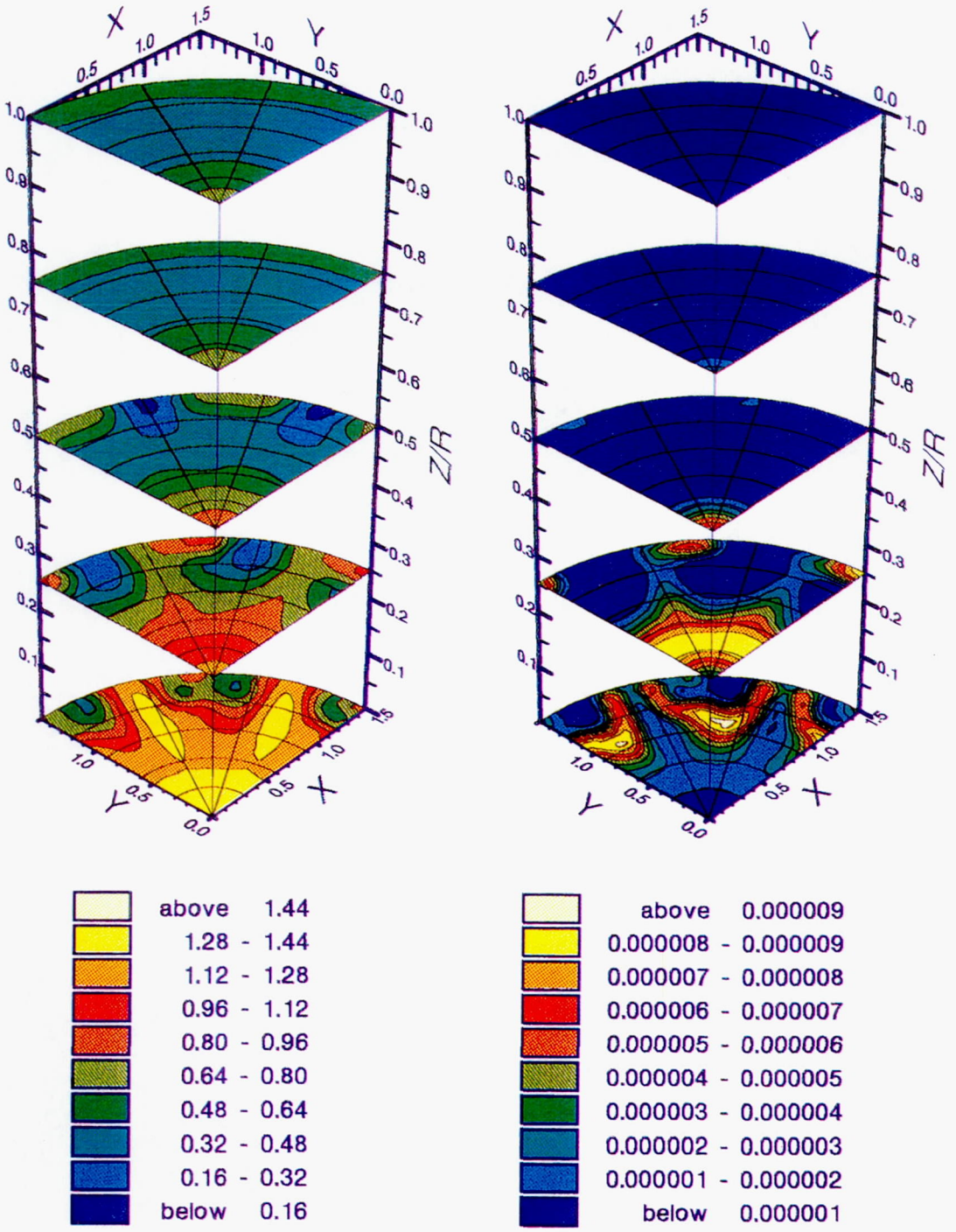

a) Equil. Ratio

b) NO Production (Mole Fraction)

Figure 5.21: Equivalence Ratio and NO Production, J80MOD2

Page intentionally left blank

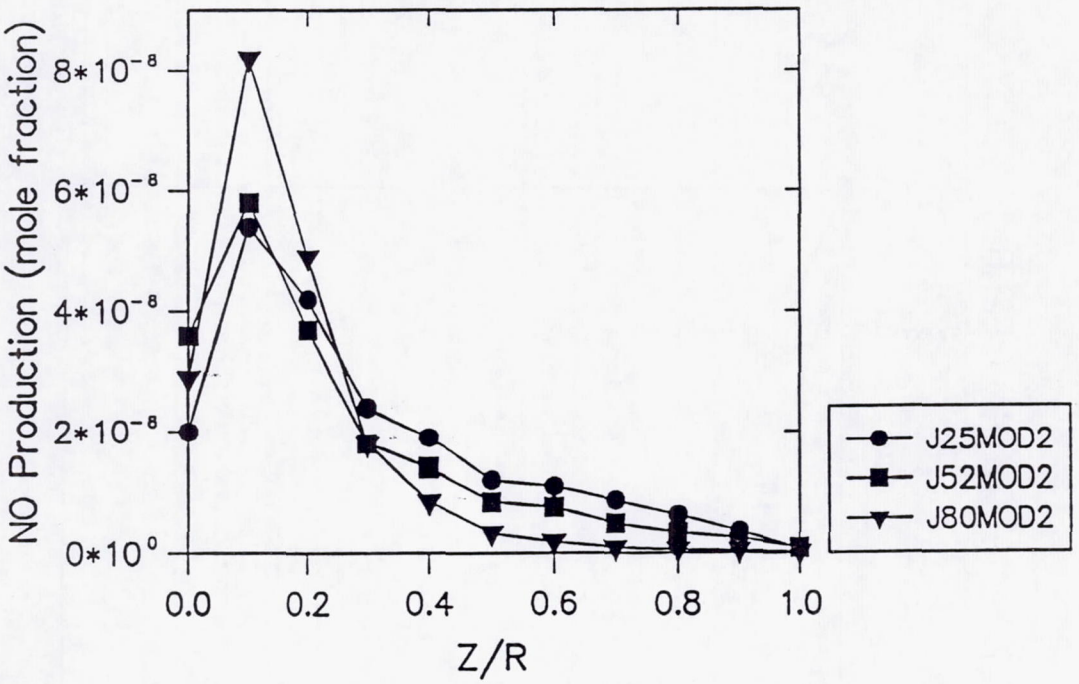

Figure 5.22 NO Production for 8:1 Aspect Ratio Modules

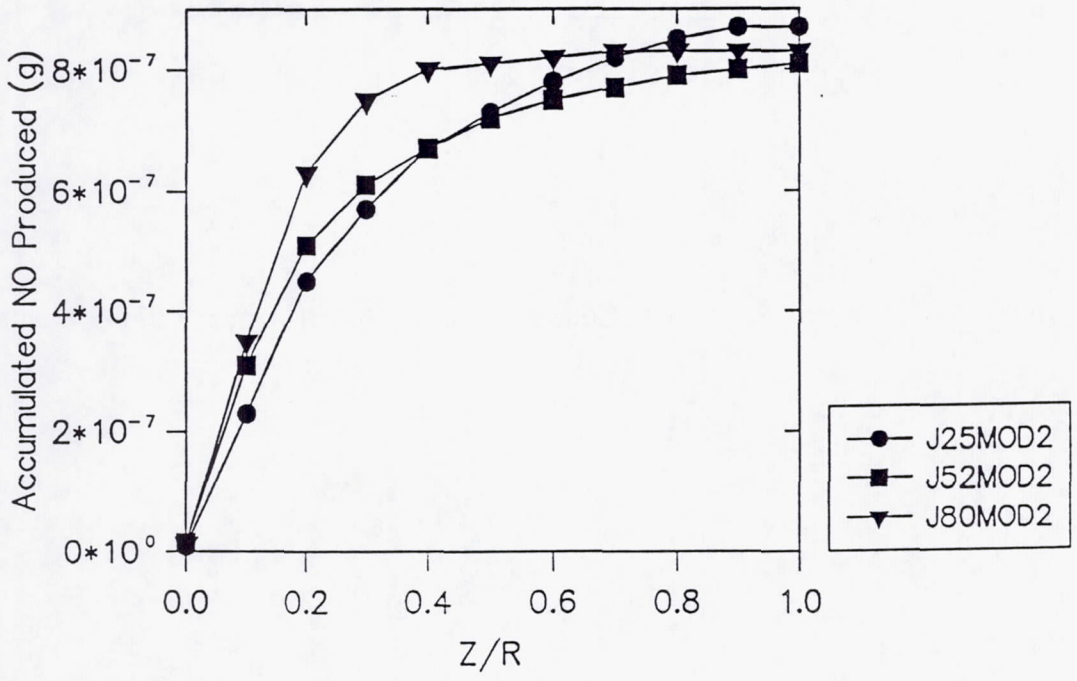

Figure 5.23 Accumulated NO Produced for 8:1 Aspect Ratio Modules

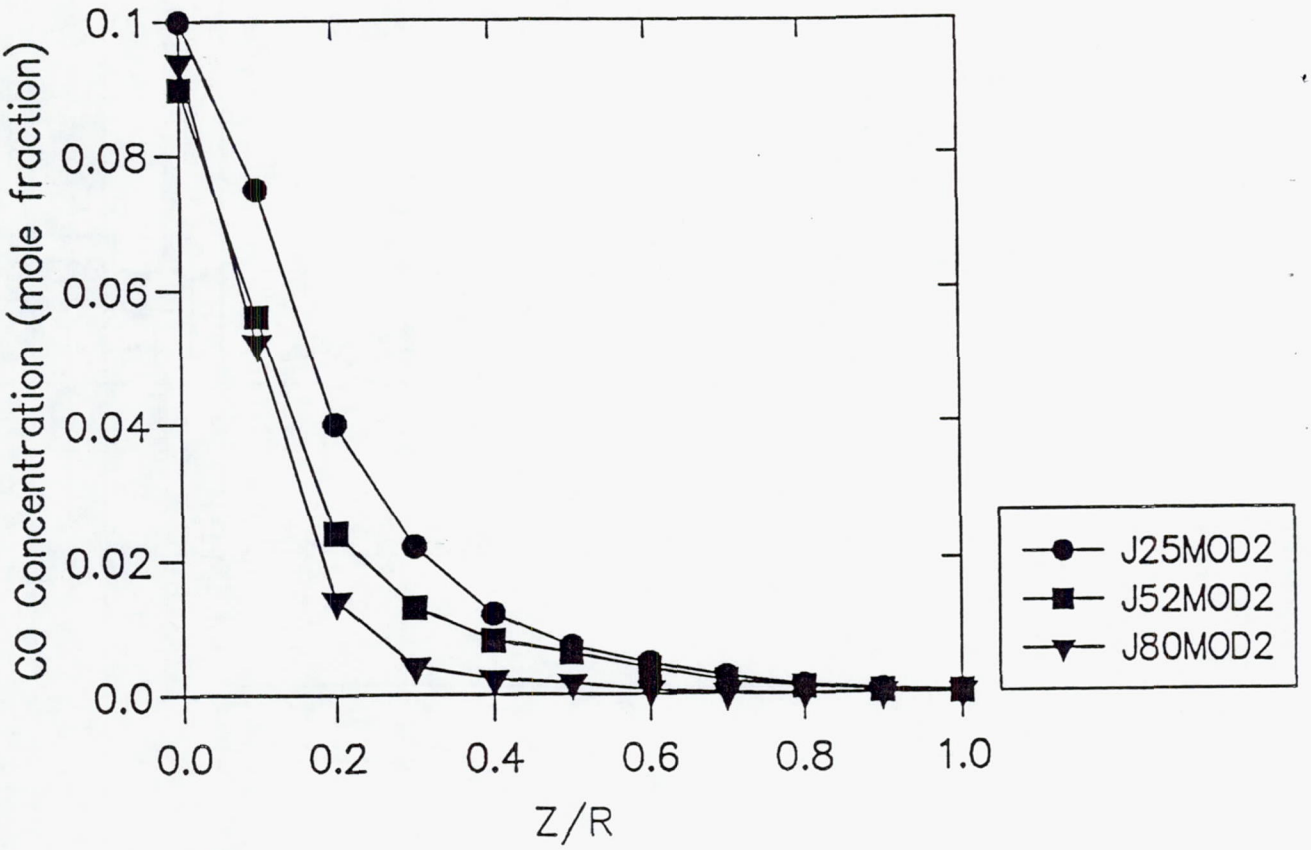

Figure 5.24 CO Concentration for the 8:1 Aspect Ratio Geometries

5.2.3 4:1 Aspect Ratio Geometry (MOD5)

Flow visualization experiments indicated that the 4:1 aspect ratio geometry behaves as an intermediate mixing configuration between the baseline and the 8:1 aspect ratio geometries. For this orifice geometry, penetration to the center is generally less than the baseline holes at the same J value, while the circumferential mixing is improved due to the presence of swirling motion. Compared to the 8:1 aspect ratio geometry, however, this swirling component is weaker but the penetration of the jets is greater. This observation was confirmed by the parametric experiments when three, 4:1 aspect ratio geometries were examined at three momentum-flux ratios.. Figures 5.25 through 5.27 present the mixture fraction distribution for the modules.

The first axial location for J25MOD5 (Z/R=0.0) shows a relatively large central region with a mixture fraction value in the range of 0.8 - 0.9. This f value is less than unity, suggesting slight jet penetration and mixing at the center of the module. The $f > 0.8$ region, however, is larger for J25MOD5 compared to that of J25MOD1. Jet penetration for the baseline geometry is stronger at this J value, therefore, the high mixture fraction region is smaller. As described previously, the 8:1 aspect ratio module at the lowest J value (J25MOD2) represents a case of under-penetration with central f values above 0.9. At downstream locations, J25MOD5 produces a relatively well mixed flow field with no indication of unmixed wall regions. At Z/R = 1.0, however, a slightly unmixed core is observed.

As J is increased, the penetration to the center is enhanced and the mixture fraction values at the core of the module at initial axial locations decreases. As previously observed for J52MOD1, the increase in jet penetration degrades the mixing along the walls. For J52MOD5, the circumferential mixing is slightly reduced, resulting in relatively unmixed wall regions. This degradation in mixing along the walls, is less severe for this module compared to J52MOD1 due to the swirling flow induced by the module geometry.

Page intentionally left blank

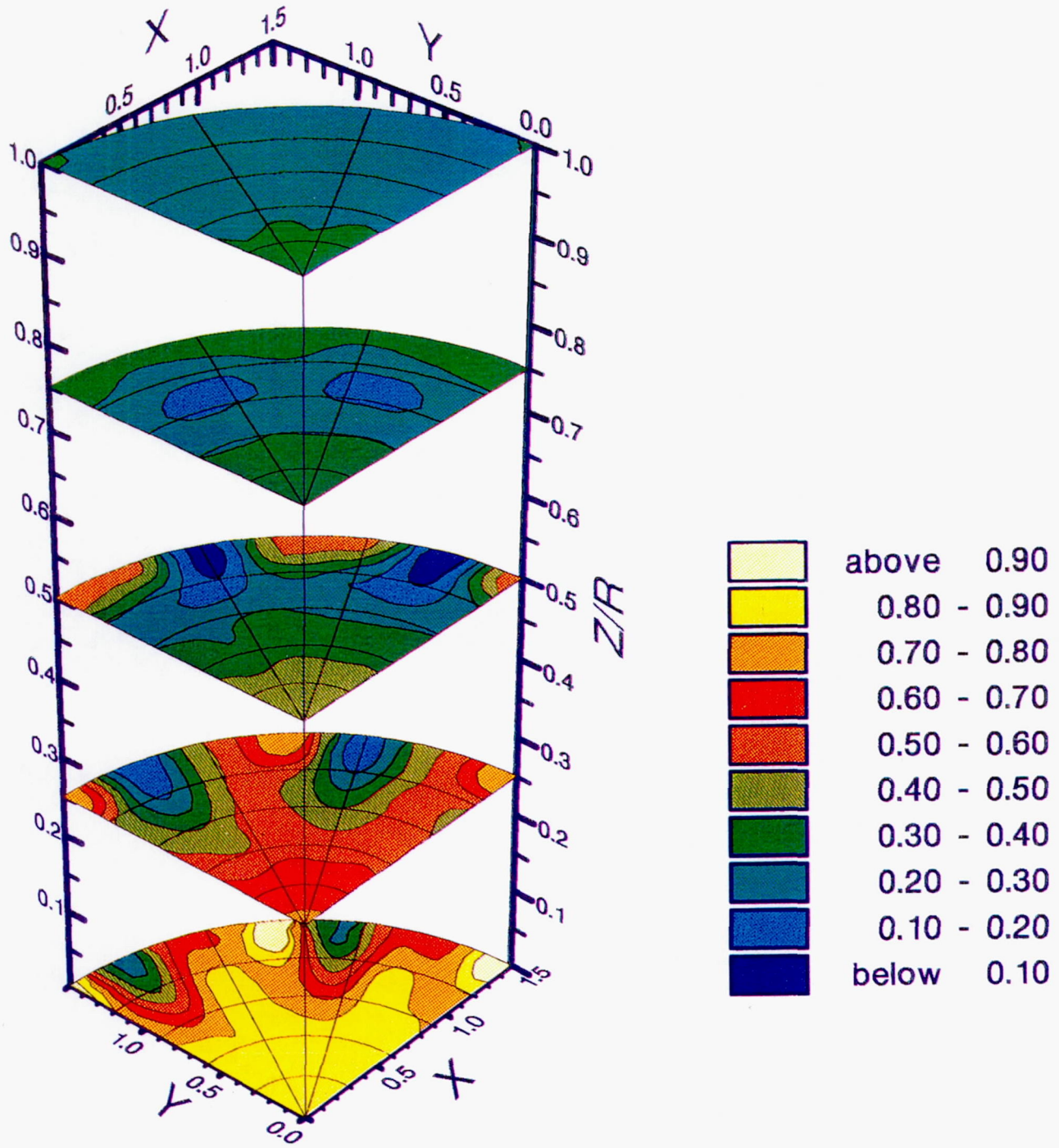

Figure 5.25: Mixture Fraction, J25MOD5, 4:1 Aspect Ratio Slanted Slots, J = 30.5

Page intentionally left blank

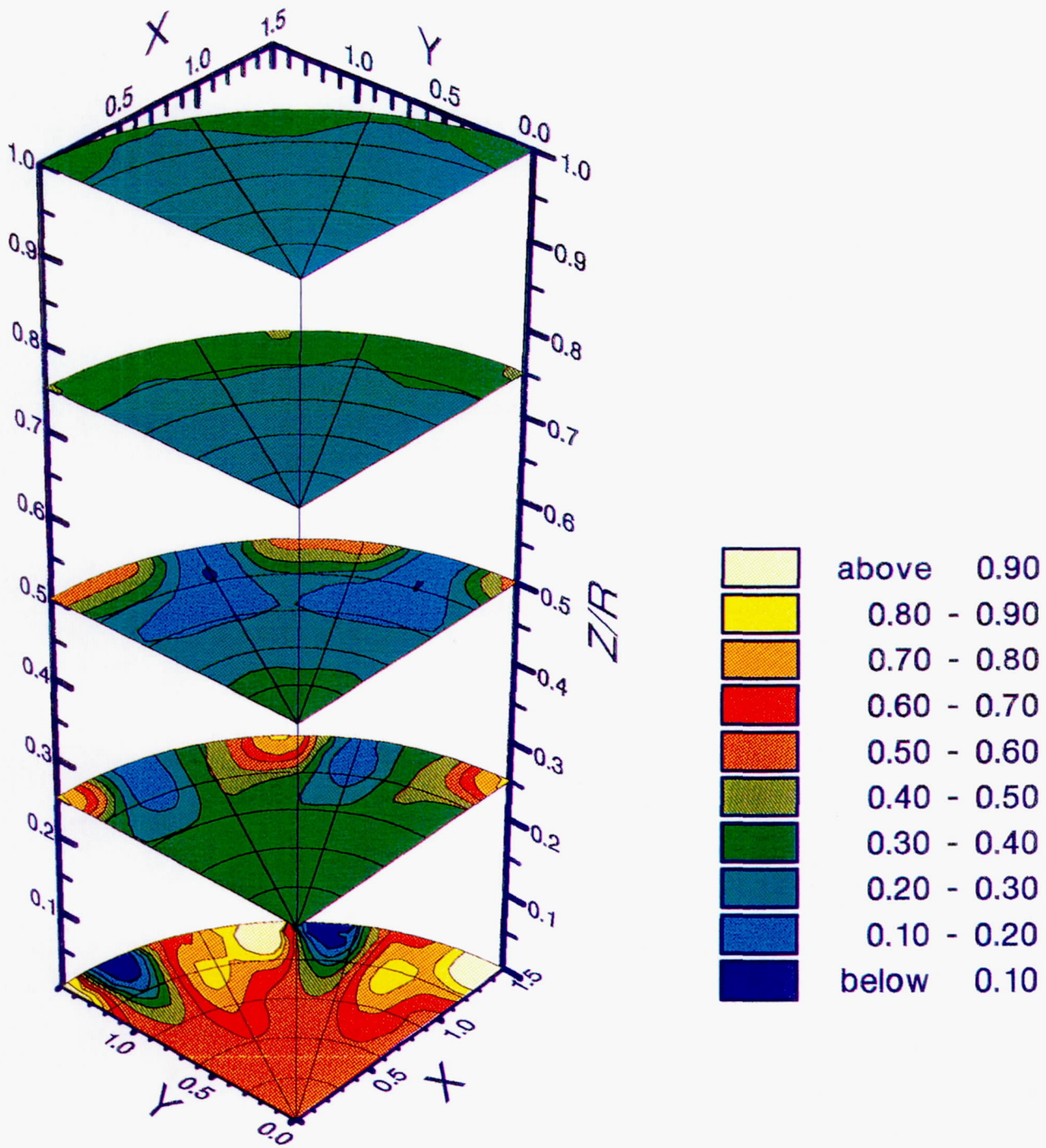

Figure 5.26: Mixture Fraction, J52MOD5, 4:1 Aspect Ratio Slanted Slots, J = 57.7

Page intentionally left blank

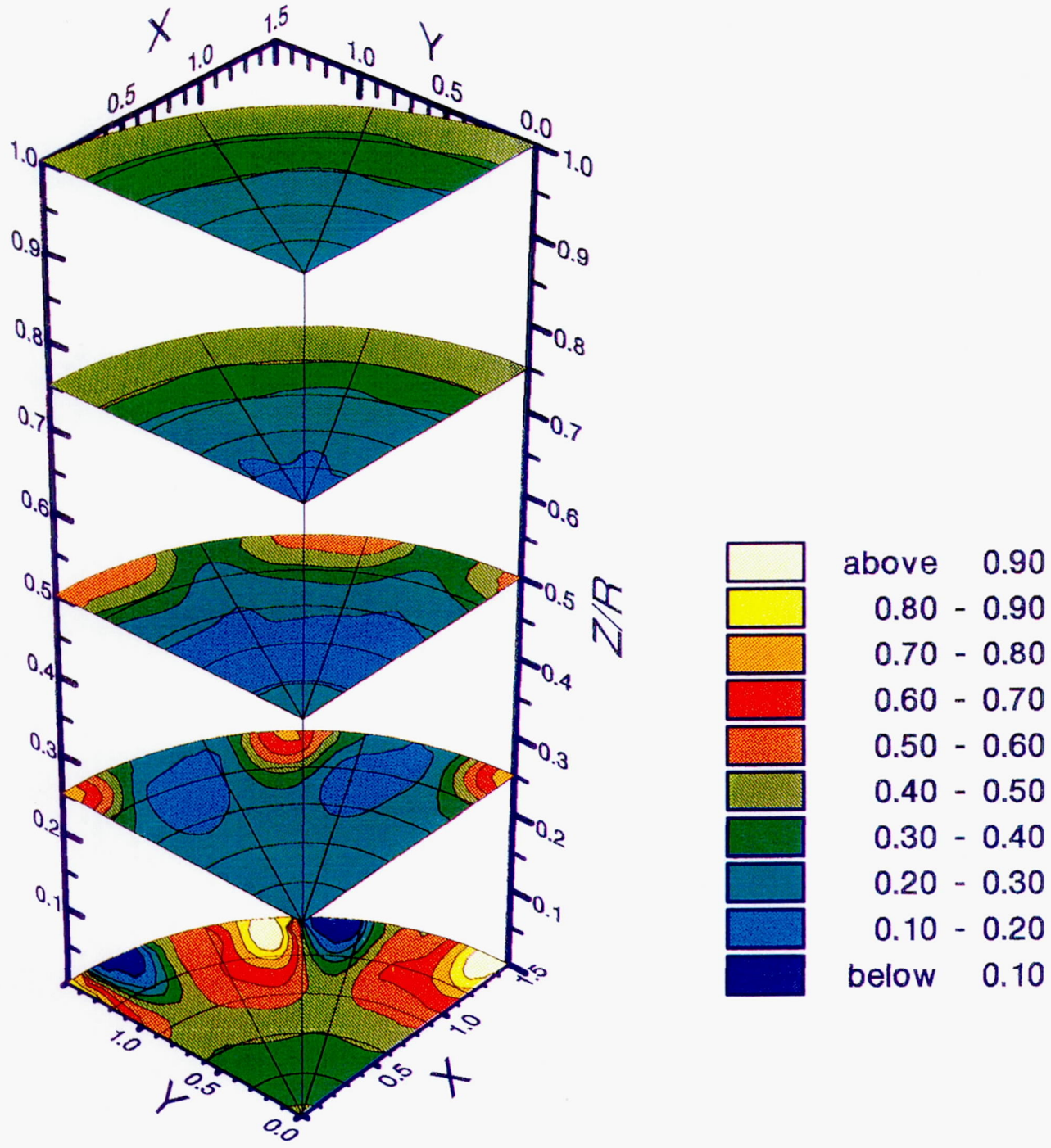

Figure 5.27: Mixture Fraction, J80MOD5, 4:1 Aspect Ratio Slanted Slots, J = 93.0

Page intentionally left blank

With further increase in J value (J80MOD5), the mixture fraction value decreases at the first axial location. At downstream locations, a low f value region at the center and relatively unmixed regions along the walls are produced. This configuration as well as J52MOD5, indicate over penetration of jets, and are not desirable from a mixing only standpoint.

Figure 5.28 compares the mixture uniformity parameter for the 4:1 aspect ratio geometries. The trend is very similar to that described for the baseline modules. At initial planes, the higher the momentum-flux ratio, the better the mixture uniformity. At downstream locations, the module with the most initial over-penetration (J80MOD5), is the poorer mixer due to degradation of circumferential mixing.

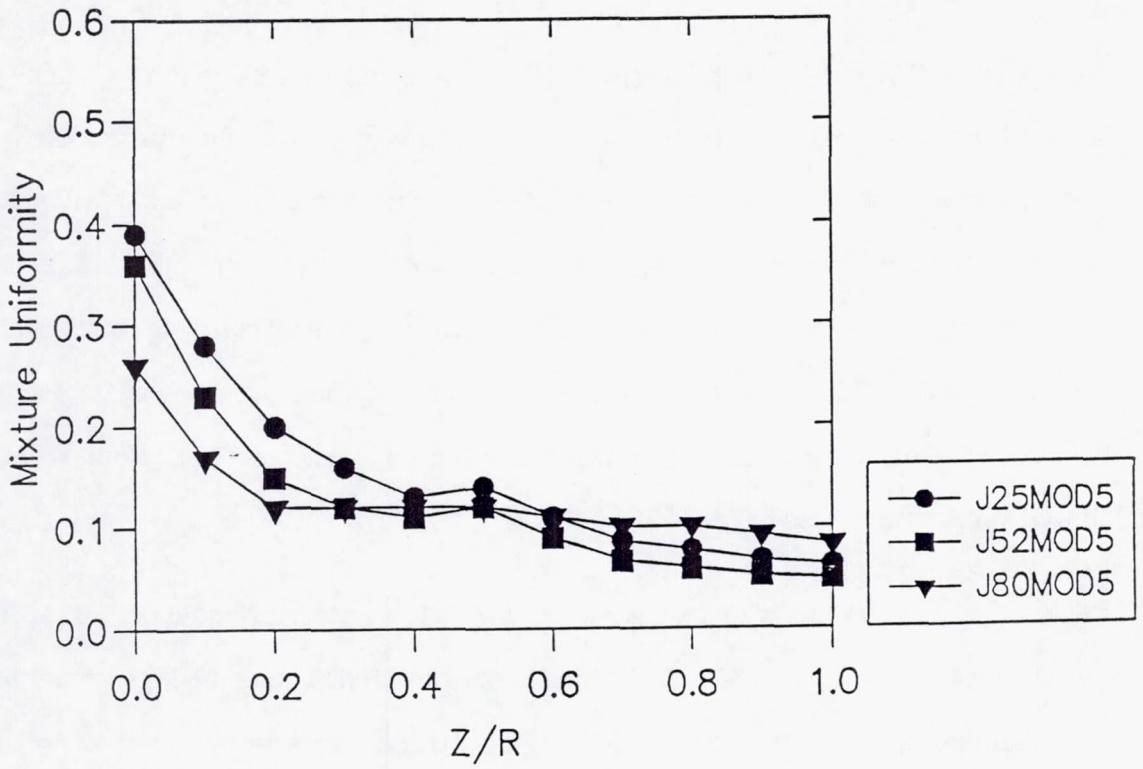

Figure 5.28: Mixture Uniformity for 4:1 Aspect Ratio Modules

Figures 5.29 through 5.31 present the equivalence ratio and NO production potential for J25MOD5, J52MOD5, and J80MOD5, respectively. As for their mixing characteristics, the NO formation potential of these configurations are similar to those of the corresponding baseline geometries. For J25MOD5, the majority of NO is produced below Z/R=0.50 in the shear layer formed between the jets and the cross stream. Beyond this axial location, the differential NO produced is negligible. For J52MOD5, the rate of NO formation is higher than J25MOD5 at Z/R= 0.0. At this plane, the jet penetration to the center is stronger for J52MOD5 compared to J25MOD5. In exchange, the near stoichiometric regions are formed between the jets at the wall region. In an axis-symmetric geometry, most of the area is concentrated along the walls. Therefore, the presence of near stoichiometric regions near the wall contribute more to NO formed than the ones present in the module center. The rate of NO production is reduced beyond Z/R= 0.3, J52MOD2 as shown in Figure 5.32. For J80MOD5, the rate of NO production between Z/R= 0.0, and Z/R= 1.0 is small due to enhanced jet penetration and mixing in initial planes. Beyond Z/R= 0.3, the rate of NO production is highest for this module, due to the relatively unmixed walls. The accumulated NO produced for the 4:1 aspect ratio modules shows the lowest NO formation potential for J80MOD5 by Z/R= 1.0 (Figure 5.33). It must be noted however, that the NO formation versus axial distance for this module has a positive slope at Z/R= 1.0. The positive slope is probably due to the NO formed at the wall region where the circumferential mixing is degraded in an over-penetrated configuration. Both J25MOD5, and J52MOD5 have flat slopes beyond Z/R=0.7.

Figure 5.34 presents the CO concentration for 4:1 aspect ratio modules as a function of downstream location. As expected, J25MOD5 and J80MOD5 have the highest and lowest CO concentrations at Z/R=0.0, respectively. At downstream locations beyond Z/R=0.4, the CO concentration is the same for all geometries.

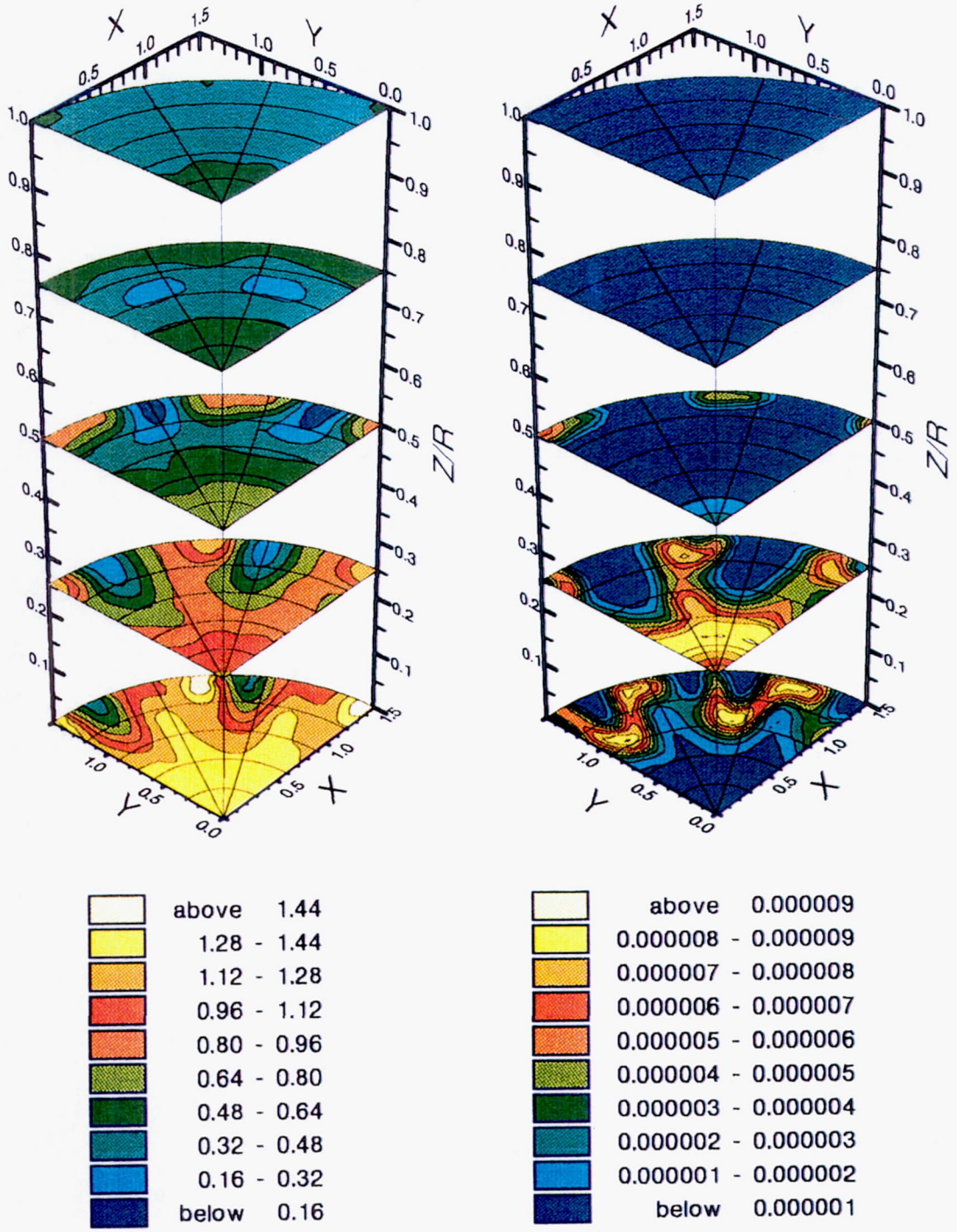

a) Equil. Ratio

b) NO Production (Mole Fraction)

Figure 5.29: Equivalence Ratio and NO Production, J25MOD5

Page intentionally left blank

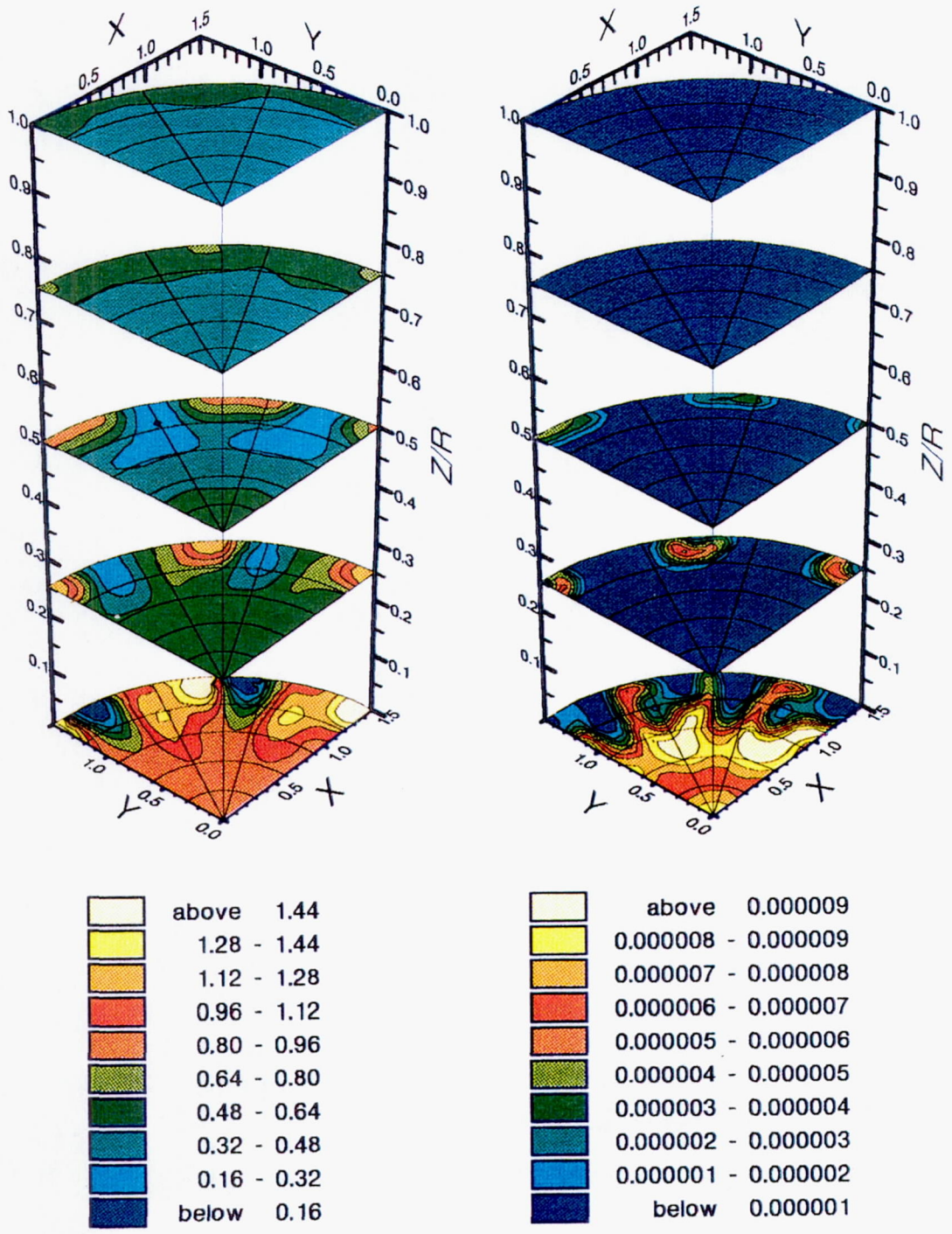

a) Equil. Ratio

b) NO Production (Mole Fraction)

Figure 5.30: Equivalence Ratio and NO Production, J52MOD5

Page intentionally left blank

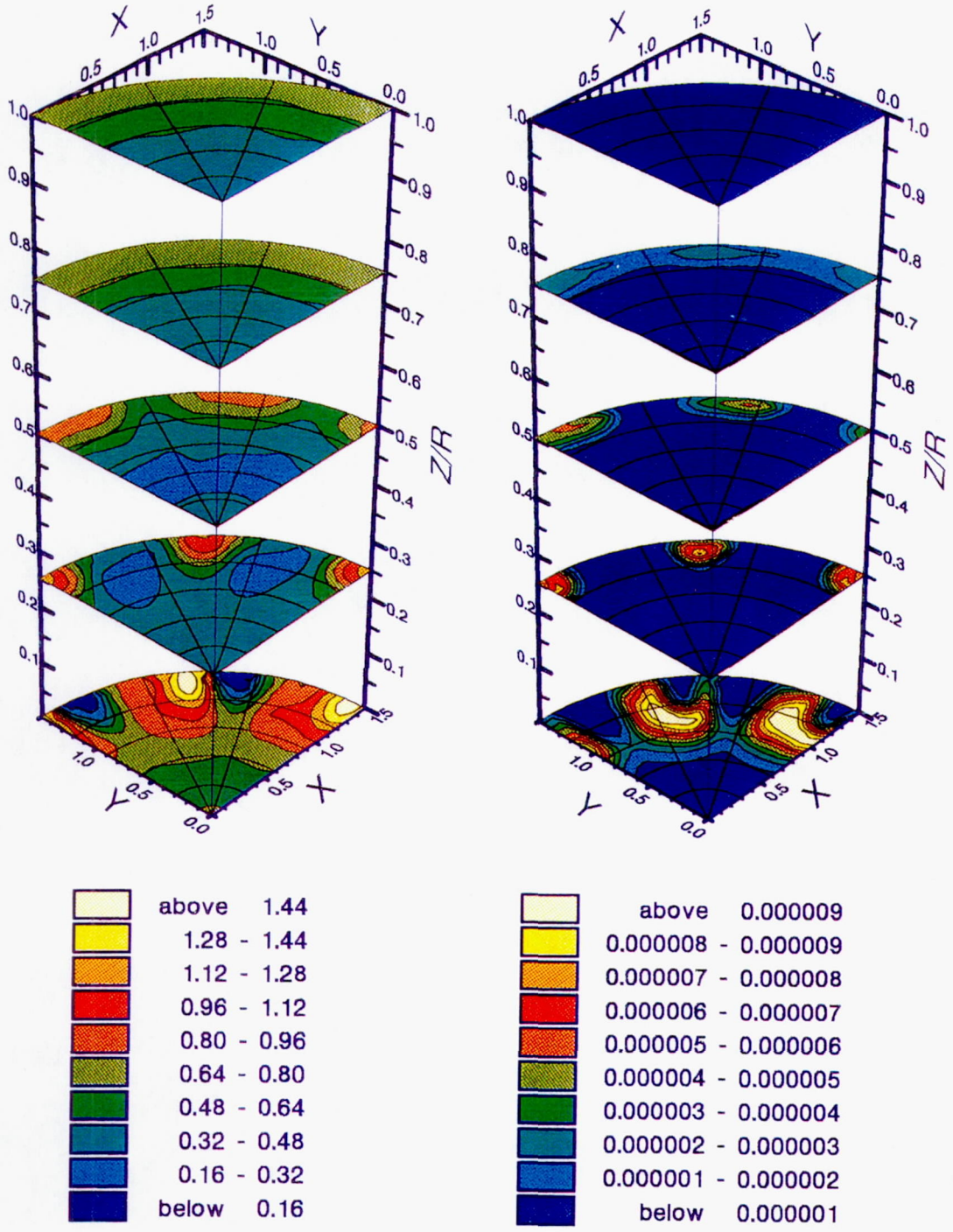

a) Equil. Ratio

b) NO Production (Mole Fraction)

Figure 5.31: Equivalence Ratio and NO Production, J80MOD5

Page intentionally left blank

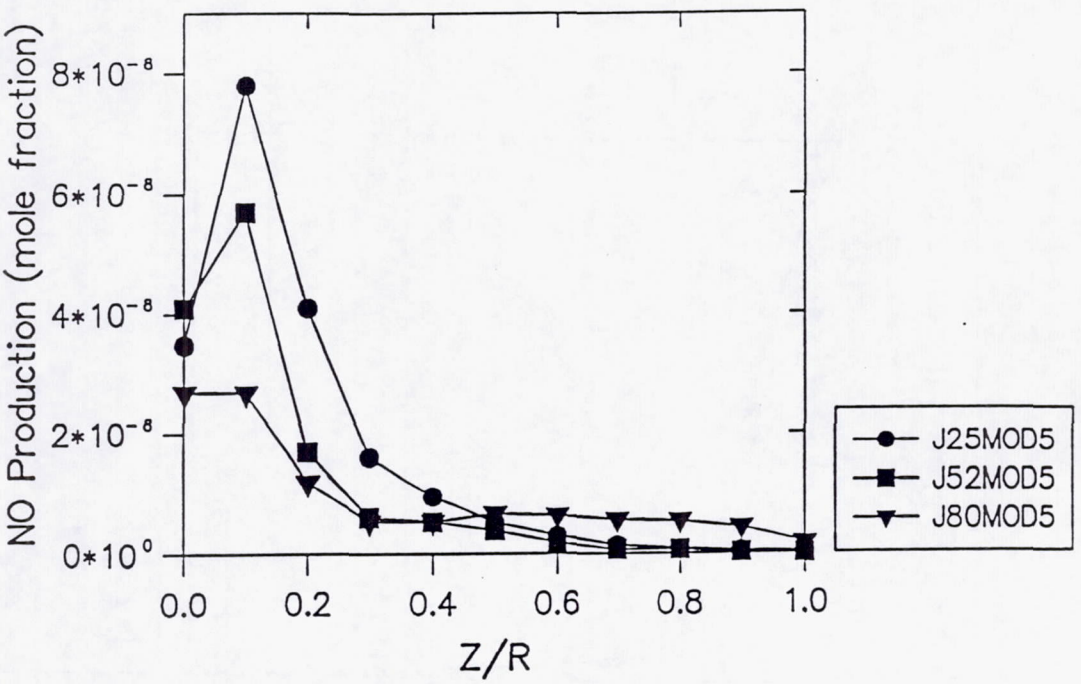

Figure 5.32 NO Production for 4:1 Aspect Ratio Modules

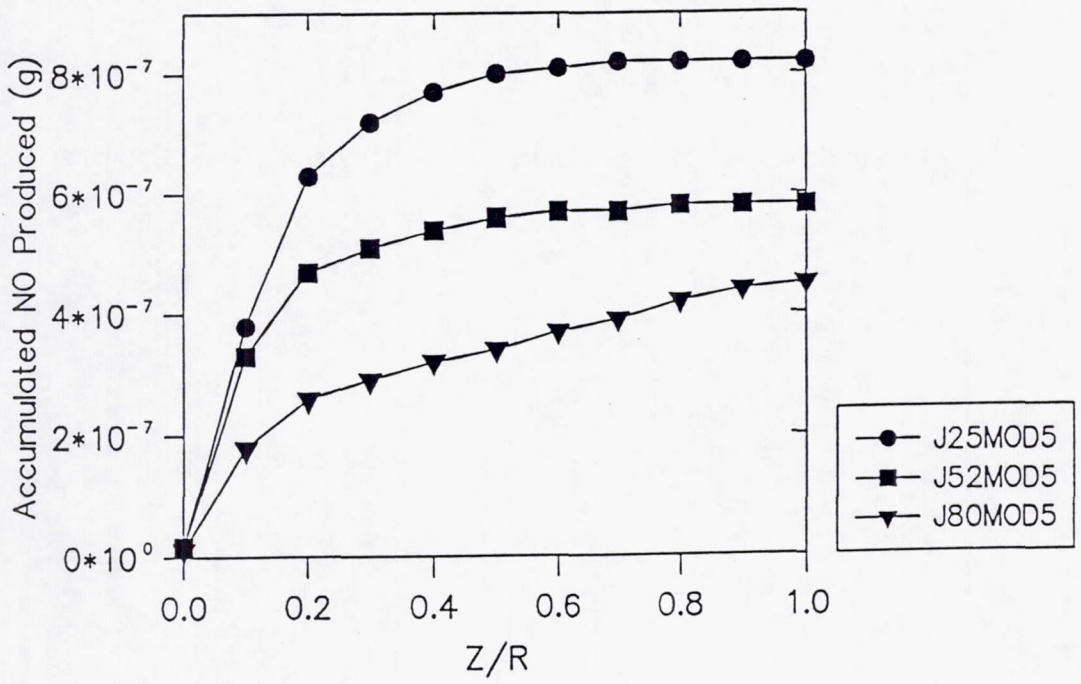

Figure 5.33 Accumulated NO Produced for 4:1 Aspect Ratio Modules

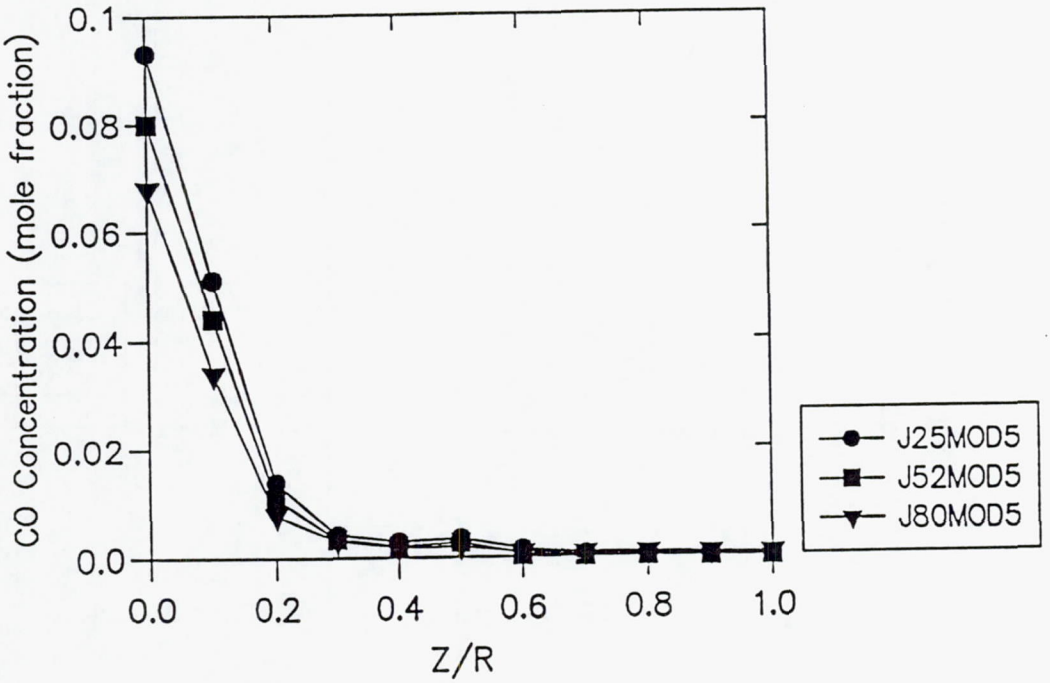

Figure 5.34: CO Concentration for the 4:1 Aspect Ratio Geometry

5.2.4 Comparison of Holes and 45 Degree Slots

This section compares the overall-mixing characteristics and NO-reduction potentials of the 8-hole baseline geometry, and the 45^{o} slanted slots configurations.

Overall-mixing For the momentum-flux ratios tested, the baseline geometry is a more effective mixing configuration at the injection plane. Figure 5.35 shows the mixture uniformity parameter for the baseline and slanted slot modules at the low and intermediate J values tested. The improved mixture uniformity at the initial planes is due to the higher jet penetration seen for the hole geometry as compared to the slanted slots geometries. At the lowest momentum-flux ratio tested (Figure 5.35a), the baseline geometry, represents a "good" mixer throughout the downstream stations examined. As J is increased, the baseline geometry still presents the more attractive mixer at the injection plane, but shows degraded mixing performance at downstream locations (Figure 5.35b). The degradation in mixture uniformity is primarily due to the relatively unmixed wall regions.

NO-Reduction Potential Figure 5.36 shows the differential NO production for the baseline and the slanted slots geometries at the low and intermediate J values examined. At the lower J value, the baseline geometry shows a slightly higher NO production rate at the initial planes, despite its better mixing performance (Figure 5.36a). This is yet another example that shows rapid initial mixing does not necessarily reduce the early rate of NO production. At the intermediate J value, the baseline geometry shows a substantially lower rate of NO production below Z/R = 0.4. Figure 5.37 shows that the baseline geometry potentially produces the lowest accumulated NO, especially at J of approximately 52, compared to the slanted slot geometries. At the highest J value tested, the holes and the 4:1 aspect ratio modules produce the same accumulated NO which is nearly half of the total NO produced by the 8:1 aspect ratio geometry.

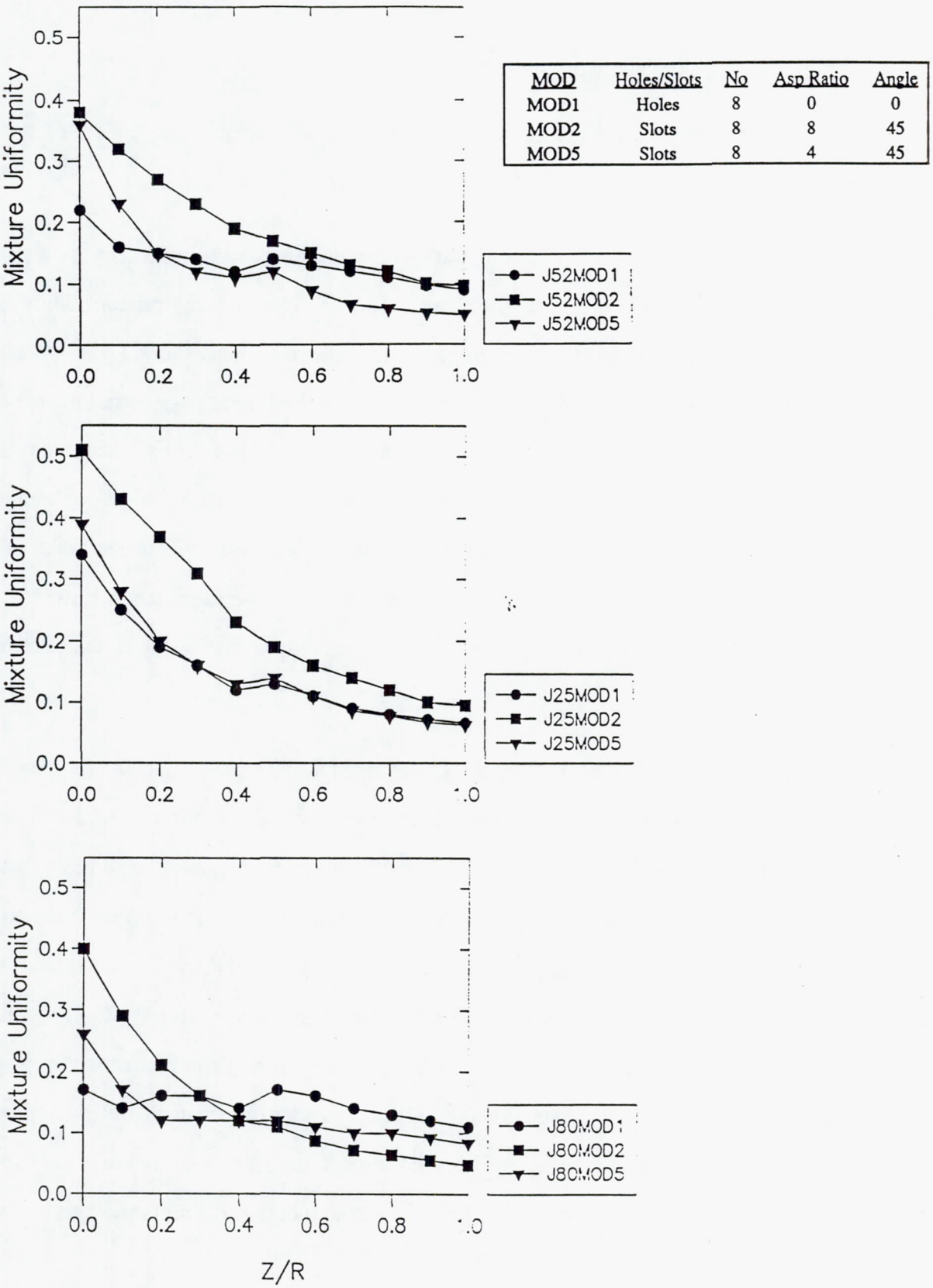

Figure 5.35: Comparison of Mixture Fraction for Holes and Slanted Slots

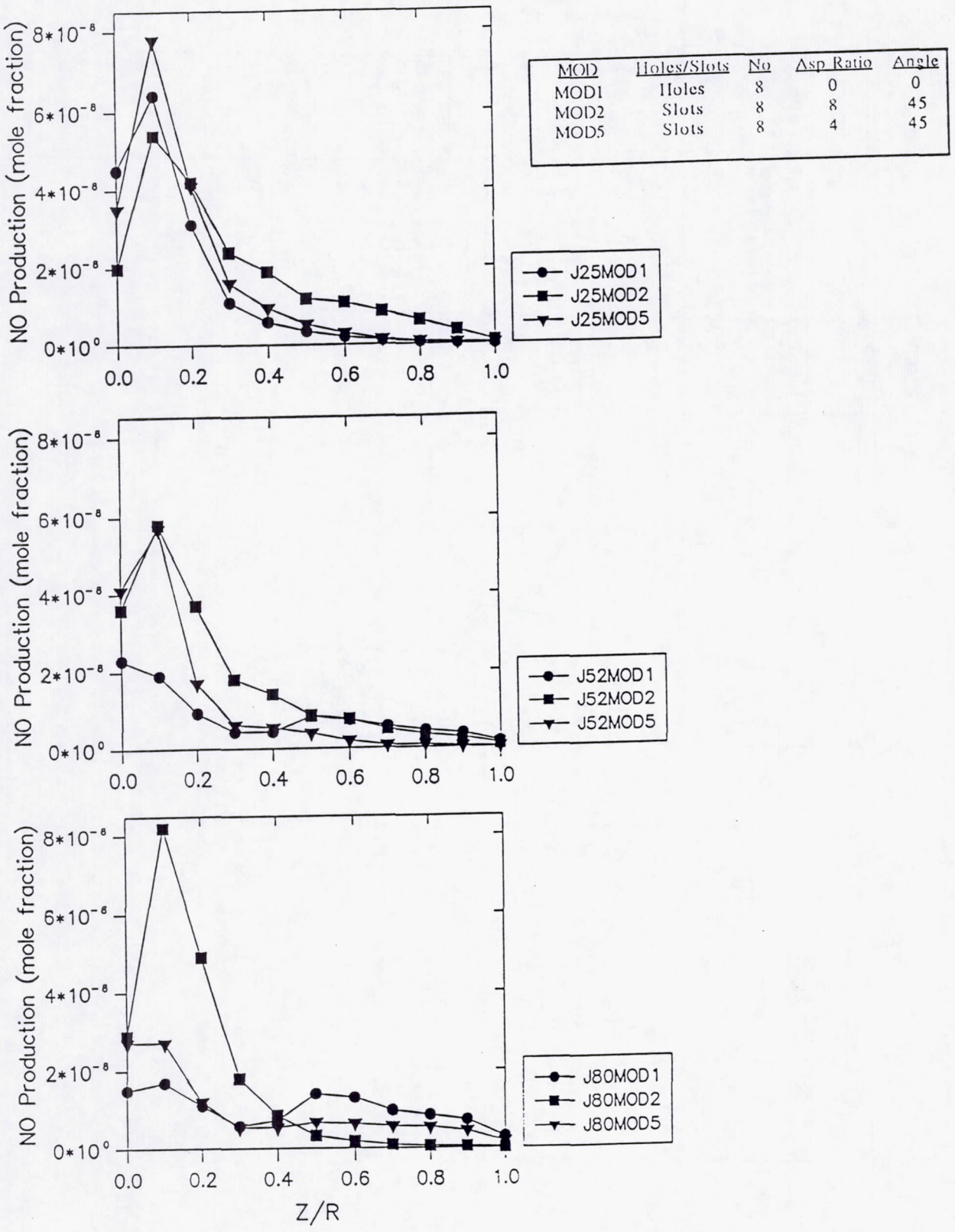

Figure 5.36: Comparison of NO Production for Holes and Slanted Slots

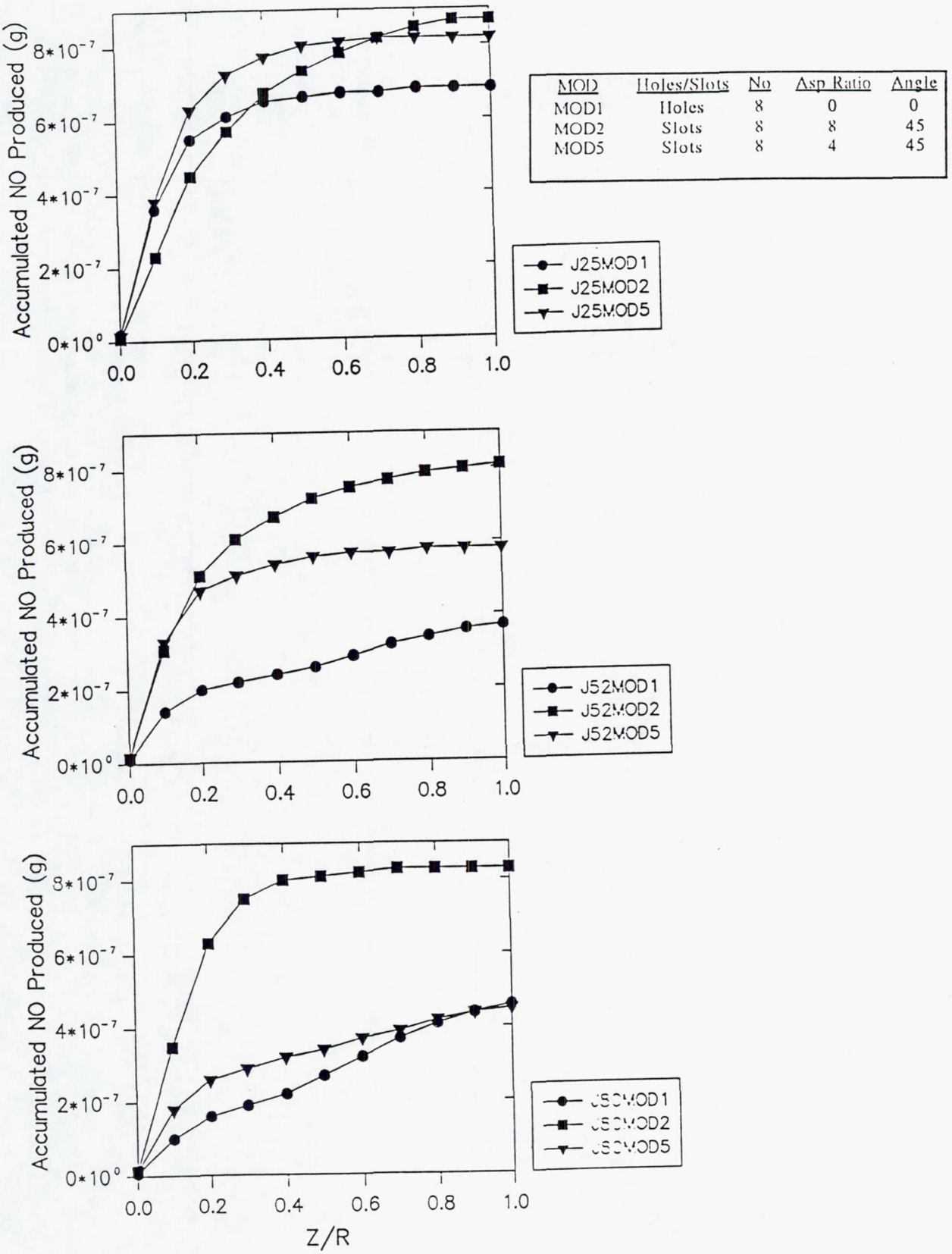

Figure 5.37: Comparison of Accumulated NO Produced for Holes and Slanted Slots

5.2.5 Effect of Momentum-Flux Ratio

As discussed earlier, jet to mainstream momentum-flux ratio was identified as the most significant parameter influencing mixing and penetration in rectangular geometries (Holdeman and Walker, 1977). The results of the present experiments show that this parameter is significant in cylindrical geometries as well.

For all geometries tested in the parametric studies, increasing momentum-flux ratio enhanced jet penetration. The degree of impact of J on penetration depends on the orifice geometry. For the baseline 8-hole geometry, increasing J from the lowest tested value (26.7) to the intermediate J (50.9) caused the slightly penetrating jets to over-penetrate. For the 8:1 aspect ratio geometry on the other hand, the highest tested J value for this configuration provided slight penetration to the center. Therefore, it is the coupling between the jet to mainstream momentum-flux ratio and orifice geometry that determines the degree of jet penetration and overall mixing for a given number of orifices.

The present results show that to minimize NO from a quick mixer, a tradeoff between effective mixing in 1) the injection plane, and 2) the wall region downstream of the injection orifices is required. Jet to mainstream momentum-flux ratio, and orifice geometry are critical parameters in optimizing this trade-off

It is noteworthy that for configurations examined, it appears that over-penetration of jets at first axial locations, reduces the rate of NO production. It must be noted , however, that over-penetration can have an additional effect not considered in this study. At high momentum-flux ratios, a strong penetration of jets can result in a backflow on the centerline. This will promote formation of NO upstream of the injection plane and contribute to the accumulated NO produced in the mixing module.

It should also be noted that this set of experiments cannot define the optimum mixing/NO minimization geometry because the number of holes was kept constant. The penetration characteristics will change with the number of orifices for a given configuration.

5.2.6 Effect of Slot Aspect Ratio

Two slot aspect ratios of 4:1, and 8:1 were examined as part of the parametric studies. The mixture uniformity and emissions potentials of these configurations for three momentum-flux ratios were presented in the previous sections.

The effects of slot aspect ratio on mixing characteristics can be summarized as follows: For a given momentum-flux ratio and number of orifices, the smaller aspect ratio slots penetrate further into the cross stream. The larger aspect ratio slots on the other hand, produces a stronger swirl component and enhances the circumferential mixing. The degree to which the overall mixing in an axis-symmetric can geometry is impacted by the slots aspect ratio, depends on the momentum-flux ratio. For example, if an 8:1 aspect ratio geometry produces an under-penetrated configuration at a given J, the corresponding 4:1 aspect ratio module will improve penetration, but may produce relatively unmixed regions along the walls.

Figure 5.35 compares the mixture uniformity parameter for the 8:1 and 4:1 aspect ratio slots. At the lower and intermediate J values, the 4:1 aspect ratio geometry is a better mixer at all axial locations. At the highest J value tested, however, the 8:1 aspect ratio behaves as the better mixing geometry beyond Z/R=0.5. This is because of the over-penetration of jets for J80MOD5 which improve mixing at the initial planes, but produces unmixed regions along the walls at downstream axial locations.

The impact of slot aspect ratio on emissions potential of a module, is far less straight-forward. Figures 5.36 and 5.37 compare the NO production and accumulated NO produced for the 4:1 and 8:1 aspect ratio geometries. It is shown that J25MOD2 has a lower rate of NO production at the

initial planes compared to J25MOD5. As discussed previously, for J25MOD5, a large near stoichiometric region exists at the shear layer formed between the jets and the mainstream. This is not the case for J25MOD2, in which the majority of the flow field is at equivalence ratios in the range of 1.28- 1.44 .

As J is increased, the jets penetrate further for the 4:1 aspect ratio geometry, and the rate of NO production in the initial planes decreases. At the intermediate J value, the 4:1 aspect ratio geometry maintains the lower rate of NO formation at all axial locations. At the highest J tested, the 4:1 aspect ratio initially presents the lower NO formation potential. As Z/R is increased, this module shows a higher NO production rate due to the NO formed in the poorly mixed wall region.

The corresponding accumulated NO produced for the two aspect ratio slanted slot, reiterates the fact that at the low J tested, the 8:1 aspect ratio geometry has the potential to produce slightly less NO. For the intermediate and high J values, however, the 4:1 aspect ratio geometry can potentially produce half the amount NO formed by an 8:1 aspect ratio configuration.

5.2.7 Effect of Slot Angle

The effect of slot angle on mixing and emissions potentials are presented for the intermediate J value. Four modules were tested incorporating eight, 4:1 aspect ratio orifices oriented at 0° (J52MOD3), 22.5° (J52MOD4), 45° (J52MOD5), and 67.5° (J52MOD6) with respect to the mainstream direction.

The mixture fraction distribution plots for J52MOD3, J52MOD4, and J52MOD6 are shown in Figures 5.38 through 5.40, respectively. [The corresponding plot for J52MOD5 can be found in Figure 5.26 and Figure 5.29.] The equivalence ratio and NO production plots for J52MOD3, J52MOD4 and J52MOD6 are shown in Figures 5.41 to 5.43.

Examining the flow field in Figures 5.38 to 5.40 at the first axial location for these modules shows that by increasing the slots angle, the jet penetration decreases. The swirl component, and the circumferential mixing on the other hand improves.

The increased jet penetration at the initial axial location, enhances the mixture uniformity as shown in Figure 5.44. It can be seen that J52MOD6 has the highest mixture uniformity parameter at this location. J52MOD3 on the other hand, produces the most jet penetration and the lowest mixture uniformity parameter at Z/R=0.0. Further downstream the geometry with the most penetration behaves as a poor mixer due to unmixed wall regions.

The differential NO production for the above modules are presented in Figure 5.45. The accumulated NO produced is shown in Figure 5.46. For this particular orifice geometry and flow conditions, the initial NO formation rate is high for the slot angle that produces the least jet penetration. J52MOD4, on the other hand, has the lowest NO production potential. It appears that an orifice angle of 22.5^{o} produces the desirable combination of jet penetration and circumferential mixing to maintain a low overall NO production rate.

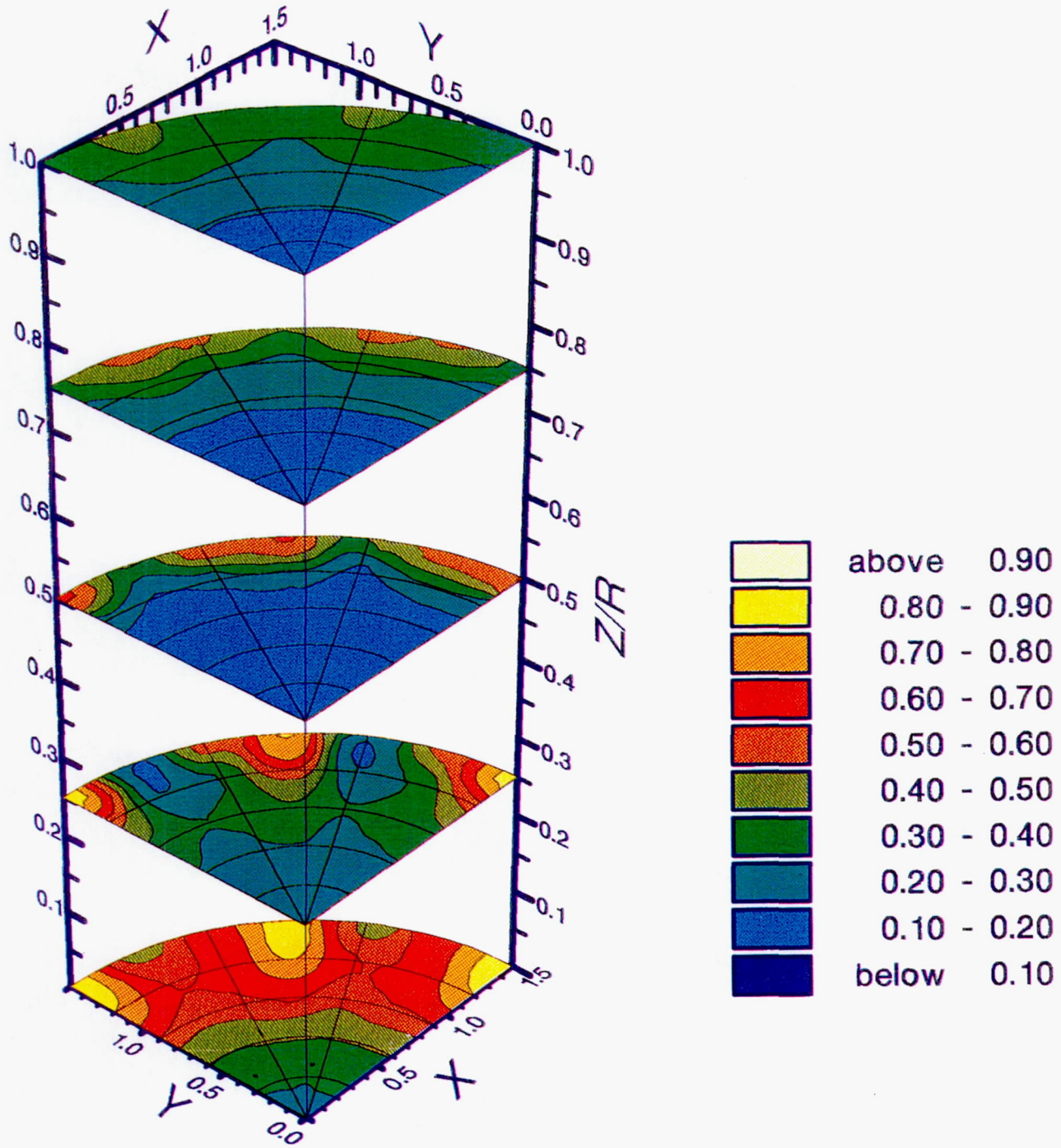

Figure 5.38: Mixture Fraction, J52MOD3, 4:1 Aspect Ratio Slanted Slots (0^{o}), J = 51

Page intentionally left blank

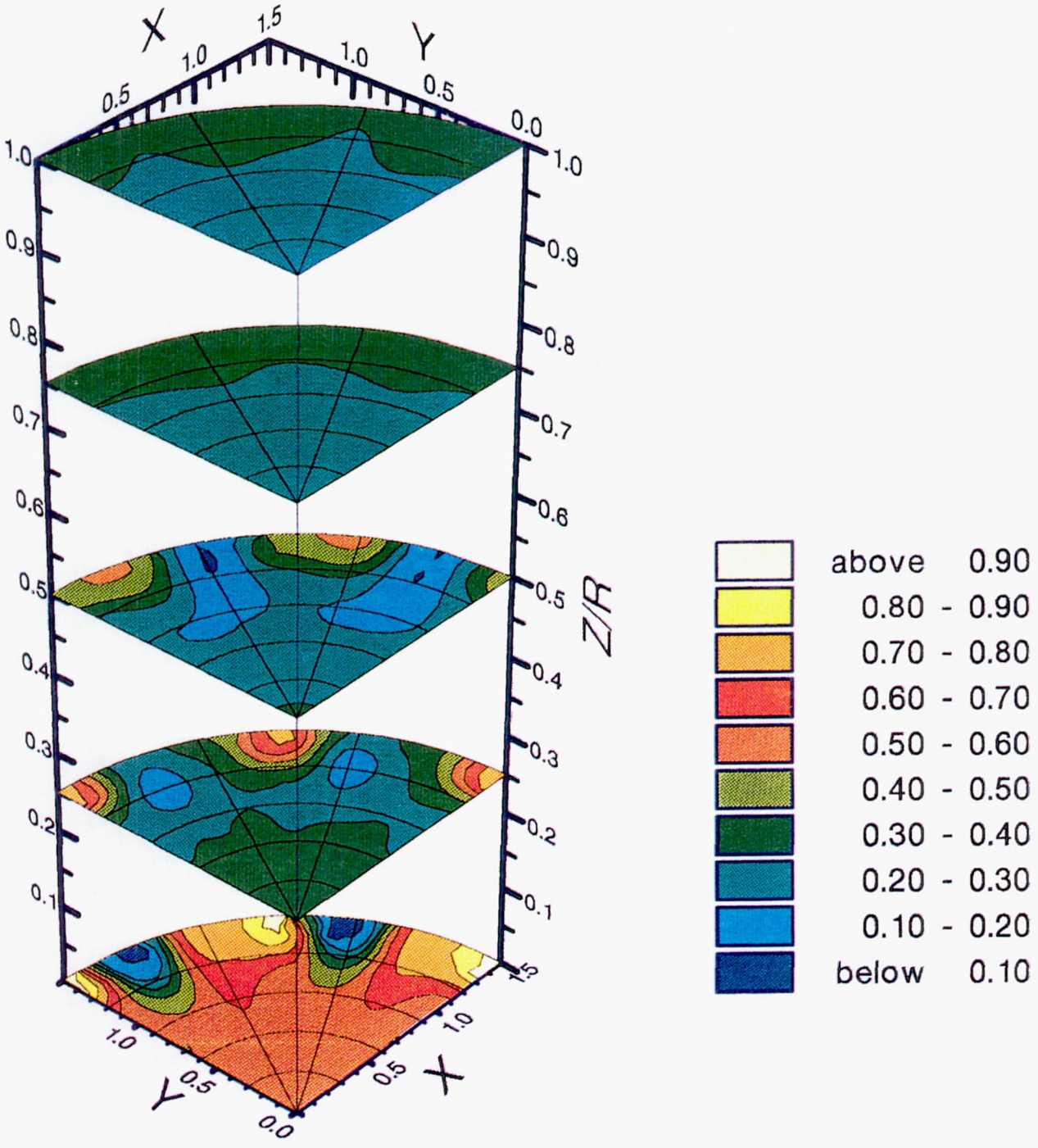

Figure 5.39: Mixture Fraction, J52MOD4, 4:1 Aspect Ratio Slanted Slots (22.5^{o}), J = 53

Page intentionally left blank

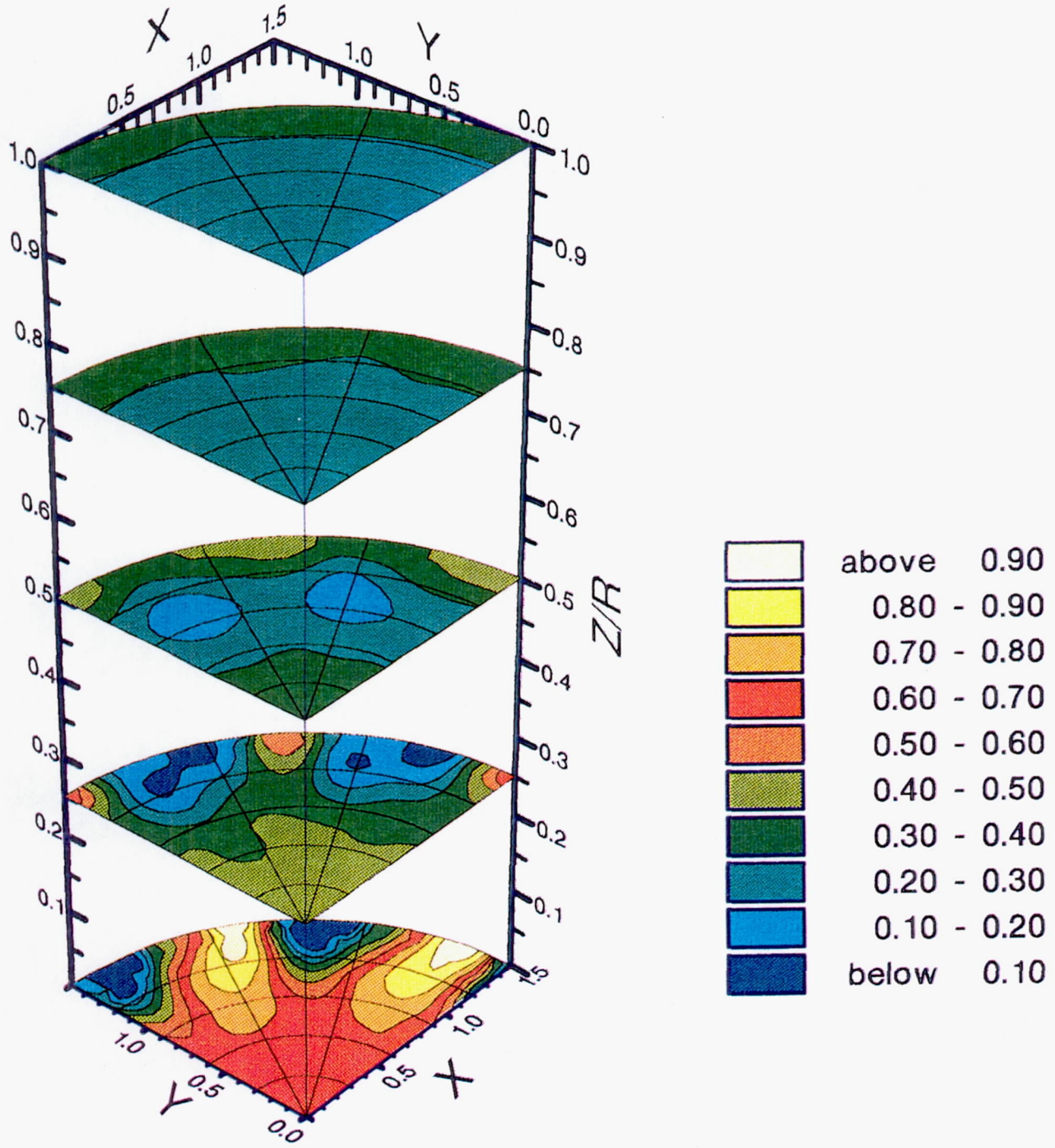

Figure 5.40: Mixture Fraction, J52MOD6, 4:1 Aspect Ratio Slanted Slots (67.5^{o}), J = 60

Page intentionally left blank

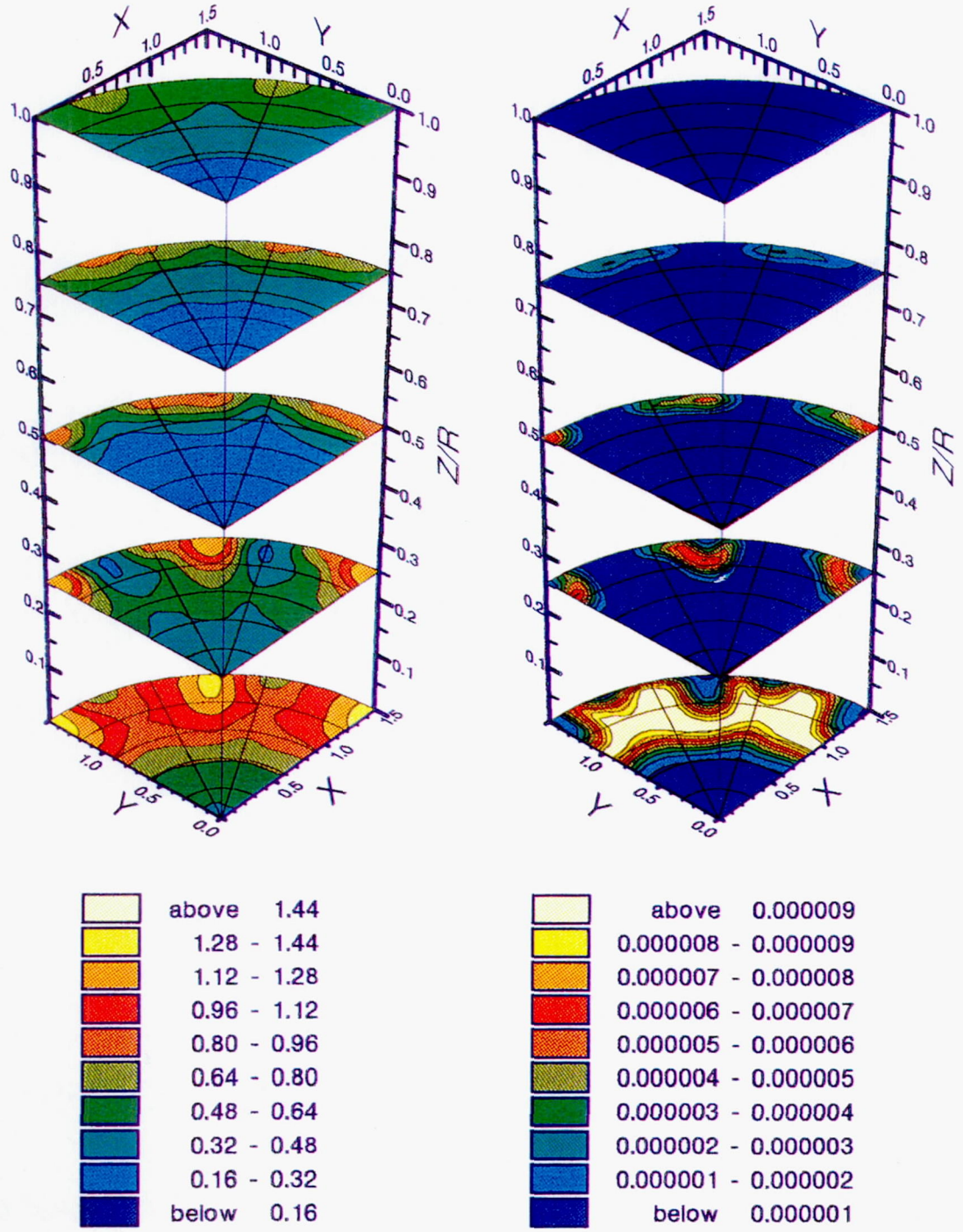

a) Equil. Ratio

b) NO Production (Mole Fraction)

Figure 5.41: Equivalence Ratio and NO Production, J52MOD3

Page intentionally left blank

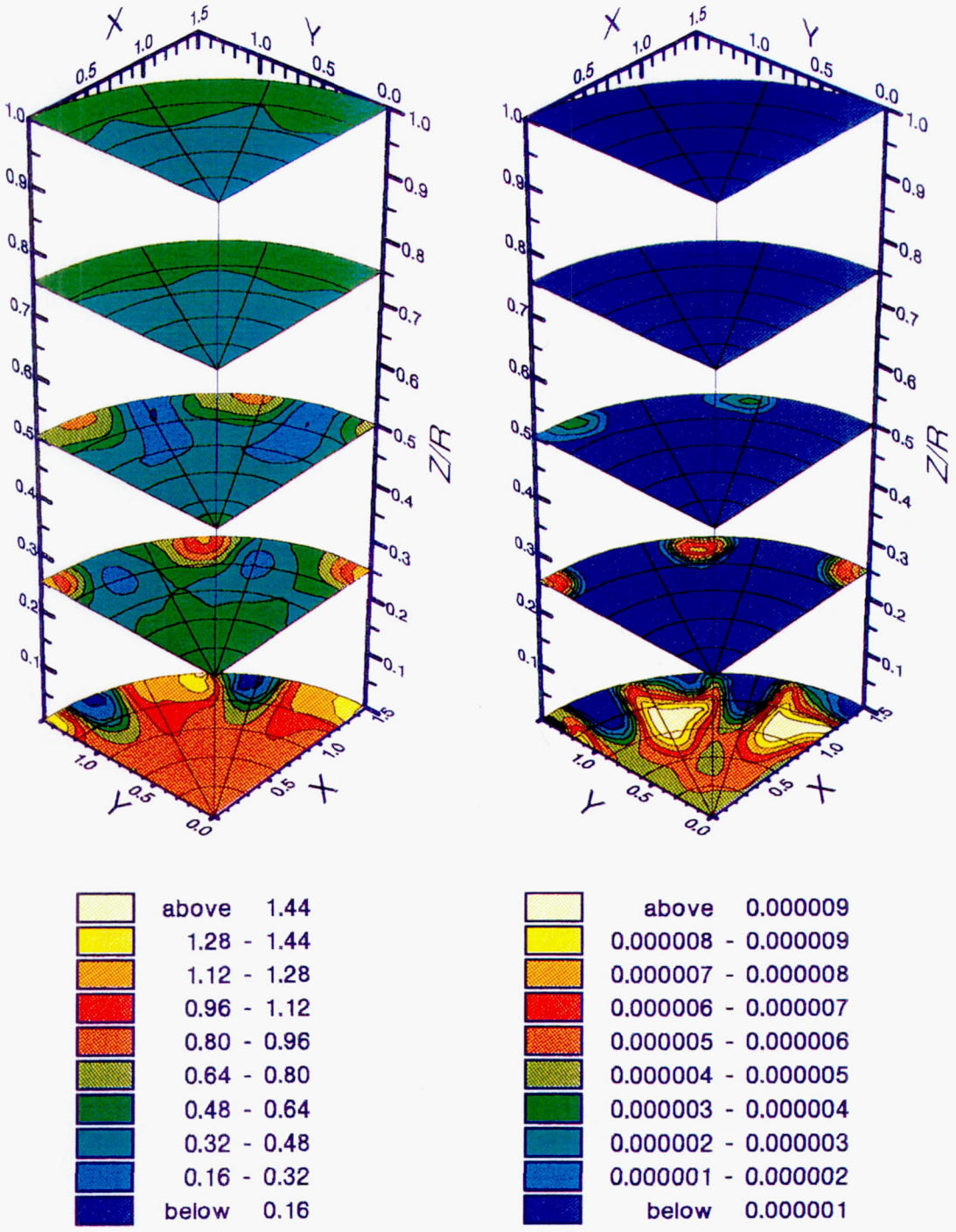

a) Equil. Ratio

b) NO Production (Mole Fraction)

Figure 5.42: Equivalence Ratio and NO Production, J52MOD4

Page intentionally left blank

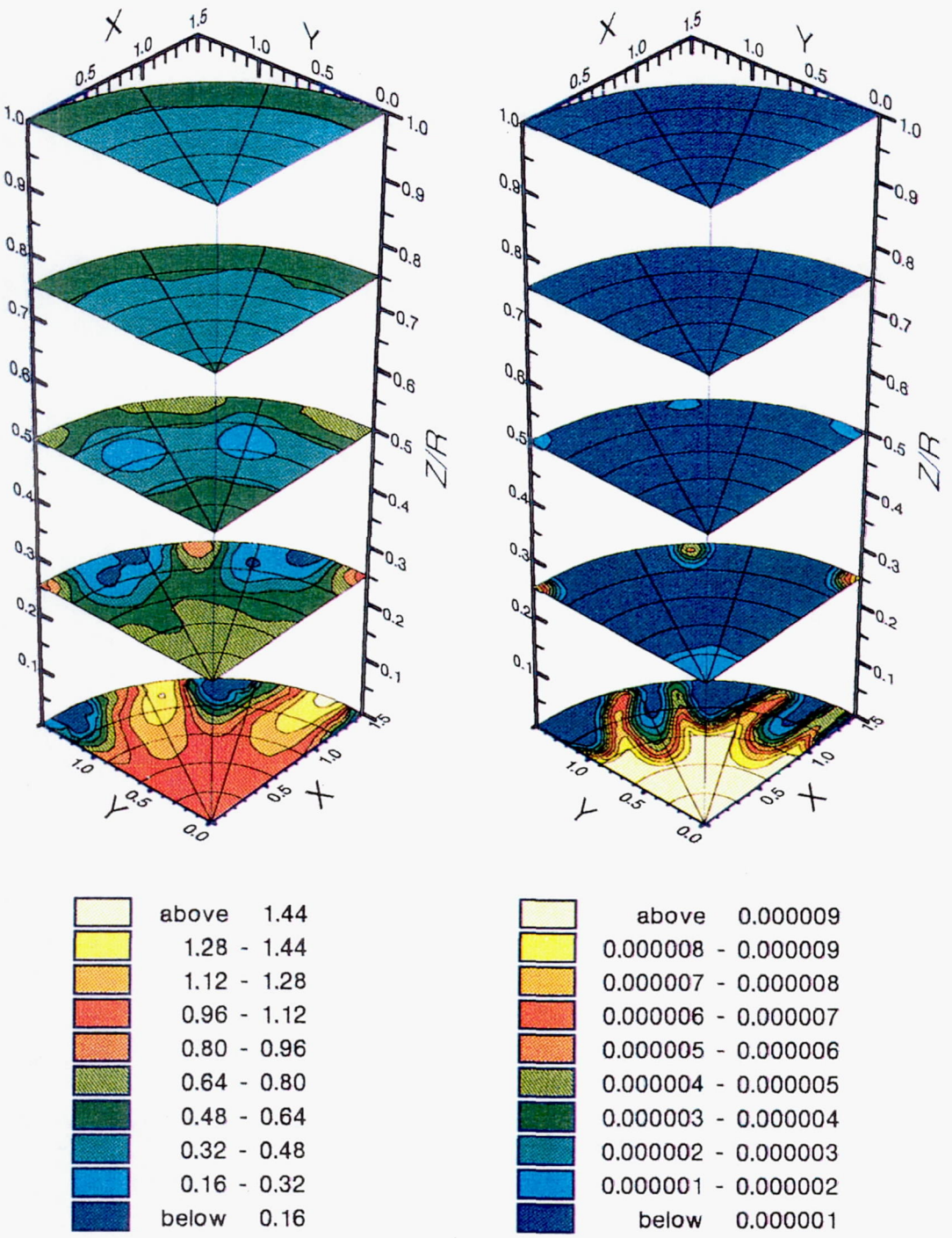

a) Equil. Ratio

b) NO Production (Mole Fraction)

Figure 5.43: Equivalence Ratio and NO Production, J52MOD6

Page intentionally left blank

MOD	Holes/Slots	No	Asp Ratio	Angle
J52MOD3	Slots	8	4	0
J52MOD4	Slots	8	4	22.5
J52MOD5	Slots	8	4	45
J52MOD6	Slots	8	4	67.5

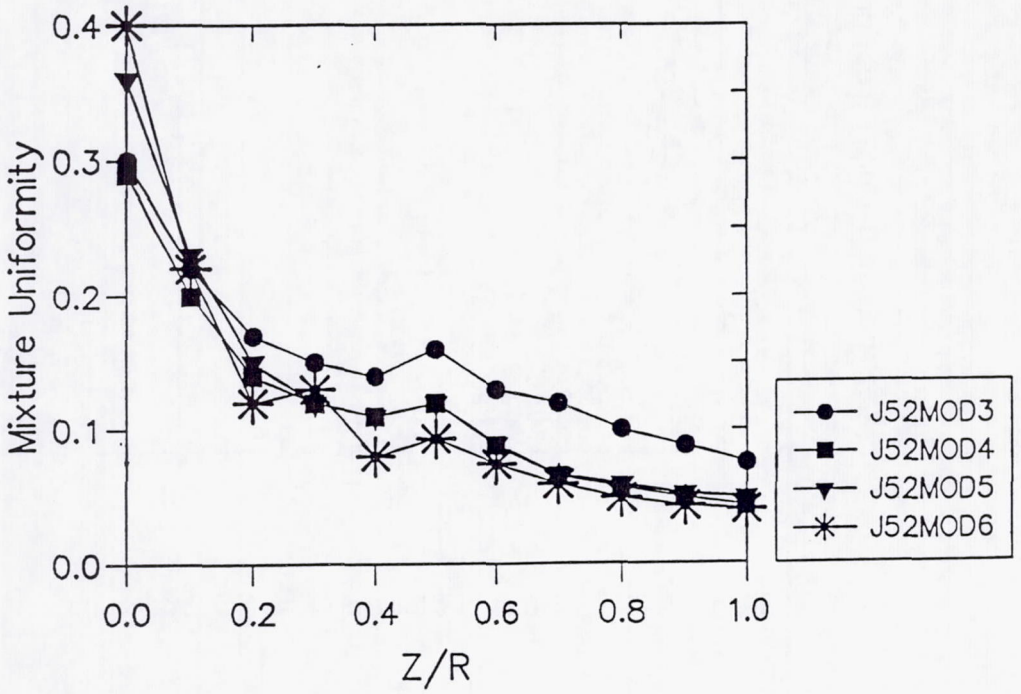

Figure 5.44 Effect of Slot Angle on Mixture Uniformity

MOD	Holes/Slots	No	Asp Ratio	Angle
J52MOD3	Slots	8	4	0
J52MOD4	Slots	8	4	22.5
J52MOD5	Slots	8	4	45
J52MOD6	Slots	8	4	67.5

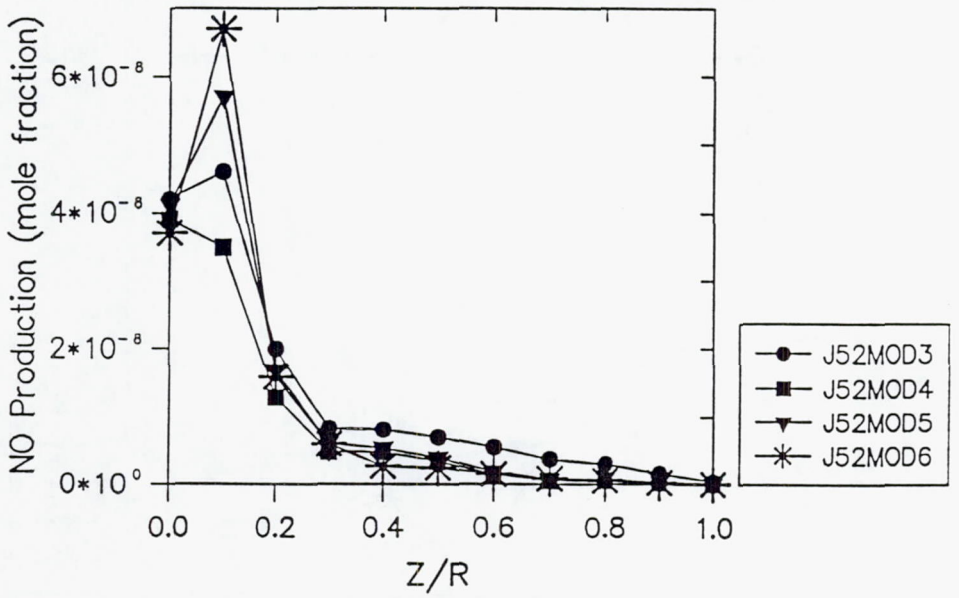

Figure 5.45 Effect of Slot Angle on NO Production

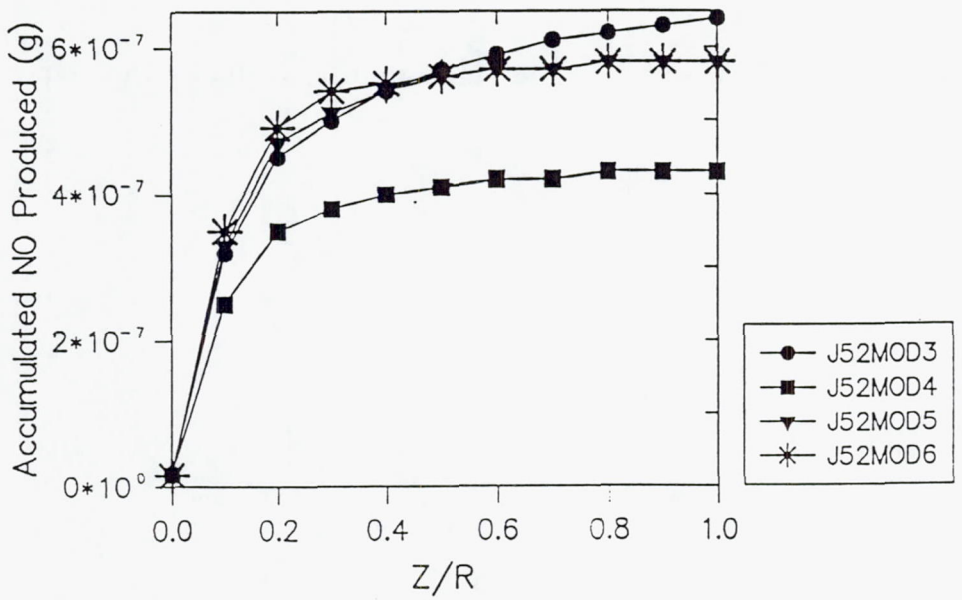

Figure 5.46 Effect of Slot Angle on Accumulated NO Produced

5.3 Demonstration Phase

Mixing studies performed in rectangular geometries concluded that jet to mainstream mass and densities ratios have a secondary effect on downstream mixing patterns (Holdeman, 1991). To examine the effects of these parameters, as well as those of reference velocity, on mixing in an axis-symmetric can configuration, a series of experiments was conducted for a 8-hole baseline geometry and an 8:1 aspect ratio slanted slots module. This section presents the results for the latter geometry.

Figure 5.47 shows the mixture fraction plot for the Demonstration Case1. This case is to be compared to J52MOD2, presented in section 5.2.2. Reference velocity, momentum-flux ratio (J = 51), and density ratio are the same for both configurations. The only difference is a mass ratio of 1.5 for the Demonstration module.

A comparison of the mixture fraction plots shows qualitatively similar flow fields for the two modules. At the first axial plane (Z/R=0.0), the jets appear to penetrate the same distance for both configurations. At downstream locations, however, a lower f value region is observed at the center of the Case1 module, indicating stronger jet penetration. At Z/R=1.0, the flow field appears better mixed for this geometry with lesser indication of a relatively unmixed center, as compared to J52MOD2.

Figure 5.48 compares the mixture uniformity parameter for the two modules. The lower mass ratio case presents a more uniformly mixed flow field in all axial locations. Because of the geometry of the slots, jet flow is introduced over a shorter distance for the lower mass ratio case. Therefore, at any axial location within the slots, the local mixture fraction value is closer to the equilibrium value and the mixture uniformity parameter is smaller . Downstream of the slots, the mixture uniformity parameter remains smaller for the lower mass ratio case. These results are contrary to what was previously observed in rectangular geometries, in which mixing performance was shown to be independent of orifice size and jet to mainstream mass ratio (Holdeman, 1991).

Page intentionally left blank

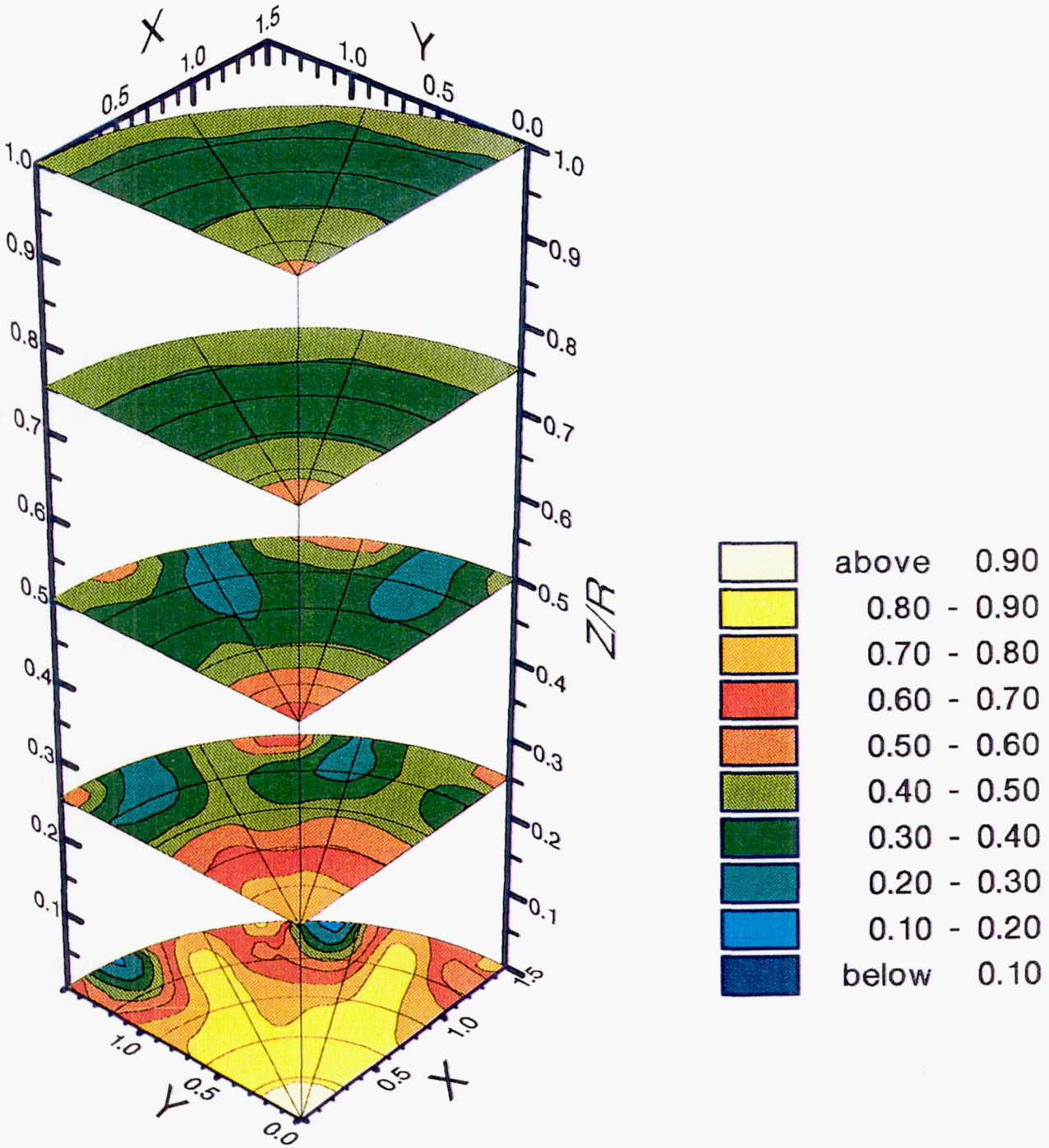

Figure 5.47 Mixture Fraction, Demonstration Case1

Page intentionally left blank

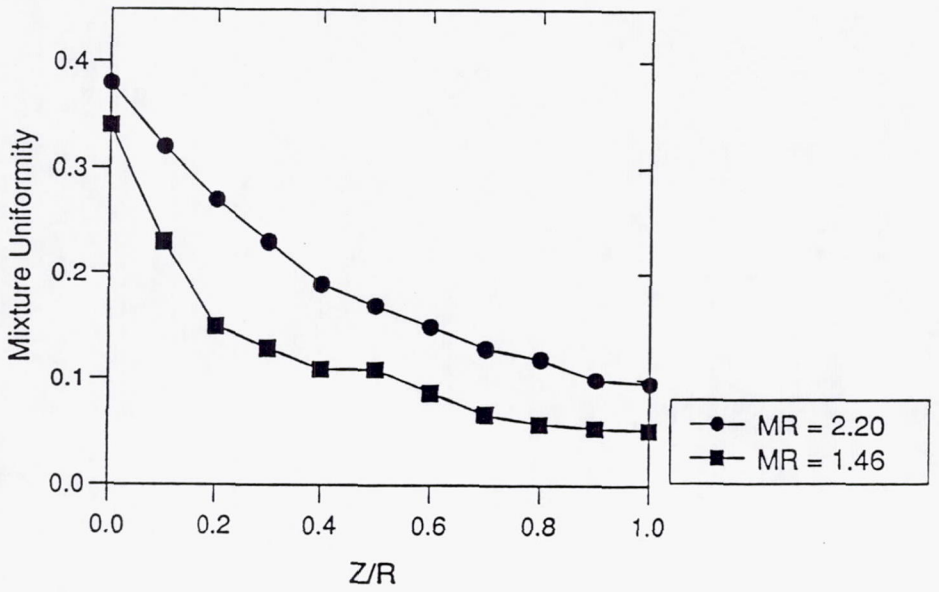

Figure 5.48 Effect of Mass Ratio on Mixture Uniformity

The effect of density ratio on mixing (Demonstration Case2) was examined by increasing the mainstream temperature (DR= 1.7). The results of this case will be compared to those of the demonstration Case1 (DR= 1.2).

Figure 5.49 shows the axial mixture fraction plots for the high density ratio configuration. The mixing pattern is similar for the two modules. Jet penetration for Case2 appears to be slightly stronger than Case1. The small $f > 0.9$ region seen at the center of the Case1 module at Z/R = 0.0, is not shown for Case2. Downstream locations for Case2, however, show slightly larger unmixed wall regions compared to Case1, further indicating higher jet penetration. Figure 5.50 compares the mixture uniformity for the two geometries. It is apparent that the mixing characteristics are basically the same for these two cases, and small difference in mixing patterns have a negligible effect on the overall mixture uniformity.

Page intentionally left blank

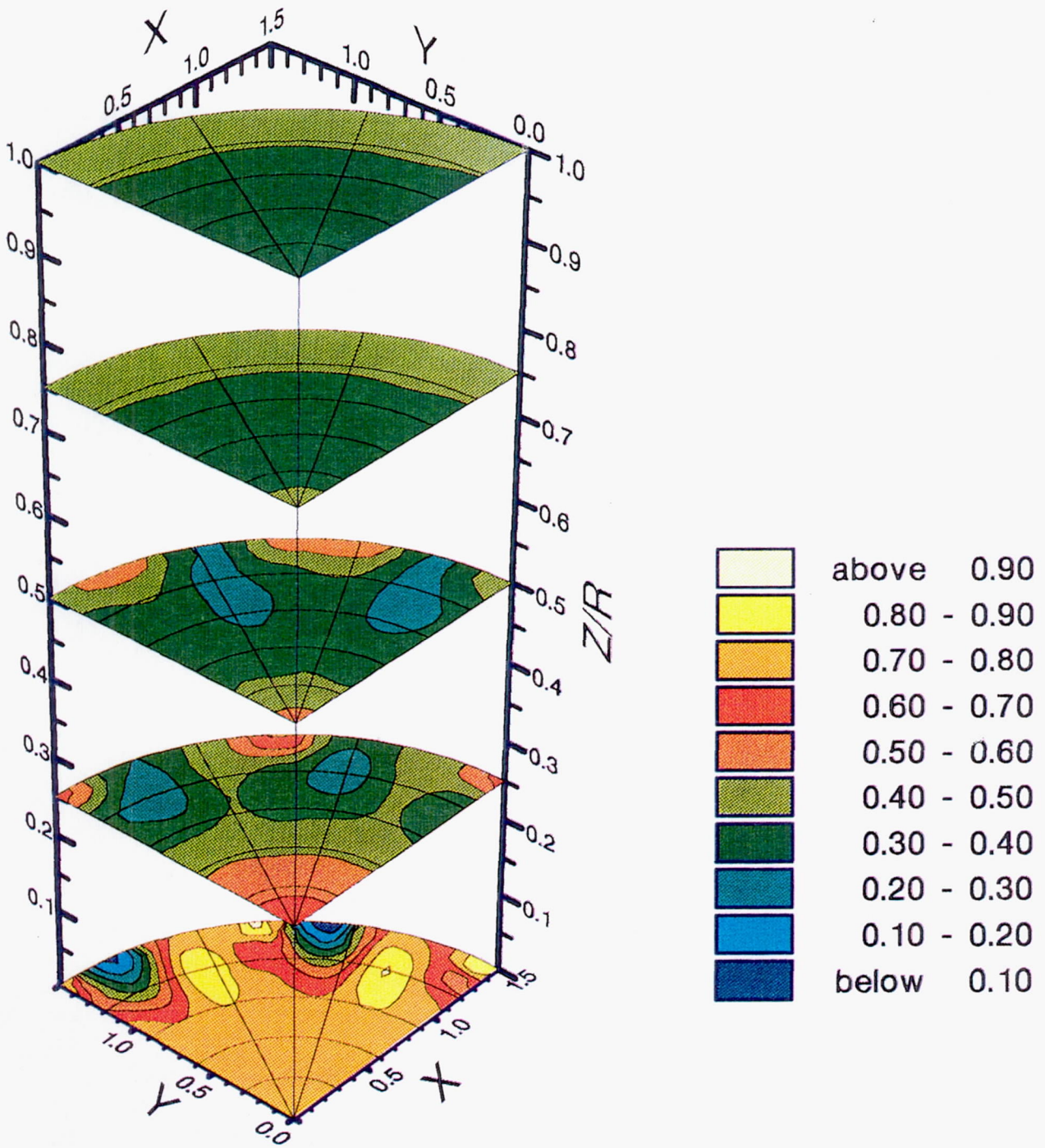

Figure 5.49 Mixture Fraction, Demonstration Case2

Page intentionally left blank

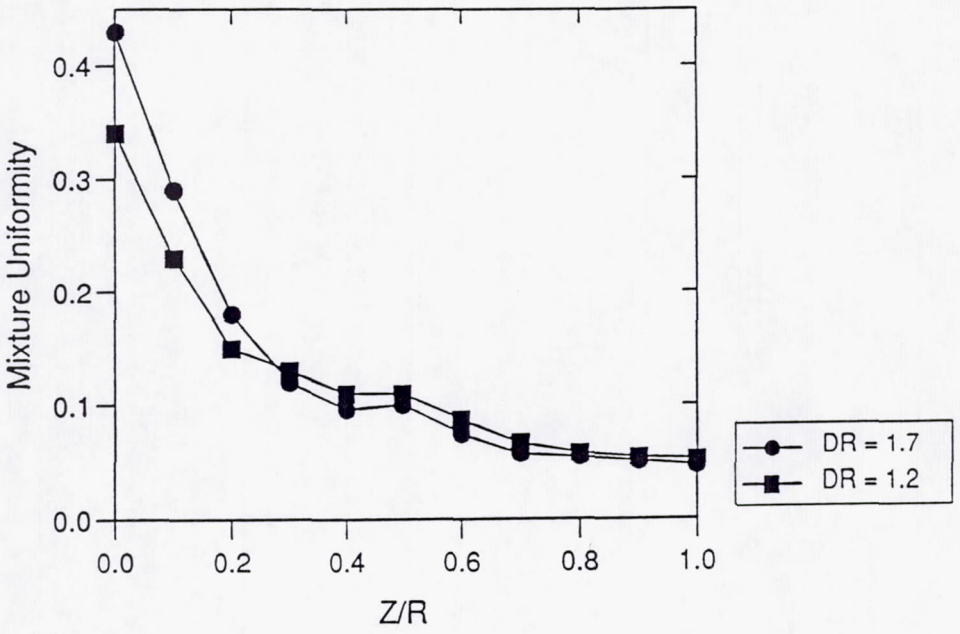

Figure 5.50 Effect of Density Ratio on Mixture Uniformity

Figure 5.51 shows the mixture fraction distribution for Demonstration Case3. For comparison to Case1 refer to Figure 5.50. At the first axial location, Case3 shows slightly higher jet penetration to the center. Mixing patterns at downstream locations also indicate stronger jet penetration compared to Case1, showing a lower f value at the center and unmixed regions along the walls. A comparison of mixture uniformity for the two cases, shows a slightly better mixed flow field for the lower reference velocity case between Z/R=0.1, and Z/R= 0.4 (Figure 5.52). This is due to better mixed central region for Case3 at these axial locations. Further downstream, the mixture uniformity is the same for the two geometries.

Page intentionally left blank

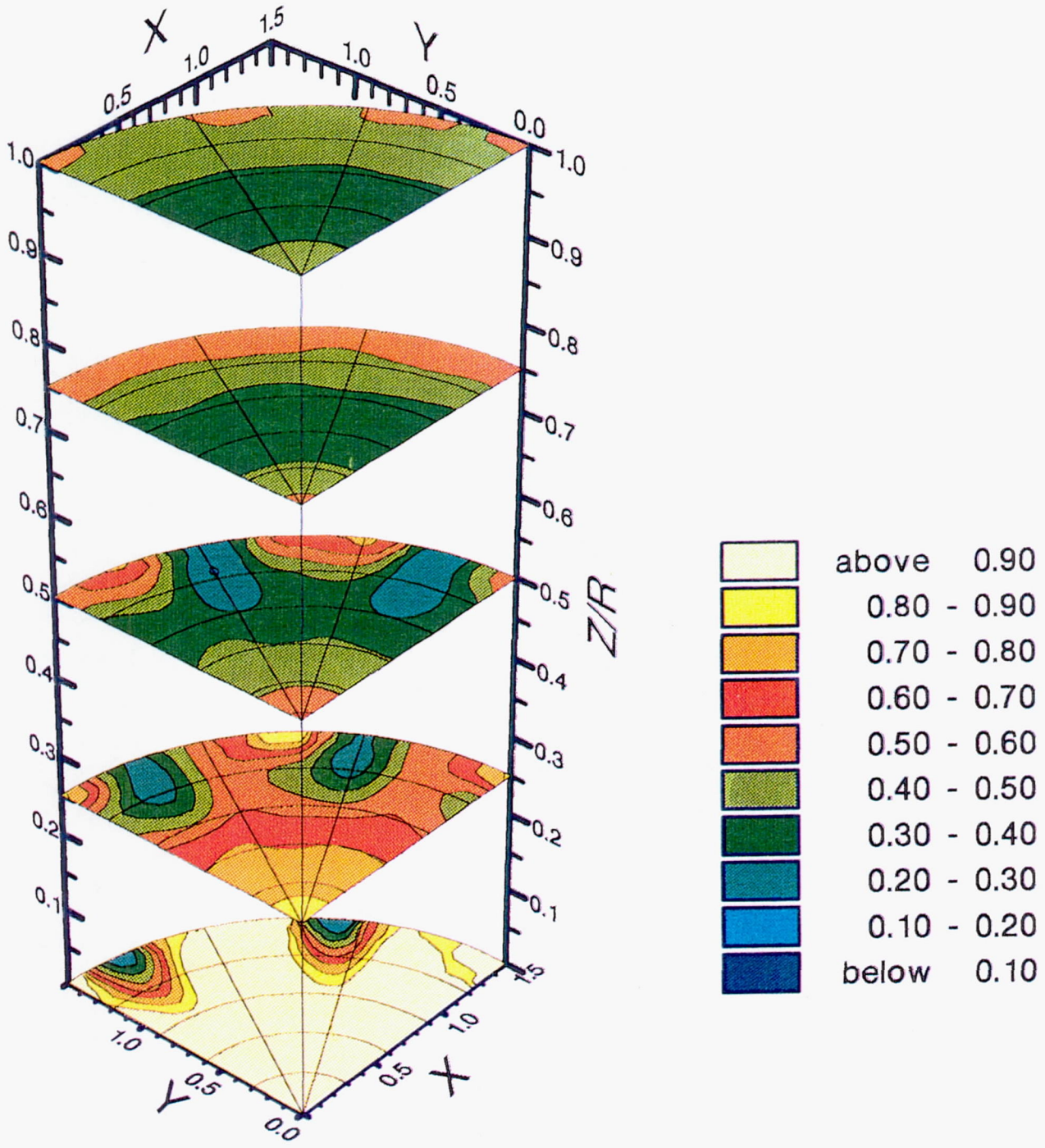

Figure 5.51 Mixture Fraction, Demonstration Case3

Page intentionally left blank

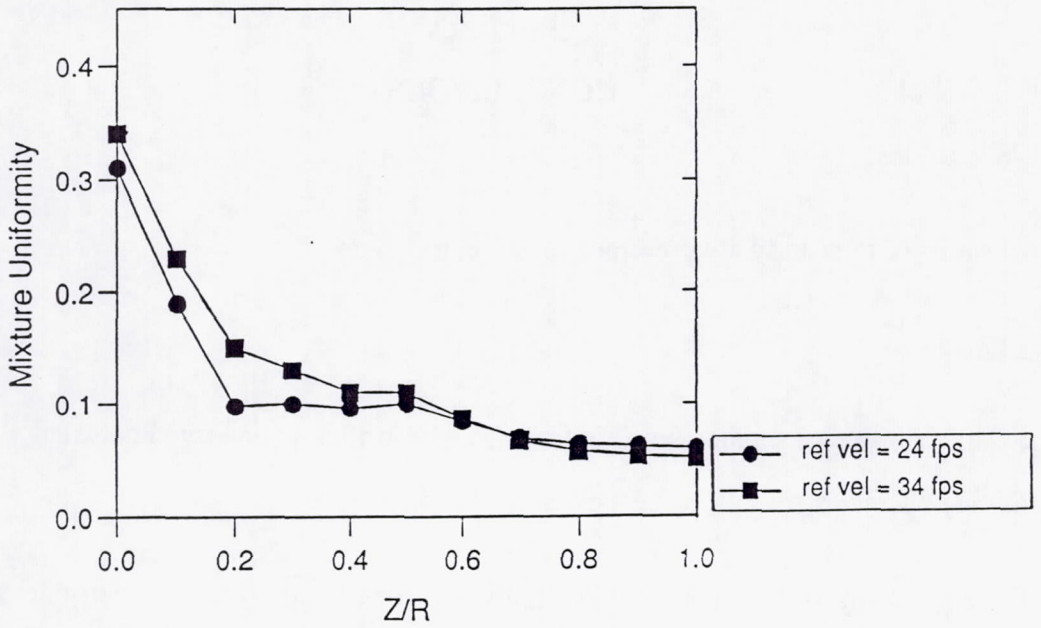

Figure 5.52 Effect of Reference Velocity on Mixture Uniformity

CHAPTER 6

CONCLUSIONS

6.1 Conclusions

The conclusions of this study are presented in two categories:

Overall-mixing

- Jet to mainstream momentum-flux ratio (J), and orifice geometry significantly impact the mixing characteristics of jets in a cylindrical geometry.
- For a fixed number of orifices, the coupling between J and orifice geometry determines the extent of jet penetration and circumferential mixing in an axis-symmetric can geometry.
- From an overall-mixing standpoint, moderate penetration to the center is desirable. Under-penetration forms a relatively unmixed core that persists at downstream locations. Over-penetration degrades circumferential mixing and forms relatively unmixed regions along the walls.
- Increasing aspect ratio of the slanted slots, reduces jet penetration to the center and enhances mixing along the walls.
- Increasing the angle of the slots with the respect to the mainstream also reduces jet penetration and enhances circumferential mixing.
- Decreasing the jet to mainstream mass ratio, in an 8:1 aspect ratio configuration enhance jet penetration and overall mixing. The effects of reference velocity and density ratio on overall-mixing are negligible at the levels of variations considered.

NO-Reduction

- An effective tool has been developed to extrapolate the non-reacting results to a reacting environment, and thereby project the NO formation and CO depletion potentials of the mixing modules.

- The NO formation potential results reveal that the majority of NO is formed near the plane defined by the leading edge of the orifices. As a result, the extent of mixing processes in this region determines the overall emissions performance of the mixer.

- Rapid early mixing does not necessarily lead to a low early rate of NO production. Very quick and uniform mixing to a local equivalence ratio of 1.0, produces large amount of NO.

- Minimizing the NO production in a quick mixer requires an optimization between two competing tradeoffs: 1) effective mixing near the injection plane, and 2) effective mixing in the wall regions downstream of the mixing orifices. Jet to mainstream momentum-flux ratio and orifice geometry are important parameters in optimizing this tradeoff. A further consideration is the rate of mass addition.

- For the cases examined in the present study, the holes at a momentum-flux ratio of approximately 52 yield the best mixer from a NO production perspective. In general, the holes result in significantly lower NO production than the 8:1 aspect ratio slanted slots for all momentum-flux ratios examined.

- At the intermediate and high J values examined, the 4:1 aspect ratio geometry produced significantly lower NO compared to the 8:1 aspect ratio slanted slot. At the lowest J, the accumulated NO calculated for the two geometries were comparable.

- The early rate of NO production increases with the increase in slot angle, except for the 4:1 aspect ratio slanted slot geometry oriented at 22.5°. This geometry shows the lowest early rate of NO production and the lowest accumulated NO among the various orifice orientations examined.

- For the modules examined, the lowest NO formation potentials at the injection plane were observed for over-penetrated cases. This observation, however, does not take into the account the possibility of backflow on the centerline and its contribution to overall NO production.

- Jet to mainstream mass and density ratios, and reference velocity do not have a notable impact on the rate and accumulated NO production at the levels of variations considered in the present study.

- The present results suggest that determining the optimum combination of momentum-flux ratio and orifice geometry for NO reduction purposes, will require an assessment of the specific application (e.g., operating conditions, mass ratio, geometrical constraints,..). In other words, further study may not necessarily lead to a universal guideline for the design of a low NO quick mixer.

REFERENCES

Atkinson, K. N., Khan, Z. A., and Whitelaw, J.H., "Experimental Investigation of Opposed Jets Discharging Normally into a Cross-stream", Journal of Fluid Mechanics, Vol. 115, pp. 493-504, 1982.

Barata, J. M. M., Durao, D. F. G., and Heitor, M. V., " Impingement of Single and Twin Turbulent Jet Through a Crossflow", AIAA Journal, Vol. 29, No. 4, pp. 595-602, April 1991.

Becker, K., H., and Schurath, U., " Photo-Oxidation of Aircraft Engine Emissions at Low and High Altitudes", NATO Advisory Group for Aerospace Research and Development, AGARD-CP- 125, London, U.K., 1973.

Brady, R. A., " A Study of Dome Region Fuel-Air Mixing in a Model Rich Burn- Quick Mix-Lean Burn Combustor", Masters Thesis, University of California, Irvine, 1991.

Brasseur, G., " Chemical Kinetics in the Stratosphere", NATO Advisory Group for Aerospace Research and Development, AGARD-CP- 125, London, U.K., 1973.

Carrotte, J. F., and Stevens, S. J., " The Influence of Dilution Hole Geometry on Jet Mixing", ASME 89-GT-292, Gas Turbine and Aeroengine Congress and Exposition, Toronto, Canada, June 1989.

Cox, G. B., " Multiple Jet Correlation for Gas Turbine Combustor Design", Journal for Engineering for Power, pp. 265-273, April 1976.

Fearn, R., and Weston, R. P., Vorticity Associated with a Jet in a Cross Flow, AIAA Journal, Vol. 12, No. 12, December 1974.

Glassman, I., Combustion, Academic Press, Second Editon, 1987.

Ho, C. M., and Gutmark, E., " Vortex Induction and Mass Entrainment in a Small-Aspect-Ratio Elliptic Jet", Journal of Fluid Mechanics, Vol. 179, pp. 383-405, 1987.

Holdeman, J. D., " Mixing of Multiple Jets with a Confined Subsonic Crossflow", AIAA-91-2458, 27th Joint Propulsion Conference, June 24-27, 1991, Sacramento, CA.

Holdeman, J. D., and Walker, R. E., Mixing of a Row of Jets with a Confined Crossflow. AIAA Journal, Vol. 15, No. 2, pp.243-249, February 1977.

Holdeman, J. D., Srinivasan, R., "Modeling Dilution Jet Flow Fields", AIAA Journal of Propulsion, vol. 2, No. 1, Jan.-Feb. 1986.

Holdeman, J. D., Srinivasan, R., Coleman, E. B., Meyers, G. D., and White, C. D., " Effect of Multiple Rows and Non-circular Orifices on Dilution Jet Mixing", AIAA Journal of Propulsion, vol. 3, No. 3, May-June 1987, pp. 219-226.

Holdeman, J.D., and Srinivasan R., "Modeling of Dilution Jet Flow Field", Journal of Propulsion and Power, Vol. 2, No.1, pp. 4-10, January/February 1986.

Holdeman, J.D., Srinivasan R., and Berenfeld, A., "Experiments in Dilution Jet Mixing", AIAA Journal, Vol. 22, No.10, pp. 1436-1443, October 1984.

Howe, G. W., Li, Z., Shih, T. I-P., and Nguyen, H. L., "Simulation of Mixing in the Quick Quench Region of a Rich Burn-Quick Quench Mix-Lean Burn Combustor", AIAA-91-0410, 29th Aerospace Sciences Meeting, Reno, Nevada, January 7-10, 1991.

Isaac, K. M., and Jakubowski, A. K., Experimental Study of the Interaction of Multiple Jets with a Cross Flow, AIAA Journal, Vol. 23, No. 11, November 1985.

Johnston, H. S., and Witten, G., " Reaction of Ozone with Nitrogen Oxides at High Altitudes", NATO Advisory Group for Aerospace Research and Development, AGARD-CP- 125, London, U.K., 1973

Kamotani, Y., and Greber, I., "Experiments on a Turbulent Jet in a Cross Flow", AIAA Journal, Vol. 10, No. 11, pp. 1425-1429, November 1972.

Karagozian, A. R., "An Analytical Model for the Vorticity Associated with a Transverse Jet", AIAA Journal, Vol. 24, No. 3, pp. 429-436, March 1986.

Karagozian, A. R., Nguyen, T. T., and Kim, C. N., "Vortex Mixing of Single and Multiple Dilution Jet Mixing in a Crossflow", Journal of Propulsion and Power, Vol. 2, No. 4, pp. 354-360, August 1986

Kavsaoglu, M. S., and Schetz, J. A., "Effects of Swirl and High Turbulence on a Jet in Cross Flow", Journal of Aircraft, Vol. 26, No. 6, pp. 539-546, June 1989.

LaRue, J. C., Deaton, T., and Gibson, C. H., "Measurement of High-Frequency Turbulent temperature", Review of Scientific Instrument, Vol. 46, No. 6, 757- 764, 1975.

Le Grives, E., " Mixing Process Induced by the Vorticity Associated with the Penetration of a Jet into a Cross Flow", Journal of Engineering for Power, Vol. 100, pp. 465-475, July 1978.

Lefebvre, A. H., Gas Turbine Combustion, Hemisphere Publishing Corporation, New York, 1989.

Novick, A. S., and Troth D. L., "Low NO_x Heavy Fuel Combustor Concept Program", Detroit Diesel, Allison Division, October 1981.

Ott, J., "HSCT Research Focuses on Environmental Issues", Avation Week & Space Technology, December, 1989.

Samuelsen, G.S., "The Combustion Aspects of Air Pollution", in Advances in Environmental Science and Technology, Vol. 5, John Wiley & Sons, 1975.

Shaw, R.J., "Engine Technology Challenges for a 21st Century High Speed Civil Transport", NASA Technical Memorandum 104363, 1991.

Smith, C. E., " Mixing Characteristics of Dilution Jets in Small Gas Turbine Combustors", AIAA-90-2728, AIAA 26th Joint Propulsion Conference, July 16-18, 1990.

Smith, C. E., and Talpallikar, M. V., and Holdeman, J. D. "A CFD Study of Jet Mixing in Reduced Areas for Lower Combustor Emissions", AIAA-90-2460, 27th Joint Propulsion Conference, Sacramento, CA., June 24-27, 1991

Sterland, P. R., and Hollingsworth, M. A., "An Experimental Study of Multiple Jets Directed Normally to a Cross Flow, Journal of Mechanical Engineering Science, Vol. 17, No. 3, pp. 117-124, 1975.

Stevens, S. J., and Carrotte, J. F., " Experimental Studies of Combustor Dilution Zone Aerodynamics, Part I: Mean Flowfield", Journal of Propulsion and Power, Vol. 6, No. 3, pp. 297-304, May-June 1990.

Stevens, S. J., and Carrotte, J. F., " Experimental Studies of Combustor Dilution Zone Aerodynamics, Part II: Jet Development", Journal of Propulsion and Power, Vol. 6, No. 4, pp. 504-510, May-June 1990.

Tacina, R. R., "Low NO_x Potential of Gas Turbine Engines", AIAA-90-0550, 28th Aerospacse Sciences Meeting, Reno, Nevada, January 1990.

Tacina, R. R., Private Communication, 1991.

Talpallikar, M. V., Smith, C. E., and Lai, M-C., "Rapid Mix Concept for Low Emissions Combustors in Gas Turbine Engines", NASA Contractor Report 185292, October 1990.

Vranos, A., Liscinsky, B., True, B., and Holdeman, J. D."Experimental Study of Cross-Stream Mixing in a Cylindrical Duct", AIAA-91-2459, 27th Joint Propulsion Conference, Sacramento, CA., June 24-26, 1991,

Weston, R. P., and Thames, F. C., "Properties of Aspect ratio 4.0 Rectangular Jets in a Subsonic Crossflow", Journal of Aircraft, Vol. 16, No. 10, pp. 701-707, October 1979.

Witting, S. L. K., Elbahar, O. M. B., and Noll, B. E., "Temperature Profile Development in Turbulent Mixing of Coolant with a Confined Hot Crossflow", Journal of Engineering for Gas Turbines and Power, Vol. 106, No. 1, pp.193-197, January 1984.

Zeldovich, J., "The Oxidation of Nitrogen in Combustion and Explosions", Acta Physicochimica, USSR, Vol. 21, 4, pp. 577-628, 1946.

ACKNOWLEDGMENTS

The authors are grateful to NASA Lewis Research Center for providing the funding for this project (contract number: NAG3-1110), and especially to the program monitor, Dr. J.D. Holdeman, for his active participation and valuable technical guidance.

We would like to thank Howard Crum and Brian Bissell for their help in developing the facility. Many thanks to undergraduates Ryan Brink and Armen Markarian who helped construct the facility, and to Steven Lee whose assistance in data acquisition and analyses was invaluable.

APPENDIX A

TIME SERIES MEASUREMENTS

In a turbulent environment such as the one of the present experiment, examining the fluctuating component of the measured quantity is of interest. For this experiment, temperature fluctuations were measured for a selected number of modules. Temperature fluctuations above the mean value are especially important in the HSCT application, since they can contribute significantly to NO formation (Brady, 1991).

To measure the fluctuations and intermittencies in the temperature field, a cold wire technique was employed. Figure A-1 presents the schematic of the cold wire electronics. A 0.0001-inch (2.54 μ) diameter, 0.31-inch (0.8 mm) long Platinum-Rhodium wire, manufactured by the Sigmund Cohn Corporation (Mt. Vernon, NY), is operated in a AC- wheatstone bridge with a current of 120 μA. The current is low enough that the velocity sensitivity is negligible. Over a limited temperature range, the wire resistance can be approximated by the following linear expression:

$$r_w = r_o[1+\alpha_w(T_w-T_o)]$$

where r_o is the wire resistance at a reference temperature T_o , and α is the temperature coefficient of resistivity (LaRue, et al. 1975). The resistance fluctuations are converted to voltage fluctuations by passing a small current through the wire. The voltage fluctuations are amplified using low noise, high gain amplifiers. The voltage fluctuations, e(t), are related to wire temperature fluctuations by the following relationship:

$$e(t) = \alpha_w I r_o[\, T_w(t) - T_o]$$

The frequency response of the cold wire is a function of the wire diameter. A detailed description of the cold wire technique can be found in LaRue et al. (1975).

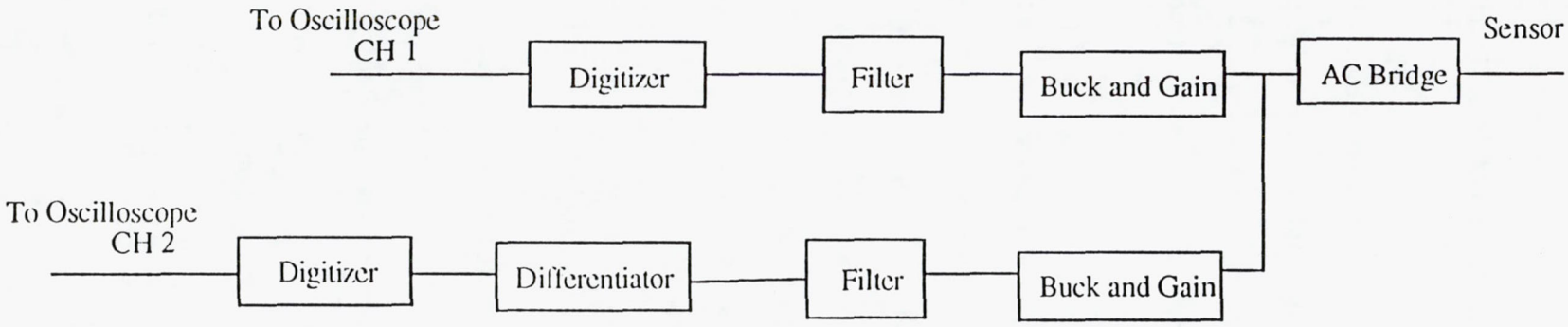

Figure A-1: Block Diagram Of Cold-Wire Electronics

The temperature fluctuations measured for the 8:1 aspect ratio quartz geometry are presented here. The operating conditions for this experiment are the same as those described for Demonstration Case3 (Table 4.5). The low reference velocity case was selected to ensure the survival of the cold wire sensor throughout the tests. Measurements were conducted in 20 points in a quarter sector, for which the corresponding mean temperatures were measured. The majority of measurements were obtained at planes Z/R=0.75, and Z/R=1.0. At lower planes, the sensor would survive only a few minutes, especially in the wall region, due to the impact of the turbulent jet flow.

The temperature fluctuation results presented in this section were made at two points in the flow field, one at the center and one near the module wall. Fluctuations were measured in several planes to examine the effect of axial location on the amplitude and general features of the fluctuations.

Figure A-2 shows the instantaneous temperatures obtained at a center point (X = Y= 0.0), for axial locations of Z/R= 0.08, 0.50, 0.75, and 1.0. The mean mixture fraction distribution can be found in Figure 5.59 At the first axial location examined (Z/R = 0.08), the temperature fluctuations indicate the injection of cold flow into a relatively constant temperature flow field at approximately 210^{o} F. This is expected since this axial location is immediately downstream of the injection plane, and the cold streaks represent the jets injected into the cross flow.

At Z/R=0.50, the jets and the mainstream have begun to mix, and the constant temperature fluid is no longer present. Instead, the mean temperature is reduced and high amplitude temperature fluctuations are seen. As the downstream distance is increased, smaller fluctuations are expected. At Z/R=0.75, temperatures fluctuations are surprisingly small, indicating low turbulence in the flow field. A verifiable explanation is not available at this point that accounts for the low fluctuating point especially since, at Z/R = 1.0, temperature fluctuations are again present. The

amplitude of fluctuations are slightly lower at this point as compared to Z/R = 0.50. More data are required to determine whether the low rms signal is repeatable.

The temperature fluctuation results for a point near the wall (X=Y= 0.88) are presented for planes Z/R = 0.50, 0.75, and 1.0 only (Figure A-3). Below Z/R = 0.5, the sensor did not survive the direct impact of jet flow.

Temperature fluctuations at Z/R = 0.50, are similar to those measured at the center point of this plane. The mean temperature, however, is lower due to the better circumferential mixing for an 8:1 aspect ratio geometry.

The instantaneous temperature measured at Z/R = 0.75 shows that colder fluid is injected into a relatively constant temperature stream. The presence of cold streaks are explained by the position of the sensor, which was placed near an air jet. The presence of low fluctuating flow field at a mean temperature of approximately 130° F is also consistent with the measurements obtained at the center point of the plane. At Z/R = 1.0, the fluctuating temperatures are present. Compared to the center point instantaneous signal at this plane, the fluctuations near the wall are smaller.

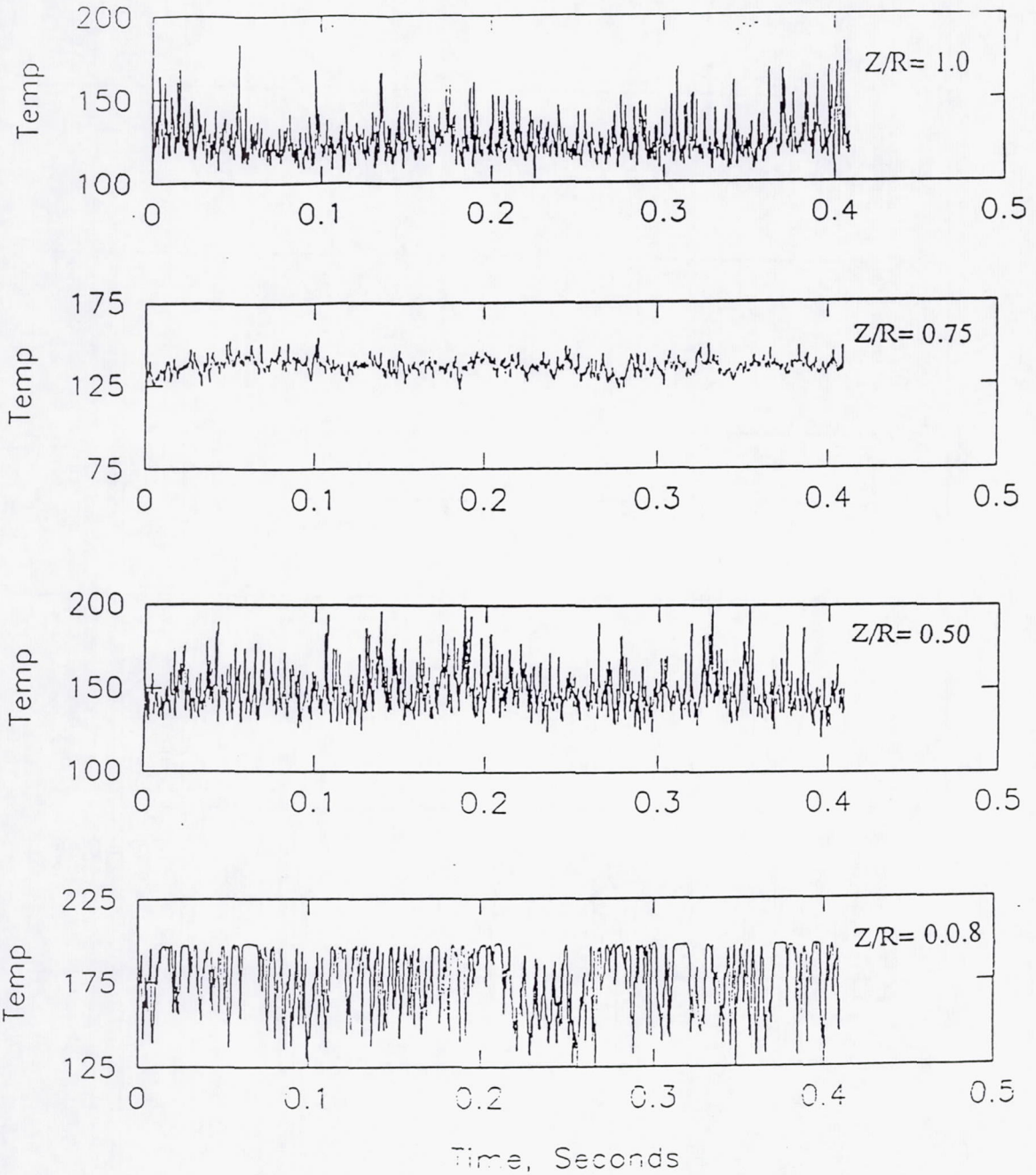

Figure A-2 Instantaneous Temperature Measurements for 8:1 Aspect Ratio Geometry, J= 54, X= 0.0, Y= 0.0

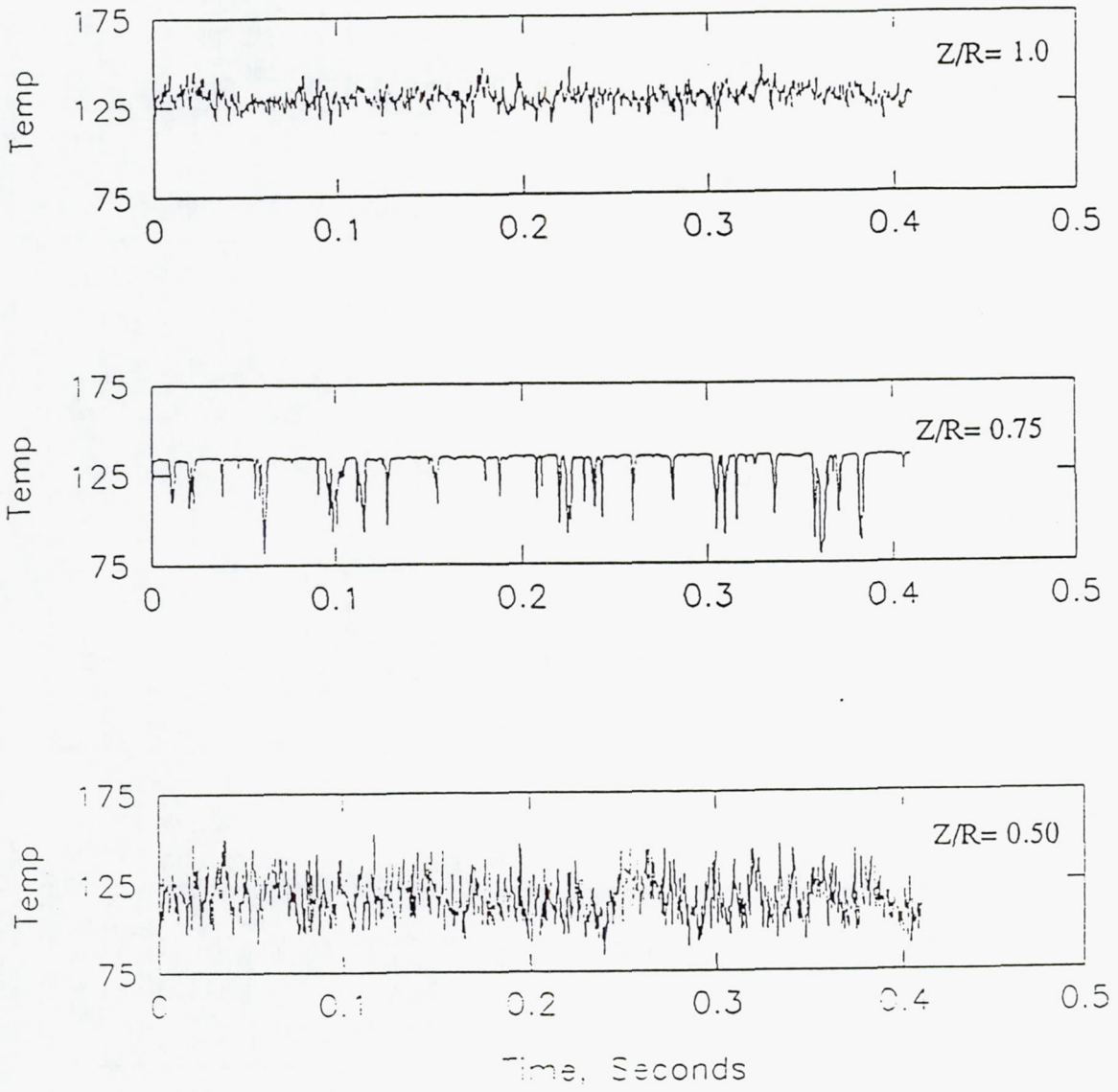

Figure A-3 Instantaneous Temperature Measurements for 8:1 Aspect Ratio Geometry, J= 54, X= 0.88, Y= 0.88

REPORT DOCUMENTATION PAGE

Form Approved
OMB No. 0704-0188

1. AGENCY USE ONLY (*Leave blank*)	2. REPORT DATE	3. REPORT TYPE AND DATES COVERED
	June 1996	Final Contractor Report

4. TITLE AND SUBTITLE

Influence of Geometry and Flow Variation on Jet Mixing and NO Formation in a Model Staged Combustor Mixer With Eight Orifices

5. FUNDING NUMBERS

WU–537–02–20
G–NAG3–1110

6. AUTHOR(S)

M.S. Hatch, W.A. Sowa, and G.S. Samuelson

7. PERFORMING ORGANIZATION NAME(S) AND ADDRESS(ES)

UCI Combustion Laboratory
University of California
Irvine, California 92717–3550

8. PERFORMING ORGANIZATION REPORT NUMBER

E–8614

9. SPONSORING/MONITORING AGENCY NAME(S) AND ADDRESS(ES)

National Aeronautics and Space Administration
Lewis Research Center
Cleveland, Ohio 44135–3191

10. SPONSORING/MONITORING AGENCY REPORT NUMBER

NASA CR–194473

11. SUPPLEMENTARY NOTES

Project Manager, James D. Holdeman, Internal Fluid Mechanics Division, organization code 2650, NASA Lewis Research Center, (216) 433–5846. (Actual work done in 1992.)

12a. DISTRIBUTION/AVAILABILITY STATEMENT

Unclassified - Unlimited
Subject Category 07

This publication is available from the NASA Center for AeroSpace Information, (301) 621–0390.

12b. DISTRIBUTION CODE

13. ABSTRACT (*Maximum 200 words*)

A series of non-reacting parametric experiments was conducted to investigate the effect of geometric and flow variations on mixing of cold jets in an axis-symmetric, heated cross flow. The confined, cylindrical geometries tested represent the quick mix region of a Rich-Burn/Quick-Mix/Lean-Burn (RQL) combustor. The experiments show that orifice geometry and jet to mainstream momentum-flux ratio significantly impact the mixing characteristic of jets in a cylindrical cross stream. A computational code was used to extrapolate the results of the non-reacting experiments to reacting conditions in order to examine the nitric oxide (NO) formation potential of the configurations examined. The results show that the rate of NO formation is highest immediately downstream of the injection plane. For a given momentum-flux ratio, the orifice geometry that mixes effectively in both the immediate vicinity of the injection plane, and in the wall regions at downstream locations, has the potential to produce the lowest NO emissions. The results suggest that further study may not necessarily lead to a universal guideline for designing a low NO mixer. Instead, an assessment of each application may be required to determine the optimum combination of momentum-flux ratio and orifice geometry to minimize NO formation. Experiments at reacting conditions are needed to verify the present results.

14. SUBJECT TERMS

Dilution; Jet mixing flow; Gas turbine; Combustion chamber; Emissions

15. NUMBER OF PAGES
173

16. PRICE CODE
A08

17. SECURITY CLASSIFICATION OF REPORT	18. SECURITY CLASSIFICATION OF THIS PAGE	19. SECURITY CLASSIFICATION OF ABSTRACT	20. LIMITATION OF ABSTRACT
Unclassified	Unclassified	Unclassified	